UNIVERSITY OF STRATHCLYDE

FACULTY OF ENGINEERING
BIOENGINEERING UNIT

SIZE-DEPENDENT MECHANICAL PROPERTIES OF SINGLE POLYURETHANE NANOFIBRES

MILOVAN JOE CARDONA

A DISSERTATION SUBMITTED IN PARTIAL FULFILMENT
OF THE REQUIREMENTS OF THE AWARD OF

MASTERS OF SCIENCE IN BIOENGINEERING

DECLARATION OF AUTHENTICITY

This thesis is the result of the author's original research. It has been composed by the author and has not been previously submitted for examination which has led to the award of a degree.

Signed: ……. Date: …… / …… / 2012

The research work disclosed in this publication is partially funded by the Strategic Educational Pathways Scholarship (Malta). This Scholarship is part-financed by the European Union – European Social Fund (ESF) under Operational Programme II – Cohesion Policy 2007-2013, "Empowering People for More Jobs and a Better Quality Of Life".

Operational Programme II – Cohesion Policy 2007-2013
Empowering People for More Jobs and a Better Quality of Life
Scholarship part-financed by the European Union
European Social Fund (ESF)
Co-financing rate: 85% EU Funds; 15%National Funds

Investing in your future

ABSTRACT

Electrospinning is a process in which a high-voltage electric field is used to create a fibre that is nanometres in diameter and meters in length. These nanofibres are then collected onto a target to create a non-woven, fibrous structure of variable fibre diameter and morphology. These electrospun nanofibre mats have a broad range of applications including being used as chemical sensors, filtration, electrode materials and drug delivery systems. They are also an excellent candidate for engineered tissue scaffolds since the fabricated structure mimics that of an extracellular matrix.

When cells are seeded onto a fabricated mesh, their behaviour strongly depends on the biomaterial`s properties. Various studies have already confirmed the role of micro-topography, the surface chemistry and treatment of a scaffold, on cell viability, attachment and signal transduction. The strong dependency of cell behaviour on the material properties further complicates the study of mechanotransduction, which is essential for cellular processes such as cell differentiation, growth, survival and the maintenance of cellular homeostasis [1].

With the development of newer technologies, namely atomic force microscopy, we are now able to visualise and characterise the properties of single nanofibres. In this study, the mechanical properties of single electrospun polyurethane nanofibres are investigated using atomic force microscopy. It was found that the elastic modulus varies significantly with a change in fibre diameter and multiple experiments were performed to confirm this observation. An attempt was also made to explain this change in fibre modulus by using nanoindentation and we hypothesise that a shallow, hard surface layer forms on the nanofibres caused by a change in the crystal structure of the polymer. The implications that these observations have on cellular mechanotransduction were then discussed and suggestions were given on how these can be limited.

ACKNOWLEDGMENTS

First and foremost, I would like to thank my supervisor Dr. Richard A. Black, who was responsible for the successful progress and completion of my dissertation. His ideas, suggestions, knowledge and expertise in the subject were greatly appreciated. I would also like to express my deep gratitude for his patience and continuous guidance during instruction on the operating procedures of the tools used in this project.

I would also like to give special thanks to Kit Mei Tan for providing materials along with her support, suggestions and knowledge which were essential for the completion of this thesis. My sincere thanks go to Katie Henderson and Brian Cartlidge for their expertise and technical assistance. Their availability and assistance was instrumental at the several stages of this project.

I also want to thank my new friends and colleagues at the department and my friends back home whose friendship and support was greatly appreciated.

Finally, I am as ever thankful to my family. Special thanks go to my sister for her continuous support, advice and patience throughout my thesis. My sincere gratitude goes to my parents for their love, patience and continuous support when I encountered difficulties. I am sure that this dissertation would not have been possible without their help.

TABLE OF CONTENTS

LIST OF FIGURES

NOMENCLATURE

A - Cross-sectional area

d - Displacement in x- direction

D - Reduced diameter of nanofibre

D_1 - Measured height of nanofibre

D_2 - Measured width of nanofibre

dP/dH - Elastic unloading stiffness

E - Elastic Modulus

E_{eff} - Effective elastic modulus

E_i - Young's Modulus of the indenter

F - Force applied

I - Cross-sectional moment of area

L - Suspended length

r - Radius of fibre

v - Poisson's ratio of the specimen

v_i - Poisson's ratio of the indenter

σ - Stress

ε - Strain

LIST OF ABBREVIATIONS

AFM – Atomic Force Microscope

DMAC - Dimethylacetamide

ECM - Extra-cellular matrix

PAMS – Poly Alpha-Methyl-Styrene

PLLA - Polylactic acid

PU - Polyurethane

PVA - Polyvinyl alcohol

SEM - Scanning Electron Microscope

1 INTRODUCTION

Tissue engineering is an interdisciplinary area combining the study of biology and engineering. It utilises expertise gained from the material and mechanical fields along with knowledge of biochemical, physiological and cellular behaviour to replace biological functions. Scientists have shown the capability of growing cells on artificial scaffolds made of engineered materials that could then be successfully implanted into humans to support or replace a biological function [1].

Tissue engineering has long promised the ability of creating a complete set of artificial organs, but this prospect is still a far from being achieved. Research in this area has been fuelled by a growing demand for organ transplant. As this demand significantly outweighs the supply, a large percentage of candidates unfortunately die while waiting for a suitable donor.

Creating artificial tissue has however proven to be significantly challenging. Cells will only grow on specialised microstructures that imitate their original extracellular matrix while chemical and mechanical stimulation have to be induced to closely mimic the cells' original environment. Most scientific research in this field has therefore been focused on any one of these areas in an attempt to find a combination of factors that would allow for a better understating of cellular behaviour and ultimately the creation of viable artificial scaffolds [2].

2 LITERATURE REVIEW

2.1 INTRODUCTION

Tissue engineering starts with a biopsy from a diseased target organ. Healthy cells are then isolated in an attempt to grow organs that are entirely made of these healthy, viable cells. These cells are then cultivated and multiplied to create an extensive supply of healthy cells to be used in the next stage. At the same time, a scaffold is created that mimics the extracellular structure of the target organ. This scaffold has to be constructed using a biocompatible material and must provide mechanical properties that are similar to those usually experienced by cells. Polymeric nanofibres are therefore the preferred material and form used for these scaffolds [1].

Cells are then seeded onto the scaffold while chemical and mechanical stimuli are applied in an attempt to convince the cells that they are actually growing on the original organ. If this is done successfully, cells would not only survive but also grow and proliferate on the scaffold creating an organ that closely mimics the original. This artificial organ would then be implanted into the patient with the hope of having it replace the function of the original organ [1].

There are multiple complications in this process. This thesis discusses the challenges faced when trying to create a scaffold that closely mimics the extracellular matrix. Common techniques used to create and characterise these scaffolds are discussed in this chapter.

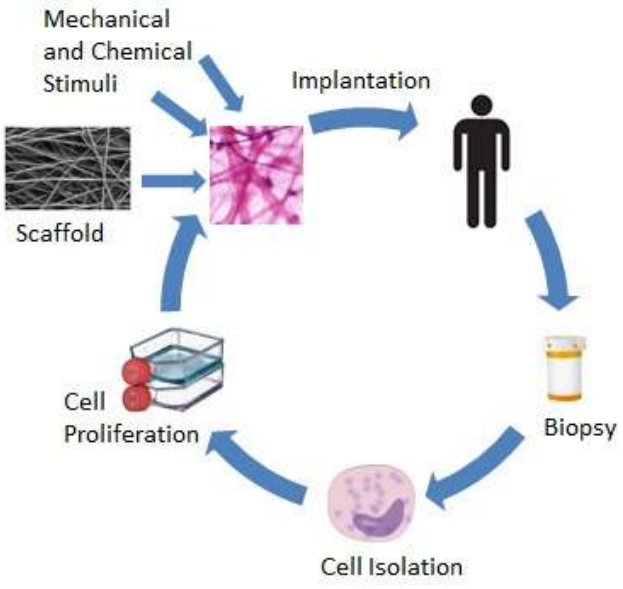

Figure 2.1 - Showing the various stages in tissue engineering

2.2 NANOFIBRES IN BIOENGINEERING

2.2.1 INTRODUCTION

Advances made in the last two decades have sparked an interest in using nanotechnology for bioengineering applications. Polymer nanofibres, defined as slender, elongated and threadlike structures with a diameter less than 1000nm [3], are of particular interest as their size range closely matches structural features present in natural tissue. Other advantages of nanofibres include their superior mechanical properties, ease of fabrication when compared to other nanostructures, large surface areas to volume ratio when assembled into a fibrous mesh and the ease of functionalisation into various purposes, as indicated by a considerable number of patents in this area [4].

Various studies look into the use of nanofibre structures for drug-delivery systems, wound dressings and the manufacture of artificial scaffolds amongst others [5]. Multiple *in vitro* studies on the use of nanostructures in these areas have shown that they can outperform their micro and macro-metric counterparts even when composed of the same material [6].

2.2.2 TISSUE ENGINEERING

Tissue engineering is a multidisciplinary field requiring knowledge from biology, medicine, engineering and material science. Fibres are collected into meshes with a high density of nanofibres and therefore a large surface area to volume ratio. The discovery that different cell types adhere and proliferate on these scaffolds and the possibility of using biological or biodegradable materials for the nanofibres has encouraged research in this area. This research was further stimulated when mammalian stem cells were found to survive and differentiate on these artificial scaffolds. Tissue engineers can now design scaffolds to elicit a specific cellular response by using signalling ligands such as growth factors, adhesion peptides or DNA fragments [7]. Many studies are focusing on three dimensional tissue scaffolds for artificial organ design by using nanofibres made of biodegradable polymers to create the next generation of medical devices.

2.2.3 WOUND CARE

The creation of artificial tissue has led to an interest in using nanofibres for the wound care sector. 16,000 patients are admitted to an NHS hospitals each year requiring medical treatment on burn wounds [8]. Nanofibres can provide an alternative to autografting and traditional wound dressings for patients with larger burn areas [6]. This demographic can be further expanded by considering patients with chronic wounds such as diabetic ulcers, pressure ulcers and venous ulcers [9]. Since they can mimic extracellular matrix, nanofibres can facilitate tissue morphogenesis and the healing process of damaged tissue [10].

2.2.4 DRUG - DELIVERY

The next natural progression for this technology was into using polymer nanofibres as drug-delivery systems. Most nanofibre properties relevant for drug-delivery such as the fibre diameter, the mesh porosity and the drug binding mechanisms can be modified. Customising these factors will affect the dose and rate of the drug release to ensure optimal results on the patient [11]. Drug-loaded nanofibre meshes can also be used as site-specific drug delivery systems where drugs are placed directly into, or adjacent to, the target area. These have numerous advantages over drugs that are carried through the blood system as they will only target affected areas and therefore reduce side-effects that in some cases can be severe [12].

2.2.5 STENT COATING

In a patent filed in 2009 [13], *Dong* describe a stent covered with aligned nanofibres to reduce in-stent restenosis and the risk of embolism formation. Previously, stents had been covered using a thick physical barrier of PTFE which failed to show clinical benefits as it was bulky and required a high deployment pressure. The proposed coating on the other hand had improved biocompatibility, was easily deployed and had the potential for drug loading [14].

Figure 2.2 – Nanofibre-covered stent

2.3 CELL - SCAFFOLD INTERACTION

Artificial scaffolds aim to mimic the complexities of the human extracellular matrix's function to accommodate and encourage cell growth and proliferation. This would result in an engineered tissue where the cells would provide the biological functionality and the scaffold creates a platform for cellular growth. Understanding the interaction between the cells and the scaffold is therefore essential as it has been found to have a considerable impact on the survival of the cells and ultimately, the effectiveness of the engineered tissue. This interaction can be regulated by both the chemical and physical properties of the scaffold material including composition, size, shape, surface texture, mechanical properties and others [15].

2.3.1 TOPOGRAPHICAL EFFECTS

The topographical effects of the scaffold have been given considerable importance in the last decade and have been found to influence cell adhesion, motility, viability, apoptosis, differentiation and various other essential parameters for tissue engineers. Both natural and artificial tissues are usually split into a hierarchical structure where the topographical characteristics are important on all size scales of the scaffold. This includes the overall shape of the scaffold (the superstructure), the cellular level (microstructure) and the subcellular level (the nanostructure).

Previous studies have confirmed the impact that the micro-topography has by introducing micrometre-size features on surfaces and assessing their influence on parameters such as migration, adhesion and morphology. Unfortunately, due to the inherent difficulty in characterisation, the nanoscale features of surface are usually omitted even though these

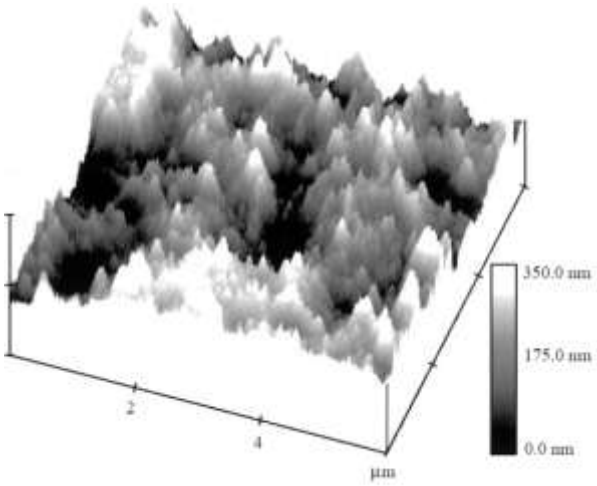

Figure 2.3 - Nano-structural surface of the corneal epithelial basement membrane underlying the corneal epithelium

might have a considerable impact on the scaffold. As the nano-topography on the artificial scaffold is different to that encountered in their natural environment, cells will encounter different physical cues, leading to a change in behaviour. One of the main areas of interest is the study of nanoscale cellular extensions such as filopodia, which provide motion and are thought to play a sensory role in the cell. These extensions might be affected by the presence of nano-topographical pores and elevations that are clearly present extracellular matrix. Figure 2.3 shows the nano-structural surface of the corneal epithelial basement membrane underlying the corneal epithelium, where one can clearly see the nano-topographical features on the surface resulting in a 400% increase in surface area. A larger area for the cell to adhere to and will have an impact on the cell movement and ultimately, the regulation of tissue growth [16].

2.3.2 EFFECTS OF MECHANICAL PROPERTIES

Many studies have shown that the mechanical properties of the extracellular matrix (ECM) have adverse effects on cells. In a study by *Ulrich et al.*, it was shown that highly rigid ECMs increase the spread of tumour cells in tissues. When the rigidity was lowered to values that mimic healthy ECMs, tumour cells appear rounded and mechanotransduction was nearly halted. The mechanical properties of the ECM also had an impact on cell proliferation as this was lowered with a less rigid ECM [17].

In another study, *Paszek et al.* take this a step further by saying that tissue stiffness can be used to predict the presence of a tumour [18]. They conclude that an abnormally stiff ECM will develop diseases and is at a heightened risk of developing malignant tumours. They found that even a small increase in the ECM rigidity would change the tissue architecture and enhance the growth of cancer cells [18]. This therefore points out the fact that an artificial scaffold would have to closely mimic the mechanical properties of the original ECM. The rigidity of the fibres should therefore be closely monitored and investigated if a viable artificial scaffold is to be created.

2.4 POLYMERS

2.4.1 POLYMERS AS BIOMATERIALS

Due to their wide range of mechanical and chemical properties, polymers are considered as the largest and most promising class of biomaterials. They are easily synthesised, can take a wide range of shapes and forms, as well as being economically feasible to mass-produce. This combination has led to plentiful research being conducted on the various aspects of polymeric biomaterials [19].

A significant number of polymers have been used for tissue engineering in the formation of scaffolds. These include biodegradable and non-degradable polymers which can be either natural or synthetic. Biodegradable polymers allow the cells to build their own extracellular matrix and slowly degrade leaving behind an organ made entirely of natural materials. Non-degradable polymers would influence the tissue turnover but have the advantage that their chemical and mechanical properties remain, to a certain extent, unaffected by time [20].

2.4.2 POLYURETHANE

Biocompatible polyurethanes and poly(ether urethanes) have been used for long term medical implants as they show excellent biocompatibility and a wide range of mechanical properties. They have been used in medical devices such as cardiac pacemakers, vascular grafts and in the production of artificial scaffolds [21].

Polyurethanes have also been extensively used in the manufacture of artificial scaffolds. A study by *Carlberg et al.* [22]investigated the proliferation and neuronal differentiation of human embryonic stem cells on polyurethane scaffolds. They confirmed that polyurethane scaffolds are a feasible scaffold for this application, displaying favourable interaction between the cells and the substrate, and indicate that the physical cues provided by the scaffold direct stem cells towards a neuronal cell fate. Another study by *Grenier et al.* [23] investigated the interaction between polyurethane scaffolds and coronary artery smooth muscle cells. They, amongst others, also concluded that polyurethane is a suitable substrate material for scaffold

manufacture [22]. With the success of bio-stable polyurethane, attempts were made to develop biodegradable polyurethanes. These have also shown considerable impact and use for medical devices [21].

The mechanical properties of polyurethane on the macro-scale have been thoroughly investigated and are suitably well understood. Unfortunately, to our knowledge, no study that investigates the mechanical properties of polyurethane in the nanoscale has been published. As shown previously, the mechanical properties of nanofibres have a significant impact on the viability of cells and a characterisation would lead to a better understanding of cellular behaviour.

2.5 MANUFACTURE OF NANOFIBRES

2.5.1 INTRODUCTION

Various procedures have been used to manufacture nanofibres namely drawing, template synthesis, self-assembly and electrospinning. An overview of the procedures and a comparison of each technique was briefly reviewed below.

2.5.2 DRAWING

A micromanipulator is used to bring a micropipette into contact with a polymer droplet. The micropipette is then withdrawn from the droplet at a fixed, slow speed resulting in a nanofibre being produced.

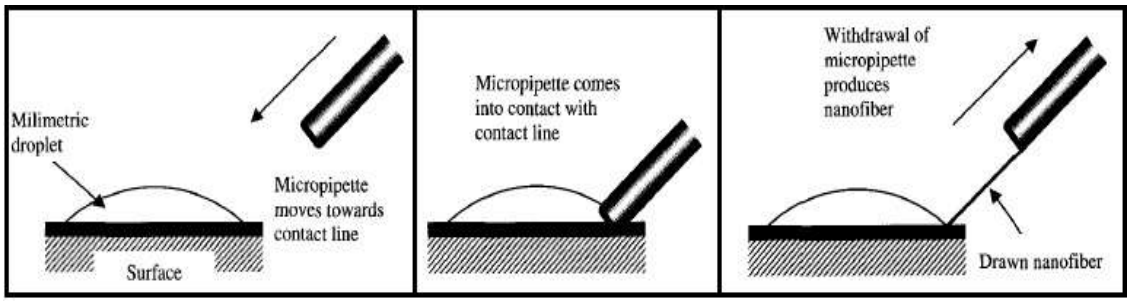

Figure 2.4 - Drawing method

Only sodium citrate nanofibres of 2nm-100nm have been successfully produced using this method. Even though the equipment required is minimal, the process is also discontinuous, producing fibres no more than millimetres long [3].

2.5.3 TEMPLATE SYNTHESIS

This procedure uses a metal oxide membrane that has pores with nano-scale diameters. This membrane is used as an extrusion dye to create nanofibres from a polymer solution under the application of pressure. The fibre diameter produced depends on pore diameter of the membrane and can be easily varied by using a different membrane. Unfortunately, this process cannot be scaled up and usually only produces fibres that are around 10 microns in length [3].

2.5.4 SELF-ASSEMBLY

Self-assembly of nanofibres is a process in which smaller molecules are used as basic building blocks for nanoscale fibres. This molecule is arranged such that bonds are formed concentrically around it using intermolecular forces that bring smaller units together to form an individual nanofibre.

Various polymers have been used to successfully create nanofibres with diameters ranging from 7nm to 100nm but the process involved is complex and the nanofibres produced are no longer then several microns [3].

2.5.5 ELECTROSPINNING

This technique uses a high voltage electric field to draw out a nanofibre from a syringe onto a collector. Various experimental parameters, such as the polymer solution, the polymer feed rate and the voltages used can be manipulated to obtain different fibre diameters and morphology.

This process has been successfully used on a wide range on polymers and diameters ranging from 3nm to 2μm can be produced. Electrospinning is also very cost-effective and the process can easily be scaled up if needed. Even though its major drawback is jet instability, fibres up to several meters in length can still be produced. This makes electrospinning the most attractive manufacturing technique for the purpose of this research and will discussed in further details below [3].

2.6 ELECTROSPINNING

2.6.1 HISTORY

The first documented record for the use of electrospinning of a polymer into a nanofibre is dated back to 1902 in a patent obtained by *J. F. Cooley* and *W. J. Morton.* This patent describes a method that deposits a viscous polymer solution onto a positively charged electrode when it is held close to an electrode of opposite charge. Another similar patent was filed the following year and specifies that the electrodes can be in the vicinity of the polymer and don't necessarily have to be in contact with the solution. The principal ideas set by these century-old patents have not been challenged and are still being used in today's electrospinning processes [3].

A significant number of patents were later filed by various other individuals, each contributing to laying down an enhanced overall technique for the electrospinning process. However, with the more recent understanding of fluid dynamics, electrostatics and the availability of newer technologies such as electron microscopy, this old technique was rediscovered, refined and expanded into numerous new applications that had not been thought of before [23].

2.6.2 EQUIPMENT AND TECHNIQUE

One of the most attractive attributes of electrospinning is that it can be set up using only a few pieces of specialised equipment. A glass syringe is used to contain the polymer dispersion while a high voltage DC generator is used to generate a potential difference between the polymer solution and a surface that is used to collect the fibres.

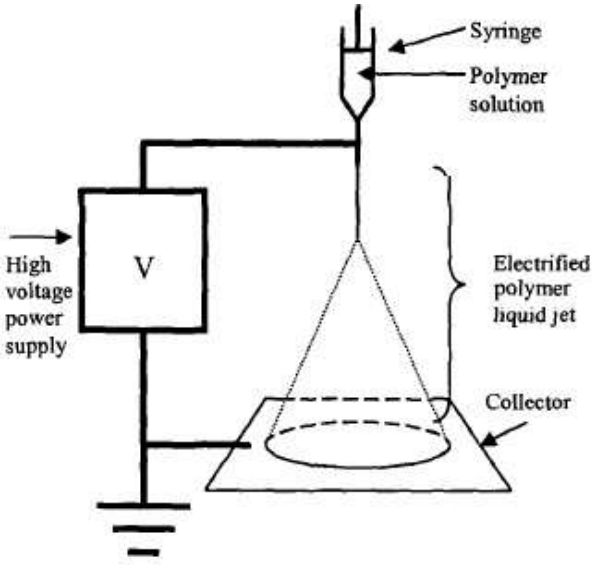

Figure 2.5 - Electrospinning Setup **[3]**

This setup is sometimes changed by using a rotating collector powered by a separate motor and a syringe activated by a linear motor to maintain a fixed polymer feed rate [24].

The voltage is switched on and at a certain threshold, governed by many factors discussed later in this section, a polymer droplet is drawn into a cone, from which a nanofibre emerges to move down the electric potential and deposit itself onto the collector. The fibrous mat created on the collector is generally composed of a single, long nanofibre arranged in a random manner due to the high electrical instability in the electrospun fibre. One can immediately see the large number of variables involved in the process, some of which cannot always be accurately controlled [25].

2.6.3 PROCESS DESCRIPTION

Electrospinning is usually initiated by a solution droplet being slowly pumped out of the syringe at a fixed feed rate. When the electric field applied is enough to counteract the surface tension of the solution and the gravitational force, the droplet elongates and assumes a cone-like shape. From this "Taylor's cone", a narrow jet of liquid is ejected in the direction of the electric field. The surface area of the jet then has to be increased to accommodate the large build-up in charge on the jet. This is achieved by producing a thin, long fibre travelling towards the oppositely-charged collector [24].

Observations show that the fibre is continually accelerated until it reaches the collector. This acceleration leads to a decrease in fibre diameter both due to extension and the evaporation of the solvent. To further accommodate surface charges, the fibres bend rapidly to increase the surface area, producing a whipping instability region that is still not completely understood [23].

2.6.4 PROCESS VARIABLES

2.6.4.1 Introduction

The final properties of the nanofibre mat produced by electrospinning highly depend on a variety of both material and process-dependent variables. Material-dependent variables include solution conductivity, concentration, viscosity and volatility of the solvent used. Process-dependent variables include solution feed rate, electric field applied, distance of tip from collector and the rotational speed of the collector amongst others. Apart from this, the environment in which the fibres are spun would also, to a certain extent, affect the resulting structure. It is therefore very difficult to create a predictive model that would factor in all these variables and foretell the final properties of the fibrous mat produced [25].

The general trends resulting from altering certain parameters on the final product are discussed in the following section. Since no quantitative data is available to help predict these results, electrospinning is sometimes considered as much an art as it is a science [23].

2.6.4.2 Polymer Concentration

Polymer concentration is usually the dominant factor in electrospinning. It is important since it has a high impact on the viscosity of the solution, which would in turn determine whether the solution would produce fibres at all. Polymer concentration is also considered as the most important factor affecting fibre diameter, where an increased concentration would generally increase fibre diameter.

It is important to note that this relationship is not linear and that a threshold value of viscosity has to be exceeded for electrospinning to be possible. Even though the solution viscosity is usually primarily changed by the solution concentration, the solvent system used can also alter the solution viscosity [23].

2.6.4.3 Solvent System

Since the solvent usually makes up for more than 80% of the solution, it has a significant impact on the solution's conductivity, surface tension and rate of solidification due to the solvent's volatility. Changing the solvent therefore impacts multiple factors that would in turn affect the product's fibre diameter [25].

Unfortunately, changing the solvent usually means that other parameters, such as applied voltage and polymer concentration, would have to be changed to make electrospinning possible. This therefore means that it is very difficult to extrapolate the effect the solvent would have on the final product by formulating experiments where the only variable is the solvent used [23].

2.6.4.4 Solvent Volatility

Solvent volatility is essential since solid nanofibres are only formed when the solvent has completely evaporated. The inherent properties of the solvent and the gap distance between the electrode and the collector determine whether the solvent is completely evaporated when the fibre reaches the collector.

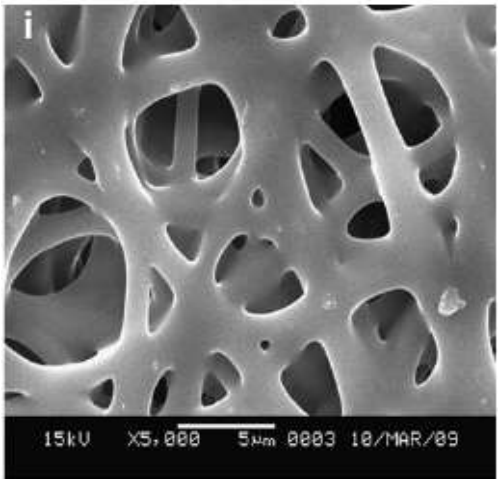

Figure 2.6 - Electrospun mesh from wet fibres **[51]**

If the solvent does not evaporate quickly enough, the wet fibres may fuse and form a reticular mat. On the other hand, if the solvent is too volatile, the fibres produced would appear to be wrinkled and needle blockage could occur [23].

2.6.4.5 Collector Geometry

The collector geometry would not only affect the shape of the final electrospun fibrous mat but can also, to a certain extent, help in controlling fibre diameter and fibre alignment. Using a circular drum, rotating at a velocity higher than a certain threshold would result in aligned fibres and, to some extent, a uniform mat of controlled thickness and porosity. A rotating collector would also increase the rate of evaporation for the solvent improving the morphology of the fibres. Stationary metal plates are the simplest collectors and also very commonly used. Apart from being inexpensive and easier to operate, this method is also used when a completely random and unaligned mesh is required.

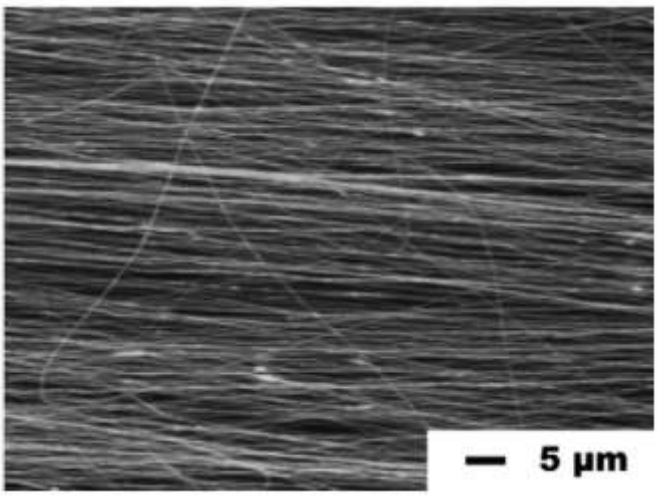

Figure 2.7 - Aligned nanofibres **[50]**

2.6.4.6 Collector material

The material used for the collector also has a significant impact on the fibres produced. The material's conduction to electricity is the most important property affecting this choice. Typically, an aluminium base covered with aluminium foil is used as it versatile, highly conductive and facilitates sample characterisation as it can be removed from the collector base. If the material used is not sufficiently conductive, the process could be interrupted as nanofibres are redirected to a more conductive surface [25].

2.6.4.7 Applied Voltage

The high voltage difference created in electrospinning is a key parameter since it is the driving force that creates the nanofibre. The voltage has to be high enough to overcome the surface tension of the solution and initiate the electrospinning process. In general, increasing the electric field would stretch the fibres further and lead to smaller diameters as well as encouraging faster solvent

evaporation yielding drier fibres [3]. On the other hand, increasing the time it takes for the fibres to reach the collector would allow them to stretch and produce thinner diameters. As increasing the voltage decreasing this time, an elevated voltage could then be seen as increasing the diameter. This highlights the need to consider all the factors collectively and not as separate entities, since modifying other parameters such as the feed rate would result in a different behaviour with a change in the applied voltage [23].

2.6.4.8 Feed Rate

For a stable nanofibre to be produced, the rate at which solution is made available for electrospinning should match the rate of removal of solution from the tip. This means that for a given feed rate, a corresponding voltage should be applied. Increasing the feed rate would somewhat increase the fibre diameter, but beads are formed when the feed rate is too high for a given voltage [3].

2.6.4.9 Gap Distance

The distance between the needle tip and the collector defines the strength of the electric field required and the time available for the solvent to evaporate before it reaches the collector. Even though some studies show otherwise, increasing the gap distance generally reduces the fibre diameter as it increases the time of flight. If the gap is too wide, electrospinning might halt completely, while the converse might lead to wet fibres being deposited on to the collector producing a network of fused nanofibres [3].

2.7 CHARACTERISATION OF NANOFIBRES

2.7.1 INTRODUCTION

Various characterisation techniques are available to measure the biocompatibility, porosity, surface area available for attachment and mechanical properties. The fibrous scaffold should retain its structural integrity and maintain the desired shape before the new tissue is completely regenerated. This section will therefore focus on the various techniques available to measure the mechanical properties of fibrous scaffolds and individual fibres, since various studies have shown the importance of scaffold stiffness on cellular function at the nanoscale size.

2.7.2 MECHANICAL PROPERTIES OF SCAFFOLDS

The techniques used to measure the mechanical properties of fibrous scaffolds have mostly been adapted from the textile industry. The most widely used and straight forward technique involves cutting scaffolds of randomly aligned fibres into rectangular or typical dumbbell shaped test samples and tested using a tensile test machine to obtain the tensile properties.

The main challenge in this technique is the handling of fragile fibre mats during sample preparation. To solve this problem, an alternative procedure to handle nanofibre mats was developed by *Huang et al*. and has considerable merit in this regard. First, a paper is cut into a rectangular frame shape as seen in Figure 2.8 and double sided tape is glued onto the top and bottom strips. This frame is then gently placed onto the fibrous mat with the adhesive surface facing the fibres. After the aluminium foil is carefully peeled off from the fibrous mat, single sided tape is placed on the top and bottom strips to secure the fibres into place. The frame is then cut into strips of the same width and the tensile tests can be performed [26].

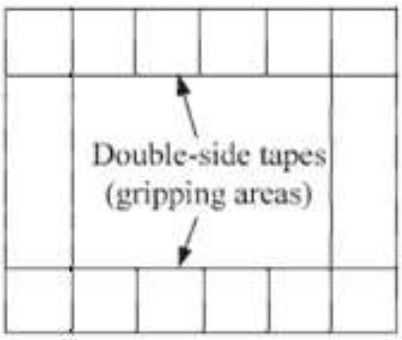

Figure 2.8 - Sample Preparation

2.7.3 SINGLE FIBRE CHARACTERISATION

Despite its various challenges, characterisation of individual fibres is critical as invariably, the mechanical properties of a fibrous scaffold are governed by the mechanical properties of the individual nanofibres. The main challenges associated with characterisation of fibres include manipulation, suitable modes of observation, sourcing accurate force transducers and the preparation of samples with single nanofibre strands [23]. To address these issues, the following 3 characterisation techniques have been compiled to obtain properties such as the elastic modulus, stress and strain curves for individual fibres.

2.7.3.1 Tensile test of single nanofibre

A technique similar to that used for characterisation of complete scaffolds can be used. A small number of fibres are spun onto a rectangular frame and individual fibres are then partitioned with additional strips of paper as shown in Figure 2.9. These partitions are then cut out, creating frames with single fibres ready for tensile testing. Using a microscope, the diameter of the individual fibre is determined along with the alignment of the fibre to the frame. The frame is then mounted onto a nano tensile tester, the vertical strips of the frame cut and the fibre is then stretched to failure at a slow strain rate [27].

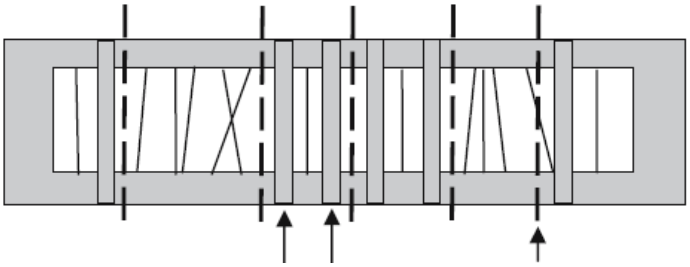

Figure 2.9 - Single fibre partitions **[27]**

2.7.3.2 Nanoindentation

Nanoindentation is probably the most straight forward technique used for nanomechanical characterisation of individual fibres as no complicated sample preparation is required. The fibres are simply deposited onto a hard, flat substrate with sufficient adhesion and nanoindentation is performed using a nanoindenter or an AFM tip to obtain the elastic modulus [28].

This technique has a considerable number of disadvantages associated with it. The surface of the fibre has an associated curvature unlike conventional nanoindentation studies that have a flat surface and this has to be taken into consideration when using Hertz theory of elastic contact. When using an AFM, the tip cannot be perpendicular to the surface, causing slip and friction between the AFM tip and the sample surface during indentation. The AFM tip shape and the cantilever spring constant are two factors that are used in the calculation of the elastic modulus. Unfortunately, these often vary from the nominal values specified by the manufacturer, leading to an error in the calculation [27]. Another factor affecting nanoindentation is the adhesion due to the effect of water condensation between the nanofibre and the AFM tip brought around by capillary action. Since the force applied is in nano newton, this adhesion force becomes significant in a high-humidity atmosphere. Nanoindentation is therefore mainly used on very short nanofibres where the other two methods of characterisation cannot be performed [28].

2.7.3.3 Oliver-Pharr

The Oliver-Pharr method was introduced in 1992 and is used to measure the hardness and elastic modulus of a material by applying an indentation load and measuring the displacement without the need of imaging the impression made by the indenter. This method is used in conjunction with sensitive equipment making it the preferred method when characterising thin films on the micro- and nano-meter scale. *Figure 2.10* shows a typical loading and unloading curve obtained from a single indentation. The important parameters obtained from this curve are the maximum load, maximum displacement, the elastic unloading stiffness *dP/dH* and the final depth after the indenter is fully unloaded [29].

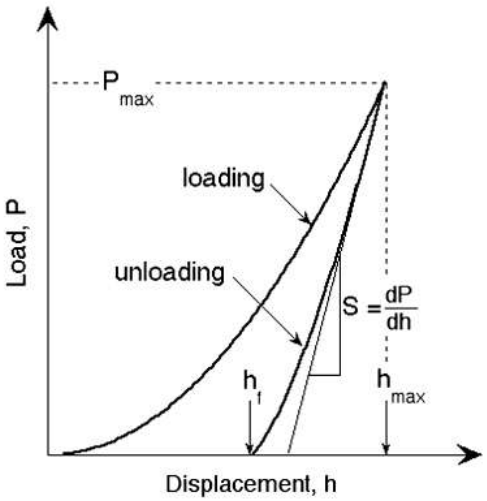

Figure 2.10 - Loading and unloading curve for indentation [29]

Knowing the geometrical properties of the indenter, the contact area can be calculated while assuming that the material deforms under the tip and does not pile up as shown in Figure 2.11. When pile up occurs, the contact area is increased significantly and the calculated value for Young's modulus is artificially increased [30]. A value for Young's modulus can then be calculated using:

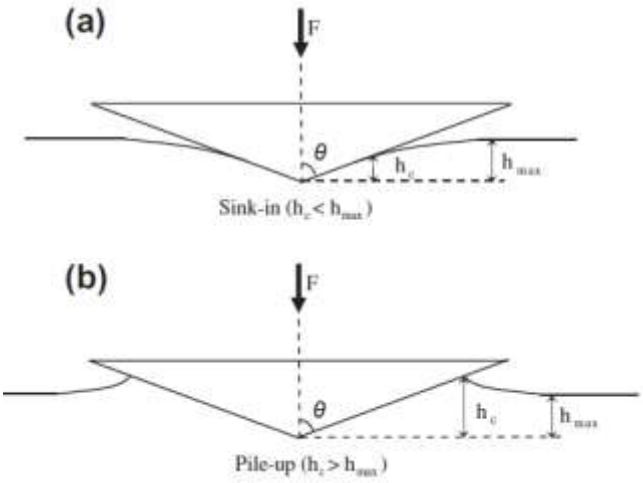

Figure 2.11 - The two modes of indentation: sink-in vs pile-up [30]

$$\frac{dP}{dH} = \beta \frac{2}{\sqrt{\pi}} E_{eff} \sqrt{A} \qquad \text{Eqn 2.1}$$

Where dP/dH is the elastic unloading stiffness

β is a dimensionless correction factor

E_{eff} is the effective elastic modulus

A is the contact area

E_{eff} is used as elastic displacements are assumed to occur both in the specimen and the indenter. This is accounted for using:

$$\frac{1}{E_{eff}} = \frac{1-v^2}{E} + \frac{1-v_i^2}{E_i} \qquad \text{Eqn 2.2}$$

Where v is the Poisson's ratio of the specimen

E is the Young's modulus of the specimen

v_i is the Poisson's ratio of the indenter

E_i is the Young's Modulus of the indenter

2.7.3.4 Three-point bend test

Three-point bending of individual nanofibres is another widely used technique due to its relative ease of preparation and repeatability. Nanofibres are deposited onto substrates with holes or trenches and an AFM tip is used to apply a small force midway along the length of a suspended nanofibre as seen in Figure 2.12. A force plot with the loading and unloading curves is obtained from the AFM and a simple calculation is used to derive the fibre's elastic modulus. Apart from this, all dimension required for this calculation can be acquired from the AFM image.

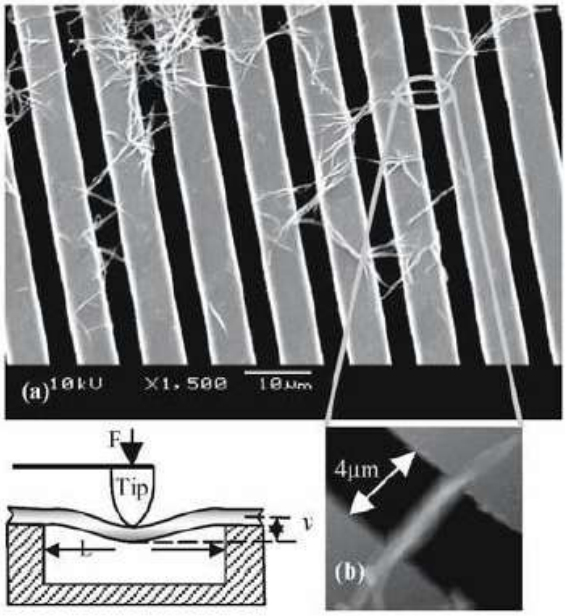

Figure 2.12 - Three-point bending **[27]**

The theoretical formula for three-point bending of a beam with two fixed ends is as follows:

$$E = \frac{F\,L^3}{192\,d\,I} \qquad \text{Eqn 2.3}$$

Where: E – Young's modulus

F – Force applied at midpoint

L – Suspended length of the fibre

d – Deflection of the wire at midpoint

I – Cross-sectional moment of area

($I = \frac{\pi r^4}{4}$ for a circle with radius *r*)

This equation is based on four major assumptions:

1) The two ends are rigidly fixed to the substrate.
2) The suspended length of the fibre is larger than the fibre diameter.
3) The weight of the fibre is negligible.
4) The vertical deflection of the fibre is very small.

A simply supported wire without any constrains at the two ends is modelled by:

$$E = \frac{F\,L^3}{48\,d\,I} \qquad \text{Eqn 2.4}$$

This shows a four times higher Young's modulus than the previous model. However, a completely constrain-free fibre is difficult to obtain due to the high adhesive forces between the fibre and the substrate [31]. Another concern is that the force applied to the fibre has to be small enough to reduce possibility of indentation being made into the nanofibre and to keep vertical deflection of the fibre as low as possible.

Various substrate surfaces have been used as a basis for this three point bend test. The two core properties for the substrate used are that it must be stiffer than the fibres to avoid buckling of the substrate itself and that substrate must not react with the nanofibres to avoid erroneous data.

2.7.4 ATOMIC FORCE MICROSCOPY

2.7.4.1 Introduction

The Atomic Force Microscope was developed in 1985 by *Binning, Quate* and *Gerber* and was made commercially available in 1989. The main advantage of the AFM is that it can image almost all types of surfaces including polymers, composites and biological samples unlike its predecessor, the scanning tunnelling microscope, which could only image conducting or semiconducting surfaces. Samples can also be imaged in air at standard temperature and pressure or while submerged in a liquid, unlike electron microscopes which require a partial vacuum [32].

2.7.4.2 Working Principles

These microscopes collect images of a sample surface by moving a probe over the surface in a raster manner. As the sample moves, the probe records the height change in the surface and an image of the surface is slowly built up [33].

Atomic force microscopes use a Si or Si_3N_4 tip with a diameter of a few 10s of nm mounted on the end of a silicon cantilever spring [34]. An increase in surface height causes a change in the force applied on the cantilever which changes the angle of the cantilever; this in turn moves the reflected beam over the photodiode. The feedback loop tries to maintain a constant force on the tip and reacts by adjusting the height of the sample. The operator can adjust the feedback controls in order to minimise the deflection of the tip and to increase the accuracy of the obtained image. This data is then used by the computer software to build up a 3-dimensional image [35].

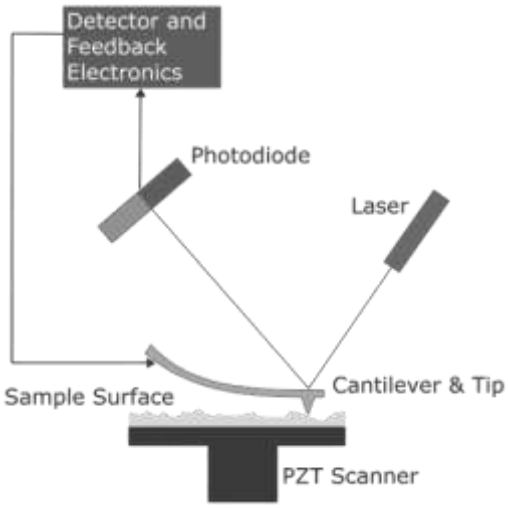

Figure 2.13 - AFM setup

2.7.4.3 Imaging Methods

Contact Mode

Contact mode is the basic mode of operation in atomic force microscopy. As explained in the previous section, the tip is maintained in constant contact with the surface and a feedback loop is used to maintain a constant force on the cantilever by adjusting the height of the sample [36]. The spring constant of the cantilever has to be less than the stiffness of the surface to allow the cantilever to bend and not impinge into the surface. The nano newton forces applied on the surface can sometimes be enough to alter the sample surface by damaging or deforming soft samples that come into contact with the cantilever [33].

Tapping Mode

In this mode, the cantilever is oscillated at high frequency and is in intermittent contact with the surface. The feedback mechanism works by maintaining a constant oscillation amplitude and hence a constant tip-sample height. This method is useful when imaging soft biological samples or samples that are loosely held on the surface as lateral forces, such as drag, are practically eliminated. As the cantilever has to oscillate at high frequency, slower scan speeds are needed and imaging in liquids is more challenging [35].

All samples, unless in a controlled ultra-high vacuum chamber, have a liquid layer adsorbed onto the surface. This layer is often exploited by atomic force microscopes to image in a non-contact mode. Here the tip oscillates over the adsorbed fluid layer and the feedback loop monitors changes in the amplitude due to the attractive Van der Waals forces that the surface has on the tip [33].

2.7.4.4 AFM Artefacts

All measurement instruments used in scientific applications generate results that may contain artefacts caused by an undesired change in the data obtained caused by one of the many stages of data collection. Since atomic force microscopy uses a complex setup that involves both mechanical and electronic components, the user must understand these artefacts so as not to misinterpret the data obtained [33].

One of the main limitations in atomic force microscopy is the physical probe used. As the probe is not perfectly sharp, the AFM image does not reflect the true sample surface but a convolution of the probe geometry and the shape of the features being imaged. Two common artefacts created by this problem are the following:

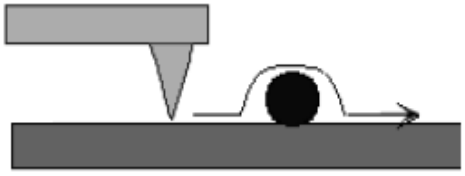

Figure 2.14 – Tip convolution **[37]**

When the AFM tip moves over a fibre or sphere attached to the surface, the data obtained would show broadening of the features in the final image [37].

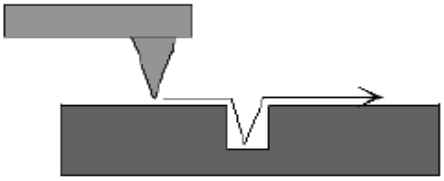

Figure 2.15 – Tip convolution **[37]**

On the other hand, when the probe moves into a hole, the width of the probe does not allow it to accurately scan the feature, resulting in a convoluted and narrower image as seen in Figure 2.15.

These artefacts only arise when the feature is very small and can be reduced by using a probe that is smaller than the features being measured. Typical probes have a tip diameter of 10nm but probes with tips that are made of carbon nanotubes or tungsten spikes with tips of 2nm in diameter are becoming commercially available. However, such probes are very fragile and are still too expensive for the purpose of standard image analysis [36].

Cantilever tips are very fragile and can easily be broken, chipped or worn down by normal use. A tip whose original shape has been changed will affect the final image obtained by the AFM [37].

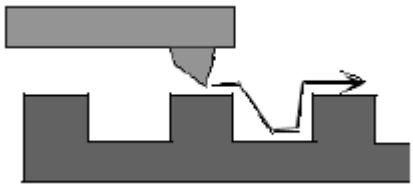

Figure 2.16 - Fractured tip convolution **[37]**

Vibrations

Any vibrations in the vicinity of the AFM can cause the probe in the microscope to vibrate and cause artefacts. The floors in a building often vibrate at frequencies below 5Hz over a distance of several microns. This can cause artefacts that are mostly noticeable when imaging flat surfaces. Acoustic vibrations have higher frequencies and can also cause artefacts while obtaining an image. These artefacts can be reduced by isolating the microscope from the ground and performing scans in sound proof chambers [37].

Other Common Artefacts

An inherent artefact in atomic force microscopes is the probe-sample angle. If the tip is not perpendicular to the surface, an artefact will be visible on the left edge of the feature. The probe would have to be realigned to obtain better image.

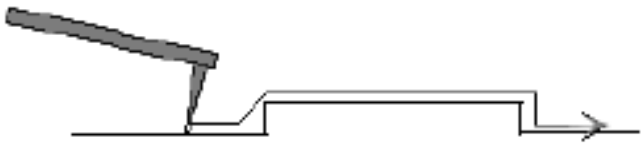

Figure 2.17 – Tip artefact

If the sample is too soft or adhesive, which is common in biological imaging, an artefact due to an altered number of probe-sample contact points occurs. Electrostatic charge can also build up on non-conductive surfaces causing long range forces on the cantilever and thus altering the image obtained. This is solved by grounding both conductive and non-conductive samples to eliminate the build-up of charge [34].

The feedback parameters are another common source of artefacts. A "*flying tip artefact*" refers to artefacts caused by tip not adequately following the sample surface. To solve this problem, the operator can increase the feedback gain and reduce the set point. Conversely, if the gain is too high, noise patterns show up when there are sudden changes in the sample height. Optimising these two parameters and reducing scan speeds often eliminates these problems and a better image can be obtained [38].

2.8 PREVIOUS STUDIES

Various studies have already been performed investigating the mechanical properties of nanofibres using various techniques. The majority of these studies have been performed on metallic or ceramic materials such as Ag, SiO2 and TiO2 [39] [40] [41]as these nanofibres have been used in creating high strength composites, low density materials and in various other applications. Some experiments have also been performed on polymeric nanofibres. Papers have been published on the investigation of elastic modulus for polypyrol, PLLA, PAMS and PVA [42] [43] [44] [45]. A review of these papers provides an insight of what problems we expected to encounter when our experiments on polyurethane were performed.

It was noted that the preferred method of characterisation by most of the studies performed was three-point bending using atomic force microscopy for its numerous advantages that have been listed in the previous section. Previous researchers have however made a number of observations that could have an impact on the results obtained. Obtaining dimensional measurements such as the fibre diameter form the AFM was problematic due to the artefacts mentioned earlier. While some papers chose to either measure the width or the height of the fibre, *Sun et al.* [46] compensated for this inevitable artefact by taking both measurements and calculating a reduced diameter using:

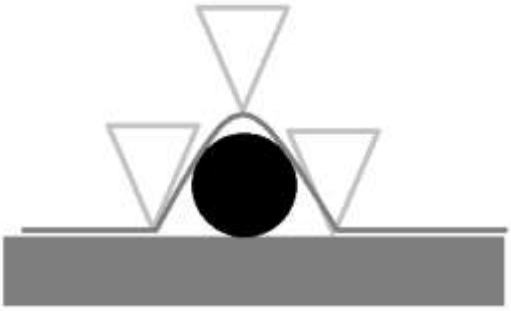

$$D = \sqrt{D_1 D_2}$$

Where D is the reduced diameter

D_1 is the measured height

D_2 is the measured width

Choosing any one of the measurable dimensions added an error into the results as the fibre diameter would not be accurately represented. Using this formula yielded more accurate results as it was a better approximation of the actual fibre diameter [46].

Determining the clamping conditions of the suspended fibres was another challenge that was highlighted in most published papers. In all the papers reviewed, calculations were made assuming that the fibres were fixed to the substrate. *Cuenot et al.* used a procedure in which the resonant frequency of the AFM cantilever tip while in contact with the fibre at different lengths was analysed. This was used as further confirmation that the fibres were indeed firmly clamped onto the substrate and the forces applied were not sufficient to detach them during testing [42].

To ensure that shear forces did not have a significant impact on the calculated values for the elastic moduli, the suspended length had to be significantly higher than the diameter of the fibre being tested. While most papers quoted that this ratio should be less than 10 [44], other papers suggested a more conservative ratio of 16 [42]. Both ratios have been backed up by previous literature from books published on the subject.

The major observation made by most papers published on electrospun polymers was that elastic modulus varied with a change in fibre diameter. Studies on polypyrol, PAMPS, PCL and PVA have all shown an increase in elastic moduli with a decrease in fibre diameter. This increase in modulus is substantial and a 5 fold increase was observed in most studies over a range of fibre diameters. In their study of PVA nanofibres, *Fu et al.* [45] report an increase of fibre modulus from 50GPa for fibre diameters of 160nm to 500GPa for diameters of 20nm. Multiple arguments were made in an attempt to explain this large increase in modulus which approached that of diamond. A recurrent argument made to explain this increase in modulus was a change in the molecular structure of the polymer as the fibres are being electrospun. It was suggested that the orientation of polymer molecules within the nanofibres arises from strong strain forces in polymer jets. This phenomenon was investigated further by *Arinstein et al.* who suggest that a resulting confinement of the supramolecular structure plays a dominant role in the alteration of moduli observed [47]. Another hypothesis that explains this increase in moduli was published by *Cuenot et al.* and refers to the heightened effect that the surface tension has on one-dimensional nano-structures [42].

3 PROJECT OBJECTIVES

Polyurethane has long been one of the few polymers that can be successfully implanted in humans and show no adverse reaction to the recipient. This polymer is therefore a suitable candidate for the scaffolds used in the manufacture of engineered tissues. If this material was to be used in artificial scaffolds, it would be valuable to understand the mechanical properties the material adopted when in the form of nanofibres as this would have an impact on the growth and survival of cells.

The main objective of this project was to analyse the mechanical properties of two grades of biocompatible polyurethane that would be used in building artificial scaffolds in the future. The elastic moduli of these materials were investigated, both in the macro and the nano-scale, in an attempt to compare the material's moduli on two different length scales. Nanofibres had to be created to mimic the form adopted when the material is being used as a scaffold and a technique had to be chosen to test the mechanical properties of these nanofibres. Electrospinning was chosen as the preferred method for nanofibre synthesis due to its relative ease of fabrication of long nanofibres. Electrospinning is also widely used and has an established role in biomedical applications. The method selected for characterisation of the nanofibres created by electrospinning was three-point bending using atomic force microscopy as this technique has been widely proven as being able to produce reliable data in the scale of interest. Polycarbonate membrane filters were used as a substrate material as these provided pores of known diameter, essential for three-point bending.

As these tests were being made on the nano-scale, the experiments faced numerous challenges that would be insignificant on the macro-scale. The reliability of the experiments performed therefore had to be confirmed by further testing and analysis of the data. The outcome of the mechanical analysis was then discussed with reference to their impact on the cell-scaffold interaction.

4 MATERIALS AND METHODS

A range of equipment made available by the Department of Bioengineering at the University of Strathclyde was utilised to successfully complete this thesis.

4.1 ELECTROSPINNING RIG

An electrospinning rig was made available by the Department of Bioengineering. The system used two Alpha III (Brandenburg, Dudley, UK) high voltage power supplies that could produce up to 25,000V each, directed towards the collector and the electric field. It also used an infusion pump (PHD 2000, Harvard Apparatus, Kent, UK) to slowly move the polymer down a needle at a fixed rate that could be set by the user. The system could also control the position of the needle for a uniform coating and the rotational speed of the target to control fibre alignment. As the system uses high voltages, a number of safety components were built into the system. These include a protective cage, emergency stop buttons and various sensors that ensure the safety of the user.

As electrospinning uses solvents that can be toxic, the rig was built to slide into a fume cupboard and could not be turned on if the fume cupboard's shutter was left open. When the rig was not being used, it could be unplugged and moved away from the fume cupboard to allow space for other experiments. With all these systems in place, the electrospinning rig was very versatile while being safe to operate.

Figure 4.1 shows the electrospinning rig mounted into a fume cupboard without the protective cage to give a better view of the components. Below is a list of the items that can be seen in the picture.

1) Needle
2) Target
3) Infusion pump
4) Syringe
5) Emergency stop button
6) Security key
7) Power supplies

Figure 4.1 - Electrospinning rig

4.2 SCANNING ELECTRON MICROSCOPE

As the process of electrospinning has a significant number of variables, producing fibres of a required diameter without bead defects can prove challenging. To find the parameters required and create a layer of nanofibres with minimal bead defects, a Hitachi TM1000 SEM was used. The main advantage of this system is its ease of use as no sample preparation is required. This meant that samples could be imaged directly from the electrospinning rig, thus facilitating the acquisition of correct electrospinning parameters. This SEM had an accelerating voltage fixed at 15kV and allowed a magnification of up to 10,000X. It also allowed for a 70mm diameter sample to be scanned and has a movement range of 15 x 18mm.

Figure 4.2 - Hitachi TM-1000 SEM

4.3 POLYMERS

Medical grade polyurethane *Z1A1* and *Z3A1* (*Biomer Technology Ltd., Runcorn, UK*) were provided for testing. The polymers being tested were a class of chemically inert, medical grade polyether-urethanes. The company states that these polymers are biocompatible and show low temperature flexibility, a wide dynamic range of hardness and can be processed in a variety in manufacturing methods.

The company also lists some mechanical properties for both polymers including the tensile modulus between 50 and 300% elongation, the ultimate elongation and the ultimate tensile strength. These values were however irrelevant, as the forces being applied on the nanofibres would only elongate the fibres by up to 1% of the original length.

Tensile Modulus (MPa)	Z1A1	Z3A1
50% elongation	3.1	10.6
100% elongation	3.9	13
200% elongation	5.8	20.3
300% elongation	10.9	32.7
Ultimate Tensile Strength (MPa)	39.6	46.7
Ultimate Elongation %	555	410

Figure 4.3 - Information provided by Biomer Technology Ltd.

For electrospinning, solutions of Z1A1 and Z3A1 were produced 13.1 and 14.7 %w/w respectively in dimethylacetamide (DMAC) by mixing on a roller for 48 hours at room temperature and atmospheric pressure. The material safety data sheets of the compounds mentioned can be found in the appendix.

4.4 SUBSTRATE

The substrate used had to be inert and display no adverse reactions to the solvent system used during electrospinning. To perform three-point bending on the nanofibres, another requirement from the substrate was for it to contain uniform trenches, or holes, of a known diameter.

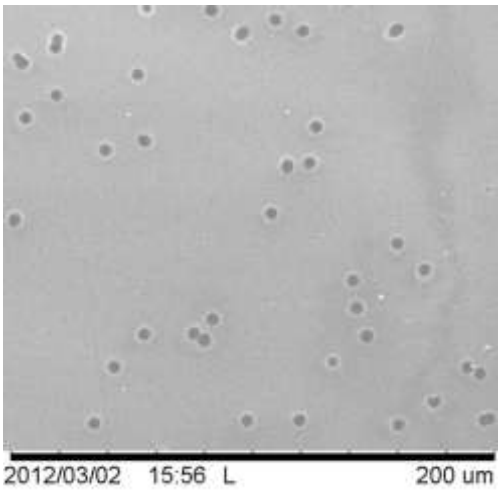

Figure 4.4 - Polycarbonate substrate imaged under SEM

Poretics hydrophilic polycarbonate filter membranes were selected as they fit the criteria required. Two sets of 100 filters were acquired for the whole experiment. The nominal pore diameter indicated by the supplier was set at 2μm for one set and 5μm for the other. This added some versatility for our experiments as the range of nanofibre diameters produced was not yet known.

To confirm that the polycarbonate membranes did not react with DMAC, one of the filters that would be used in the experiments was immersed in a DMAC solution for 5 hours. An image of the membrane was obtained using the SEM before and after immersion in solution to visually confirm that no changes had occurred.

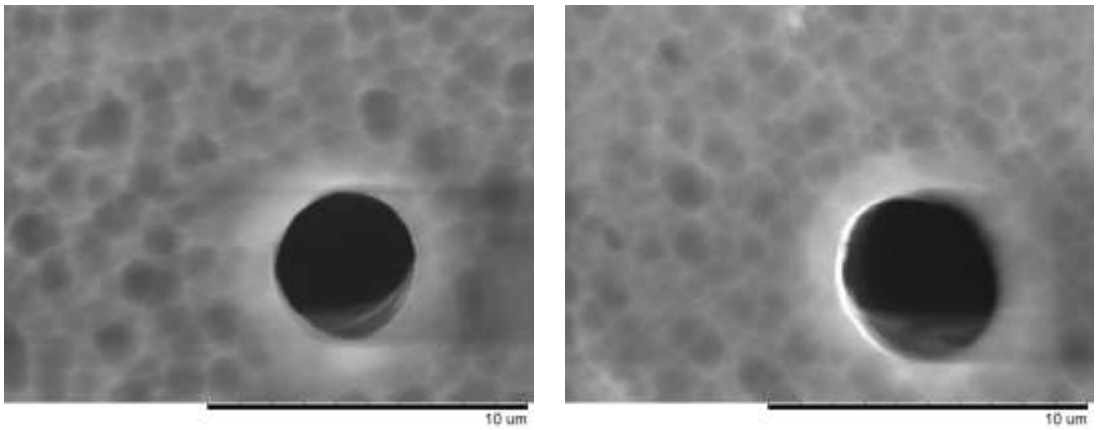

Figure 4.5 - SEM image of polycarbonate membranes before (left) and after (right) immersion in DMAC for 5 hours.

4.5 SAMPLE PREPARATION FOR AFM TESTING

4.5.1 METHODOLOGY

Both polymer grades Z1A1 and Z3A1 have been successfully electrospun in the Department of Bioengineering. Guidance was provided for a general idea of the parameters that had to be used to successfully create nanofibres. The collector material that was previously used was aluminium foil, which undoubtedly provides a different conduction coefficient to polycarbonate. As electrospinning is based on the flow of polymer down a charged electric field, changing the collector material to polycarbonate resulted into a significant change of process parameters. This step could not be avoided as nanofibres had to be spun directly onto the polycarbonate

membranes in order to ensure sufficient adhesion, thus preventing fibres from slipping while three-point bending was being performed.

The polymer concentrations and solvent system used were the only two parameters that were kept constant at the suggested values. Attempting to change these variables would have proven to be very challenging as they would have completely altered the parameters provided. The set of parameters that could be altered was still extensive; the mandrel voltage, electric field voltage, tip-collector distance, polymer flow rate and volume had to be optimised to create a sparse layer of nanofibres ideally free of bead defects. Slight variation of any of these parameters resulted in a significant change in bead formation. Since the electrospinning parameter optimisation experiments extended over several days, environmental factors were another set of variables that had to be taken into consideration. Even though a set of parameters could have produced nanofibres with close to adequate bead defects on one day, these parameters were not guaranteed to yield the same results the following day. Although these effects are usually observed when producing three-dimensional nanofibre meshes, the variability was amplified due to the fact that only a thin, sparse layer of nanofibres had to be created on the substrate. This meant that the instability created by the polycarbonate substrate was constant and was not *dampened* by the presence of sub-layers of nanofibres.

A procedure was developed where a set of parameters was used, the resulting nanofibres imaged on the SEM and compared to the results obtained by a previous set of parameters. One variable was then changed and another sample was produced. This process was repeated iteratively until a set of parameters that produced the desired results was found. When the right combination of parameters was found, samples had to be produced as quickly as possible to avoid variation brought around by a sudden change in atmospheric conditions.

Each filter provided around $2cm^2$ of area for the three-point bend test to be performed and the density of pores on the membrane was observed to be around 10^5 pores per cm^2. As this provided ample space for tests to be carried out and to avoid inter-sample variation, only two samples with identical parameters were produced.

Each sample was then split into four and stored separately to ensure that damage to one sample would not result in a complete loss of specimens.

4.5.2 RESULTS

The results obtained varied between both polymers. Z1A1 proved easier to spin when compared to Z3A1 but the latter produced thinner fibres that were desired for the three-point bend test.

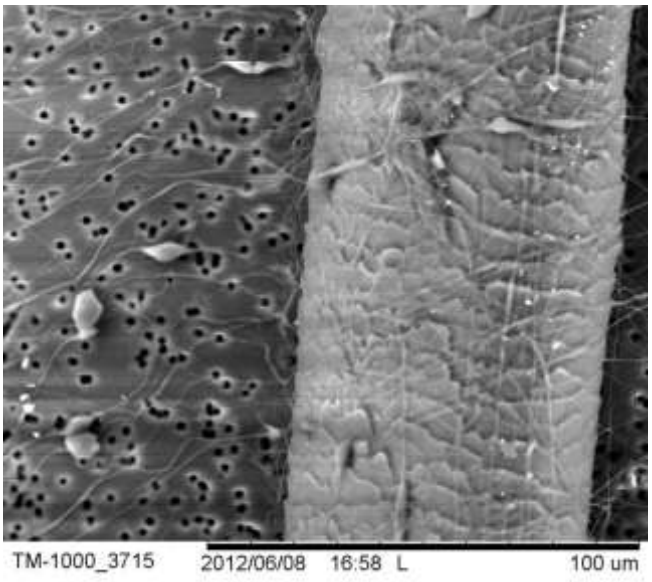

Figure 4.6 - Scale of nanofibres compared to a human hair and 2µm pores

Figure 4.6 gives an idea of the scale of the nanofibres being produced. A human hair, with a diameter of about 70µm is compared to Z1A1 nanofibres with an average diameter on 0.5µm on a polycarbonate membrane with pores of 2µm.

4.5.2.1 Z1A1

When the suggested parameters were used to spin Z1A1, unstable electrospraying was produced. This generated beads of uneven sizes sprayed over the membrane as seen in Figure 4.7 rather than creating long, thin nanofibres. After a slight modification of the parameters, fibres could be produced with low bead defects. The main challenge presented by Z1A1 was to find the right volume of polymer that would create a thin coating of nanofibres without excessive overlap. Too few fibres would reduce the chance of finding fibres on pores suitable for three-point bending, while excessive fibres would create overlap making them unsuitable for our experiment.

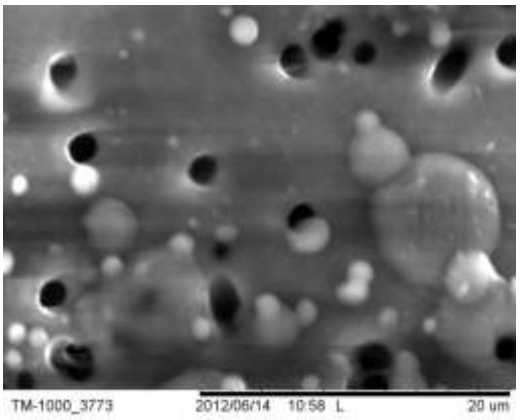

Figure 4.7 - Z1A1 Showing electrospraying

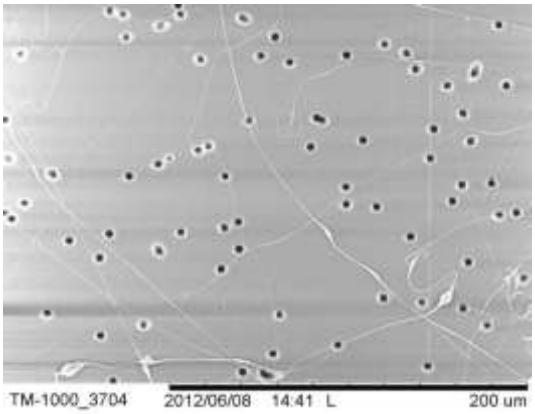

Figure 4.8 - Z1A1 with minimal coverage

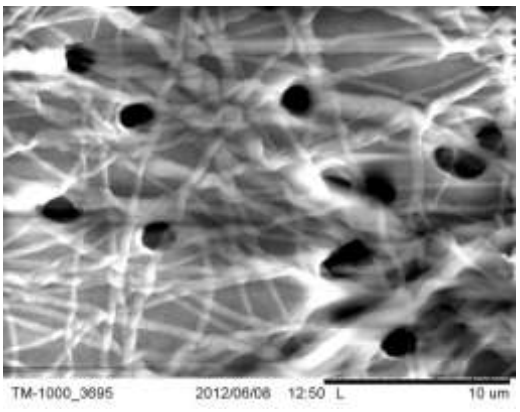

Figure 4.9 - Z1A1 showing excessive fibres

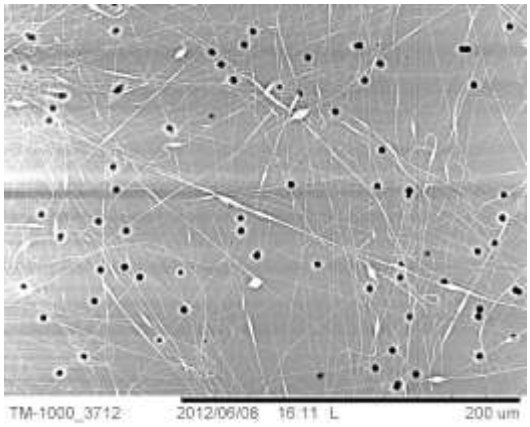

Figure 4.10 - Z1A1 Selected Sample

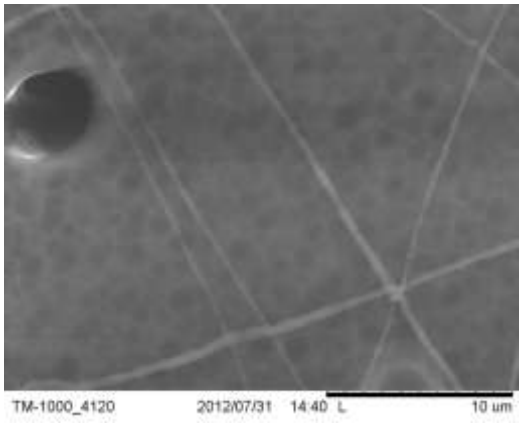

Figure 4.11 - Z1A1 Selected Sample

The final samples selected for testing showed minimal bead defects with adequate fibre density. The parameters used were: mandrel voltage - 23kV, electric field voltage - 18kV, distance to target – 15cm, flow rate – 0.2ml/hour, volume – 0.003ml with an atmospheric temperature of 22.6^{o}C and humidity at 32%.

4.5.2.2 Z3A1

Z3A1 was more arduous to spin and satisfactory results were only produced after 60 hours of trial and error. Electrospraying was not observed and fibres were always produced but bead defects were excessive and minimising them proved to be challenging. As the AFM cantilever tip would be in contact with the surface while scanning, the presence of beads could easily damage it by causing high deflections that could not be handled by the cantilever. Beads would also reduce the probability of finding fibres on pores that would be suitable for three-point bending.

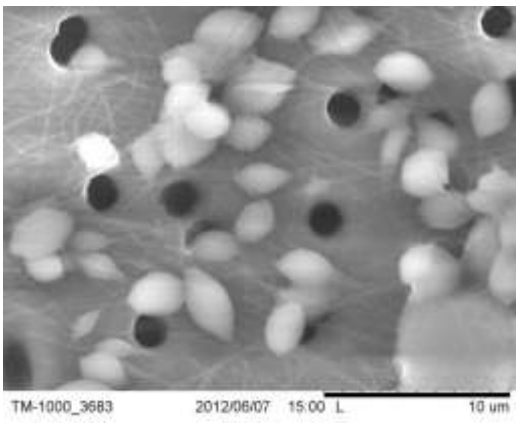

Figure 4.12 - Z3A1 with high bead defects

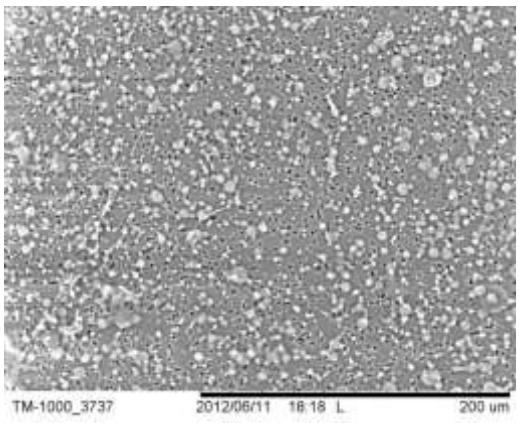

Figure 4.13 - Z3A1 with high bead defects

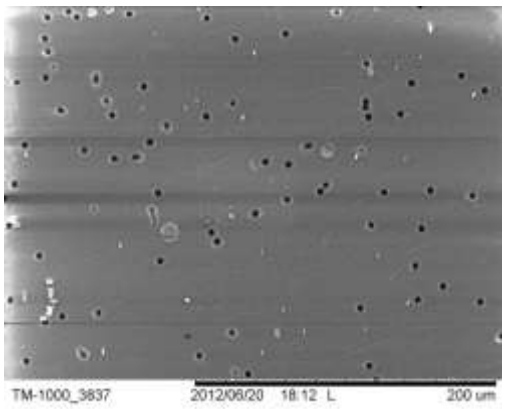

Figure 4.14 – Z3A1 with minimal bead defects

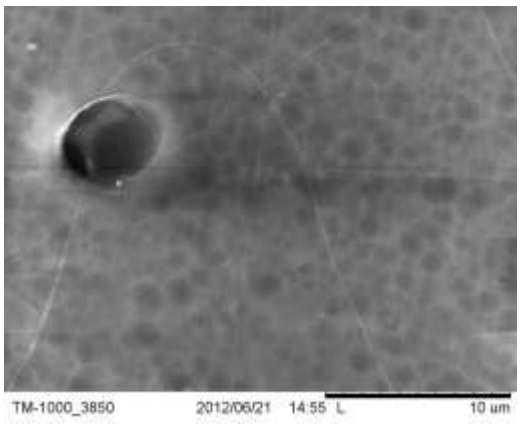

Figure 4.15 - Selected sample

The selected samples had minimal bead defects and adequate fibre density. The fibres obtained also had a smaller diameters then Z1A1 with an average diameter of 0.3µm. The parameters used were: mandrel voltage - 15kV, electric field voltage - 18kV, distance to target – 15cm, flow rate – 0.06ml/hour, volume – 0.004ml with an atmospheric temperature of 23.7^{o}C and humidity at 29%

4.5.3 DISCUSSION

The fibres obtained for testing were generally suitable for mechanical testing. However some observations were made that contributed to the limiting factors of this experiment.

A wide variation of fibre diameters was observed over the whole sample as seen in Figure 4.16. This variation was accounted for when elastic modulus calculations were made. A variation in diameter was sometimes even seen on the same fibre. As the modulus varies with the fourth power of fibre diameter, an accurate system to measure this variable had to be produced. Abrupt changes in fibre diameter over the pores would therefore lead to a significant change in the accuracy of the calculated modulus. Even though the supplier declares the pore diameter to be fixed at 5µm, a variation in this parameter could also be observed from the SEM images.

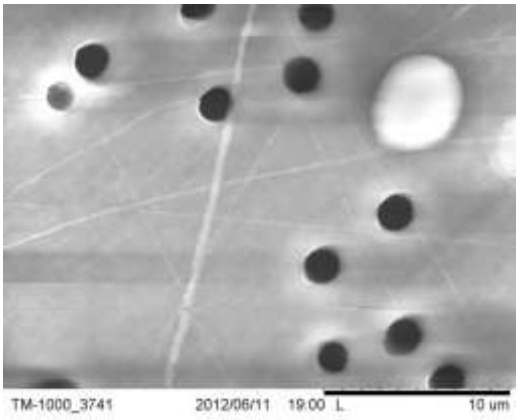

Figure 4.16 - Variation in fibre and pore diameter

The fibre diameters observed for Z1A1 were 0.45µm ± 0.15µm, while the diameters observed for Z3A1 were 0.25µm ± 0.1µm. This meant that comparing the two polyurethanes would be challenging as a different range of fibre diameters would have to be tested. To obtain thinner fibres for Z1A1, the polymer concentration would have to be changed and further optimisation of parameters performed. This procedure had to be passed up due to the project's time limitations as well as lack of available previous experience in electrospinning these polymers.

SEM imaging also confirmed that the method of electrospinning successfully created fibres that were suspended over pores. Suspended fibres could be observed for both polymers and it could be confirmed that the fibres did not collapse under their own weight or while handling the samples. The main drawback was that these suspended fibres were relatively rare and finding them on the AFM would be time-consuming as scans are limited to an area of 90µm x 90µm.

Another observation made while visualising samples under the SEM was that the energy provided by the bombarding electrons used to obtain the image was enough to dissolve the fibres that were suspended over a pore. This meant that even though it was important to visualise the samples under the SEM to identify whether the samples are of good quality, exposure to the SEM electron beam had to be minimal so as not to compromise the few fibres that were suspended and available for three-point bending.

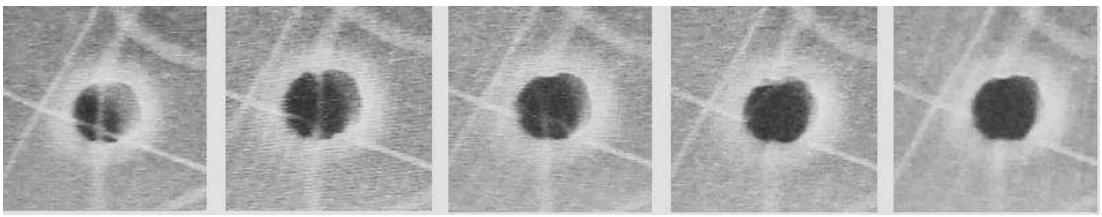

Figure 4.17 - Dissolving fibres in a Z1A1 sample under SEM

A sample from each polymer was securely mounted onto a glass slide whilst while ensuring that it lay flat on the glass surface. Each sample was clearly marked to avoid mistakes as there was no visual difference between samples generated from the two polymers.

4.6 TENSILE TESTER

The bulk properties of the materials used were tested using a *Bose ElectroForce* 3200 Load Frame System. This system is built for testing soft materials with force transducers ranging from a maximum reading of 225N to 22N. A large selection of clamps was available to perform a variety of tests on samples with different requirements. The tests could be performed in dry conditions or submerged in a heated saline bath to mimic the environment required. The software allowed the user to define a series of test conditions from simple force ramps to cyclic loading at 0.00001 - 200Hz over a prolonged period of time. The maximum displacement was set at 12.5mm with the option of adding a Hall effect sensor that would reduce the travel range to 1mm but significantly increase the accuracy of the displacement obtained.

4.6.1 TENSILE TEST ON CAST FILMS

Thin solvent cast films of Z1A1 and Z3A1 were produced by the removal of the solvent at 65^{o}C under a vacuum of 45kPa for 48 hours. The films were then removed from the petri dishes and soaked in deionised water for 24 hours to ensure that any remaining solvent was removed. The *Bose ElectroForce* system was then used to evaluate the tensile modulus of the polymers. A sensitive Hall effect sensor coupled with a 250gram load cell was used to measure small forces created by equally small displacements. Dimensional measurements of the samples being tested were obtained using a micrometre screw gauge and callipers. The data obtained from the *Bose ElectroForce* system was then analysed on *Microsoft Excel*.

4.7 ATOMIC FORCE MICROSCOPE

An Atomic Force Microscope (AFM) was used to obtain detailed images of the sample surface. The AFM was also used to apply and record forces applied to a nanofibre from which its modulus could be calculated. An *Asylum Research MFP-3D Stand Alone* AFM was used as it was readily available at the University of Strathclyde. It is a highly versatile AFM that could be used in a wide selection of modes and an even wider range of applications. Imaging could be done both in contact and in tapping mode, in air or submerged in liquid. In *Force Mode*, the surface of the sample could be tested and the system's powerful computational software could be used to analyse the data obtained.

A Class I laser system was used to accurately monitor any movements of the cantilever for precise measurements of the cantilever position. An inbuilt optical camera could also be used to locate desirable positions for the AFM to scan while giving the option to image both from the top and bottom for opaque samples. It used accurate piezoelectrics to measure exact positions and automatically corrects for hysteresis and creep. The AFM stage was limited to a 90µm x 90µm X-Y scan size with an average deviation of 0.5nm. The Z travel range is limited to 15µm with a lower average deviation of 0.06nm for accurate measurement of forces. The system's inbuilt software provides complete control over the AFM and various additional features that make the system highly versatile and adaptable. To avoid unwanted noise while obtaining measurements, a vibration isolation table was used along with an acoustic isolation enclosure. This system therefore ensures accurate data acquisition with minimal noise for optimum results.

1) AFM head
2) Movement table
3) Light source and camera controls
4) Vibration isolation table
5) Acoustic isolation table

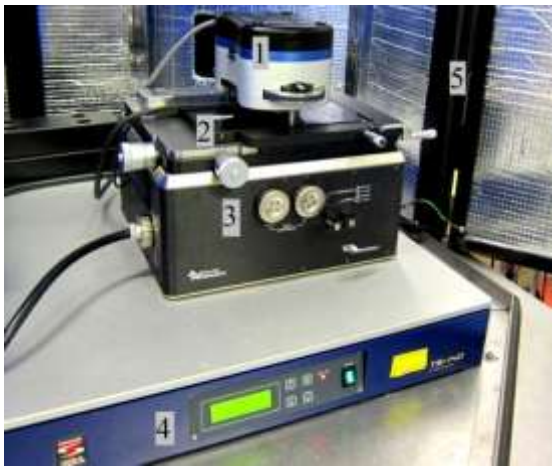

Figure 4.18 - AFM on vibration isolation table inside an acoustic chamber

4.7.1 MECHANICAL TESTING USING AFM

4.7.1.1 Outline

To test the mechanical properties of individual nanofibres, setting up the AFM correctly was crucial to obtain reliable data. A cantilever was carefully mounted onto the AFM head and a tuning was performed to confirm the integrity of the cantilever tip. A thermal tuning was then performed to acquire the real value of stiffness for the specific cantilever. This value varies between two cantilevers from the same batch and was essential for our measurements as a change in cantilever stiffness would completely alter the values of elastic moduli obtained. A procedure instructed by the AFM user manual was then followed to calibrate the force curves obtained from the software.

One of the samples was placed underneath the AFM and the optical microscope was used to find an area that was suitable for scanning. An area of 90 x 90μm was scanned and the image produced was analysed for any fibres that appeared to be suspended on a pore. If no suspended fibre was found, the sample was moved and another large area scan was performed. When a suspended fibre was found, a smaller scan area was selected to zoom in on the fibre and obtain better calculations. A fixed force was then applied at the mid-point of the fibre for calculation of the elastic modulus.

4.7.1.2 Scanning procedure

The fibres chosen for testing had to be suspended over the pore without any obstruction to avoid artificial stiffening. The fibres also had to be suspended as close to the centre of the pore as possible to avoid fibres that might be attached to the pore walls below the visible surface. Furthermore, some pores on the polycarbonate substrate had a substantially smaller diameter then that specified by the supplier, making them unsuitable for testing.

When areas of the substrate were found to have a considerable number of collapsed fibres, scanning was moved to a completely different area of the specimen to avoid obtaining data from areas that might have been previously damaged by SEM imaging. The presence of bead defects on the substrate further complicated data collection as they created significant artefacts that could potentially permanently damage the cantilever tip. Bead defects therefore forced a lower scanning speed of the 90μm scans to extend the usable life of the cantilevers and obtain images with less tip artefacts.

When all these factors were taken into consideration, the average rate of finding a sample suitable for testing was about 1 sample every 1.5 – 2 hours, making the process very cumbersome and time-consuming. A chain of 90μm *quick* scans, each lasting around 5 minutes had to be taken before a potential fibre was seen. This was followed by smaller, more detailed scans lasting about 20 minutes to ensure accurate representation of the actual dimensions. When an adequate image was obtained, mechanical testing and dimensional analysis was performed. The data obtained was consequently tabulated and analysed. The following pages contain a series of images obtained from the AFM and show both 90μm scans and smaller 7μm scans that were used to obtain the mechanical data.

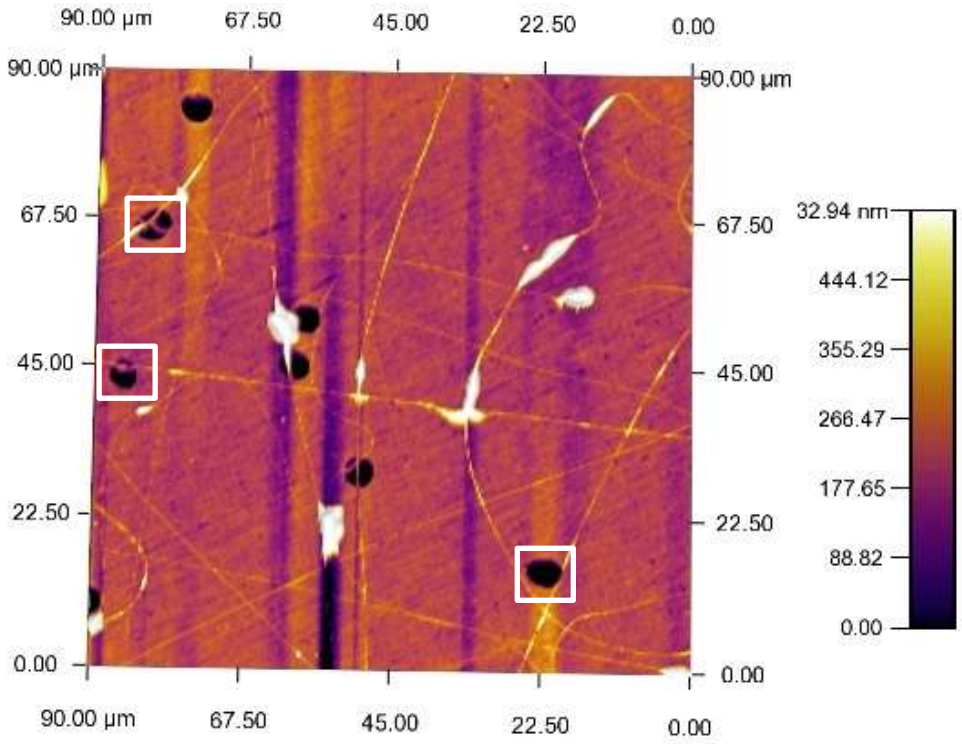

Figure 4.20 Showing a 90µm scan with multiple inadequate fibres over pores

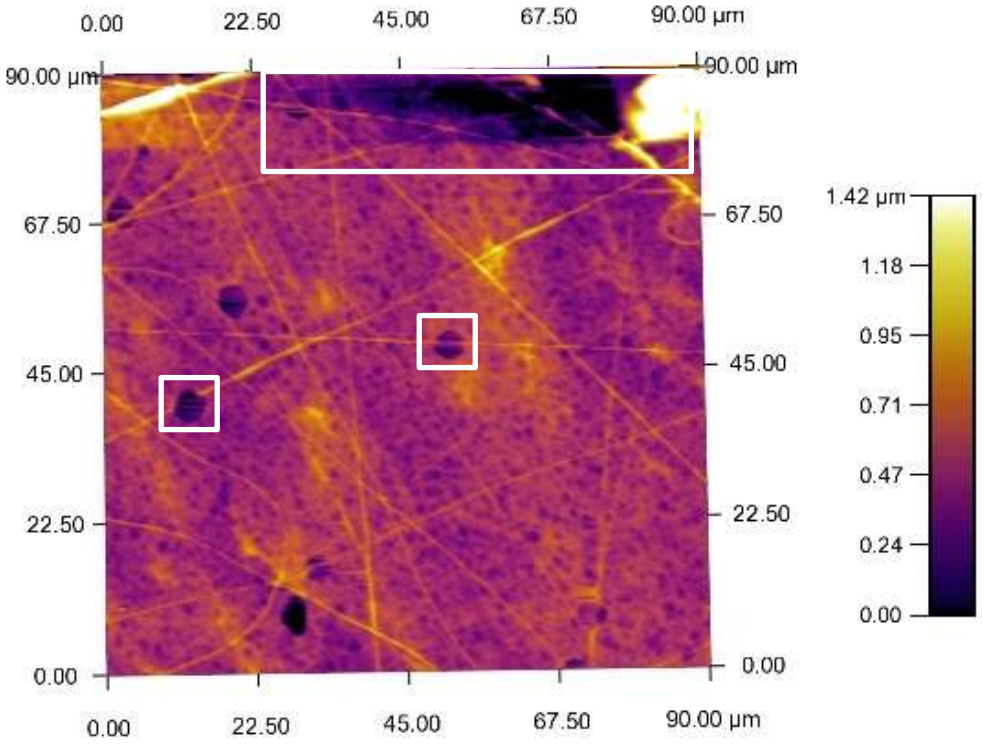

Figure 4.19 - Showing artefact created by beads, a collapsed fibre and a suitable fibre.

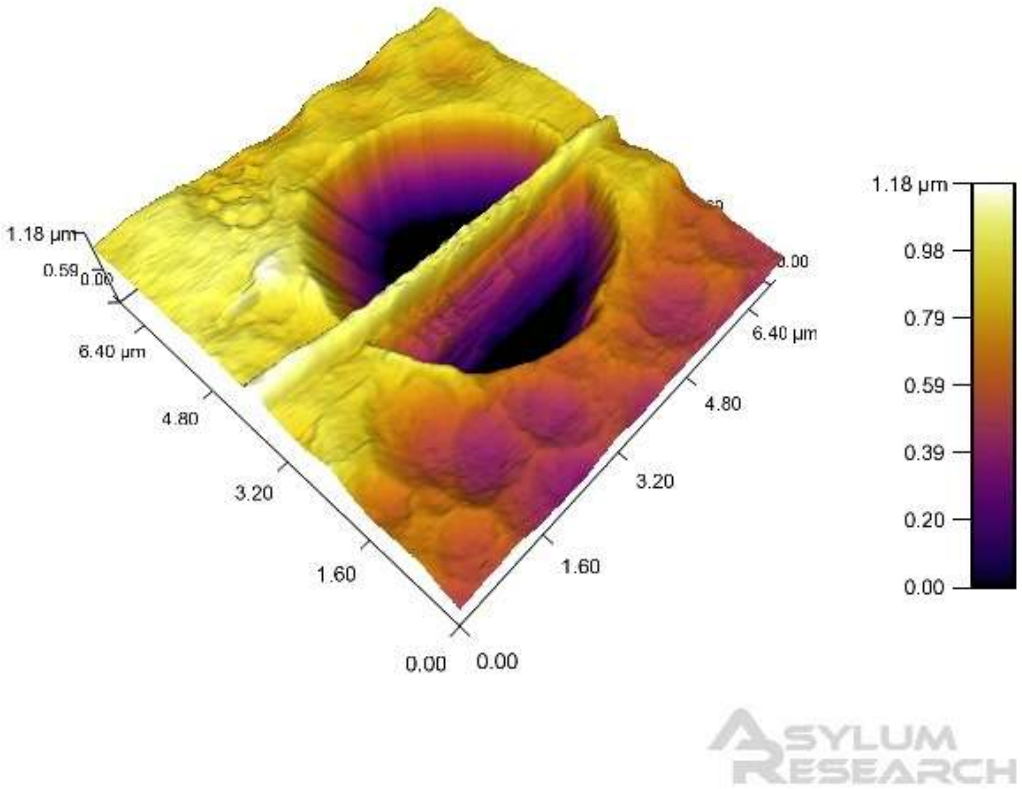

Figure 4.21 - Showing ideal fibre placement on a 5µm pore

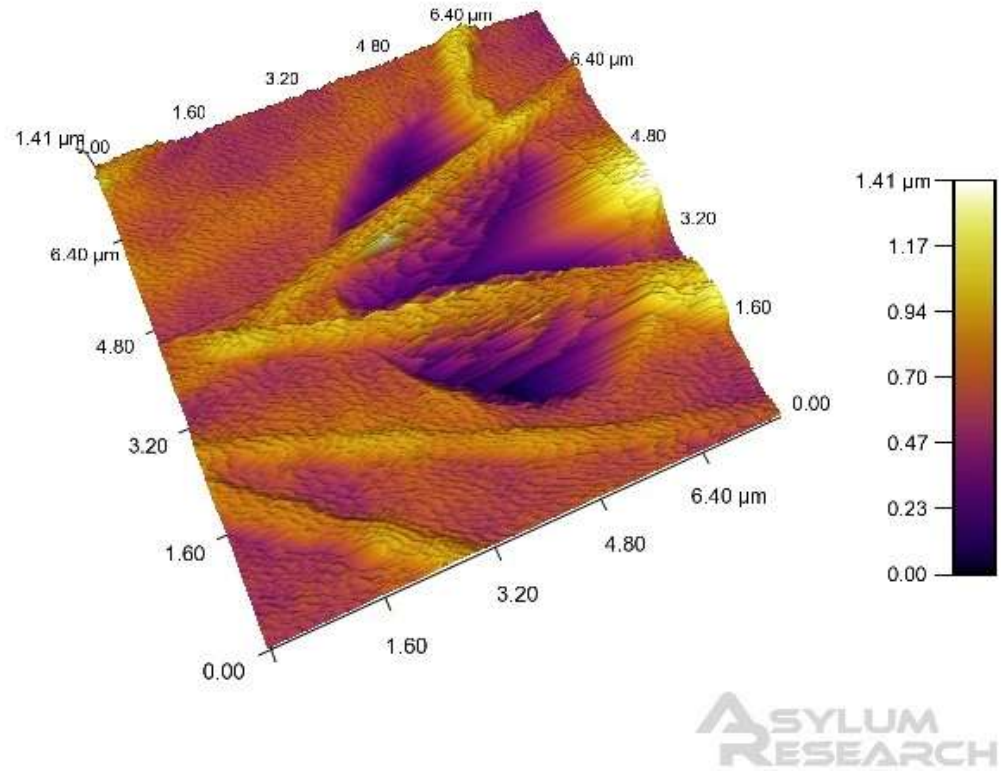

Figure 4.22 - Showing a unique occurrence with 2 suspended fibres but still inadequate for data collection as the pore is only 3µm wide.

4.7.1.3 AFM Artefacts

The Atomic Force Microscope's cantilever selection was a critical part of the experiment since apart from being the only component of the microscope that comes into contact with the sample, the forces being applied and recorded by the system also depended primarily on the cantilever tips used.

AFM tip integrity

The size of a cantilever is about 4mm making it difficult to handle and susceptible to damage as it is being mounted onto the AFM head. This cantilever holds a fragile silicon nitride tip that is about 0.1mm in length. At the end of this tip is another tip of 0.03mm which comes into contact with the surface. This final tip is pyramidal in shape and has an apex radius of about 30nm.

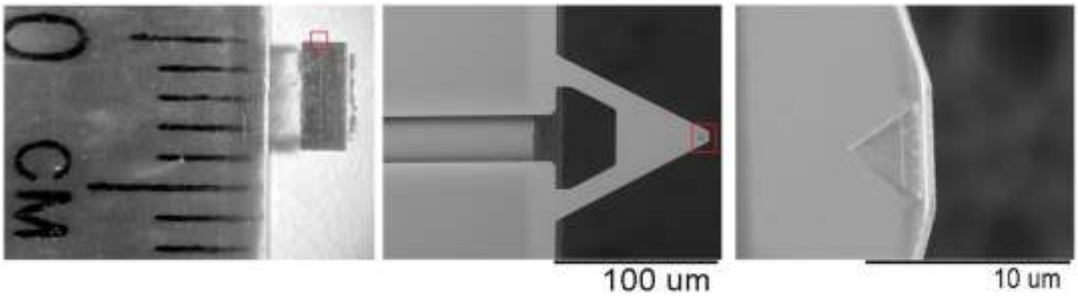

Figure 4.23 - Showing a size comparison of the cantilever tips

A balance had to be found between tip preservation and the scanning parameters such as scan speed. If the scan speed was too high or the set point too low, the tips could have been damaged quicker. Tips that were not damaged by poor parameter selection were also susceptible to damage from wear and tear as they picked up debris from the surface of the sample. The tips were therefore handled with utmost care as replacing them, apart from costing around 30GBP per cantilever, was a delicate and time-consuming process.

The SEM was used to obtain the images presented in Figure 4.24 which show a cantilever tip that was broken after being used for a prolonged period of time. The base of the tip is completely broken off leading to a change in the stiffness of the cantilever. This was detected after performing a thermal analysis of the tip which showed a significant change in the calculated stiffness.

Debris can also be seen scattered on tip. This debris contributes to an elevated amount of adhesion while scanning and while performing the tests on the fibres.

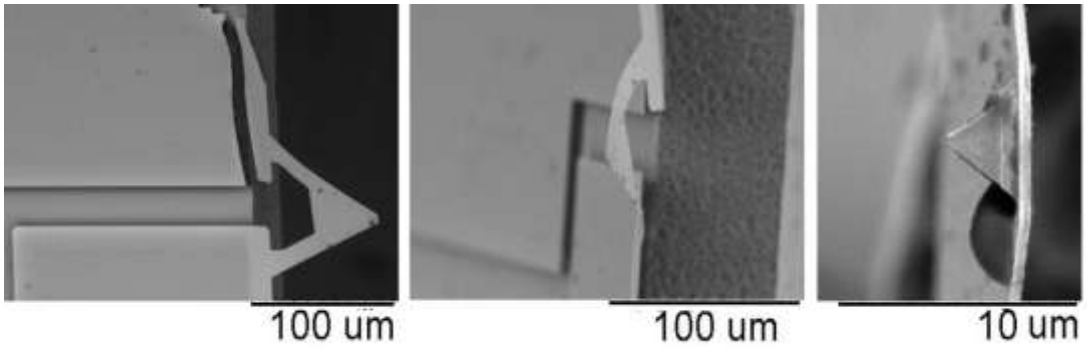

Figure 4.24- Showing a damaged cantilever tip that is broken, bent and has debris on the tip

Cantilever Stiffness

The procedure previously described was repeated for both cantilevers on the same sample. As the same fibres could not be tested, a number of different fibres were tested with each cantilever.

An experiment performed compared 2 cantilevers of different stiffness. A stiff AC160-1 cantilever with nominal stiffness specified at 10N/m was compared to a soft TR400PB-1 cantilever with a nominal stiffness specified by the supplier at 0.1N/m. The results obtained from this experiment were plotted in Figure 4.25 and show a continuous range of results for both cantilevers, ensuring that the data obtained does not vary for different cantilevers.

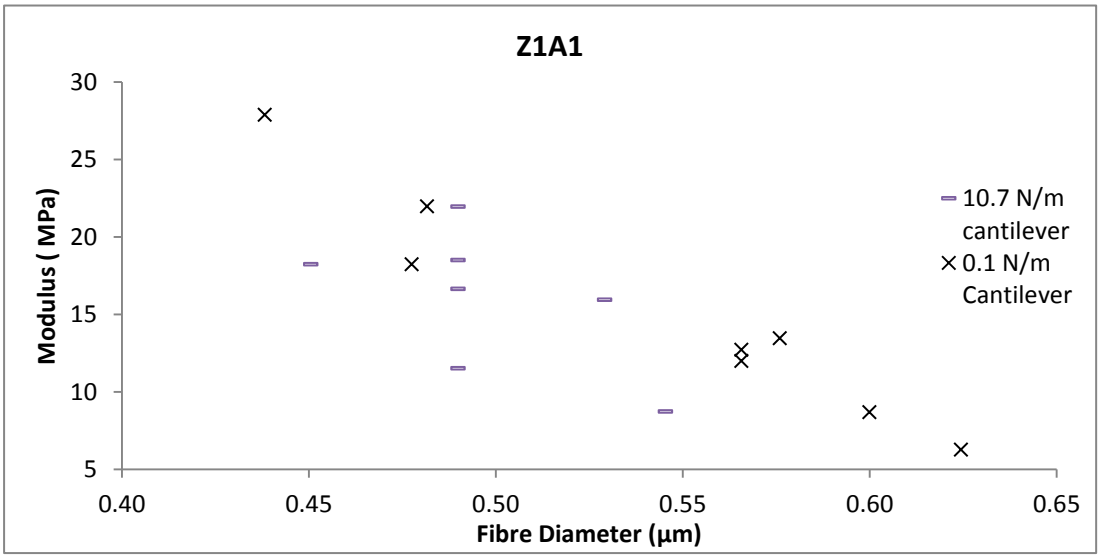

Figure 4.25 - Graph comparing results obtained from 2 different cantilevers

On further analysis of the data, a significant difference between the two cantilevers could be found. As the 10.7 N/m cantilever is stiffer by a factor of 100 when compared to the soft cantilever, it is considerably less sensitive to smaller forces as seen in Figure 4.26. This meant that to obtain a linear relationship, a larger force accompanied by an inevitably increased displacement had to be applied on the fibres. This elevated displacement could compromise the assumptions that were previously made and ensured that the softer, more sensitive cantilevers were more suited for our experiments.

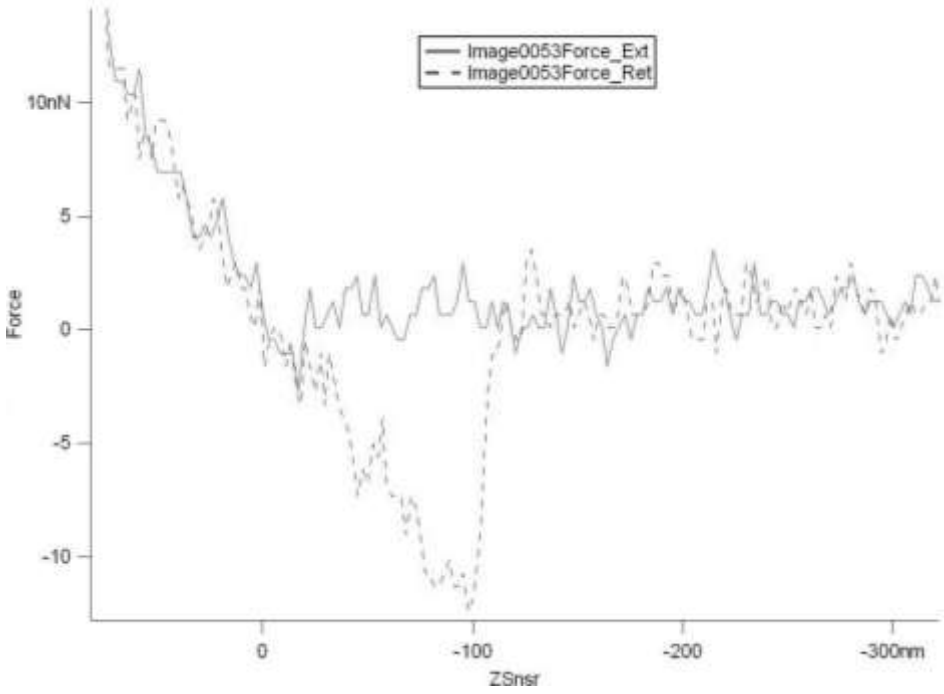

Figure 4.26- A typical force curve obtained from the stiffer cantilever

Imaging Method

Obtaining an accurate representation of the geometry involved was essential for our calculations as these had a significant effect on the calculated value of the modulus. Imaging in tapping mode would reduce the risk of moving or damaging the fibre, while imaging in contact mode gives a more accurate representation of the area being scanned as the tip is in constant contact with the surface.

A number of variables that alter the interaction between the tip and the surface along with the scanning speed can be set to obtain a better image. Unfortunately, to obtain better images, scan time has to be sacrificed.

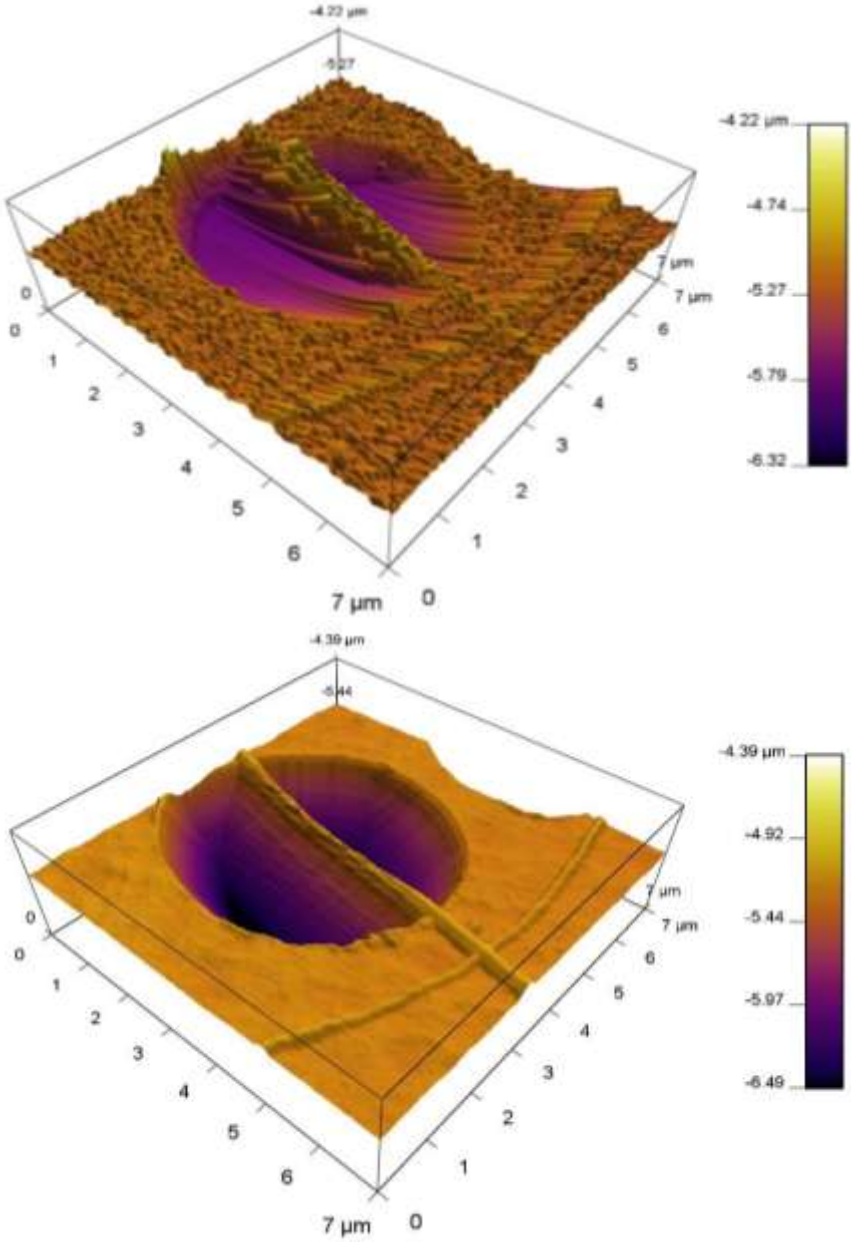

Figure 4.27 Showing the same area scanned with 2 different imaging modes. Top: Tapping, Bottom: Contact

Figure 4.27 shows the same area being scanned in tapping (top) and contact mode (bottom). For both modes, the same scan time was used to obtain a fair comparison. Even though tapping mode reduces the risk of damaging the fibres, the geometrical data obtained from these images was very unreliable. Contact mode was therefore used for the majority of the experiments conducted.

4.7.1.4 Dimensional considerations

After the scan was obtained, the AFM software was used to measure the dimensions related to the three-point bend test. The suspended length could be measured directly while a measurement for the suspended fibre diameter had to be taken from the same fibre on the substrate. Measurements for the width and the height were taken from the fibre cross section to avoid errors produced by tip convolution, to compensate for the cross-section deformation created when wet fibres impinge onto the substrate. The fibre diameter was then calculated using the formula $D = \sqrt{D_1 D_2}$ where D is the reduced diameter, D_1 is the measured height and D_2 is the measured width.

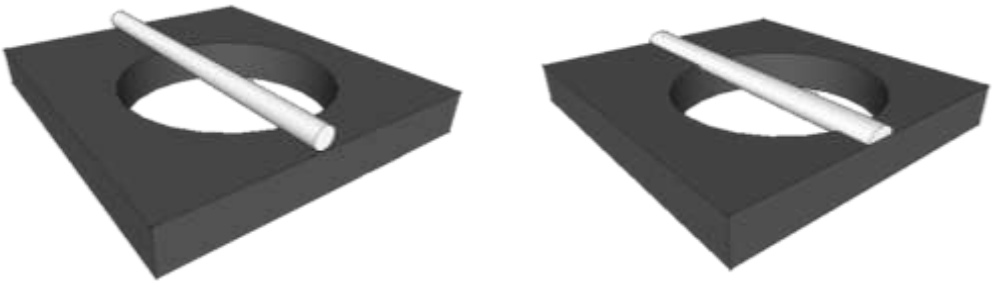

Figure 4.28 - Ideal fibre (left) and actual fibre representation (right)

While scanning was done in both contact and tapping mode depending on the cantilever used, the force curves were always obtained in contact mode to ensure repeatability of the measurements regardless of scanning mode.

A force of was then applied onto the substrate and the AFM software automatically recorded the displacement observed against the force applied. The peak of the suspended fibre was then found by applying small forces at the mid-section of fibre and observing the highest point

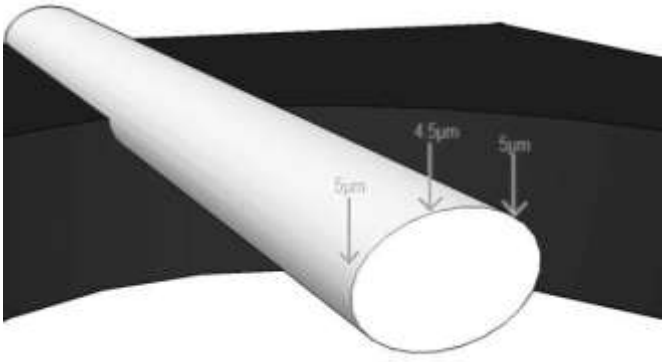

Figure 4.29 - Method to find midpoint of fibre and relative values obtained from the Z-Sensor

were the force was triggered as seen in Figure 4.29. This ensured that the midpoint of the fibre was being tested and cantilever slip was minimised. The force used during these tests was kept to a minimum avoiding plastic deformation of the fibre.

When the peak of the fibre was found, a fixed force was applied at 1μm/s for four times to ensure that the fibre did not move and no elastic deformation was present. The graphs obtained where then analysed to obtain the elastic modulus of the fibre. This procedure was repeated multiple times for different fibres from the same sample to permit the construction of a distribution of fibre moduli.

4.7.1.5 Data extraction

The procedure to obtain the relationship between the force applied and the displacement of the fibre required an understanding of the AFM data-acquisition system. Movement of the cantilever tip was interpreted by the software as the force applied while the motion of the Z-Sensor was interpreted as the displacement as shown in Figure 4.30.

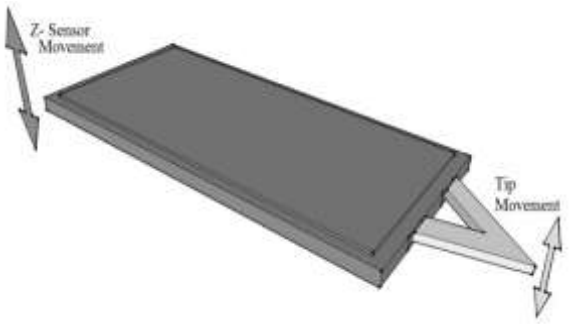

Figure 4.30 - AFM Cantilever

Figure 4.32 shows the complete graph obtained from the AFM software plotting Z-sensor against Force. The dashed line shows the cantilever approaching the surface while the solid line show the cantilever retracting from the surface. The initial segment of the approach curve (1) shows the Z-Sensor moving towards the surface without any deflection on the cantilever (or force). When the cantilever comes close to the surface, a small negative force deflection can be seen brought about by surface energy attracting the cantilever tip to the surface (2). This is followed by an increase in force as the Z-sensor travels towards the surface (3). When a set force is reached, the z-sensor changes direction and starts moving away from the surface. The solid line then shows a linear decrease in force as the cantilever is pulled away from the surface (4). The tip remains attached to the surface for longer, since surface energy causes adhesion between the tip and the surface. When the force is enough to overcome the adhesion, the cantilever tip

springs back up to its original position (5). For most of the following representations, only the approach curve was plotted to avoid confusion

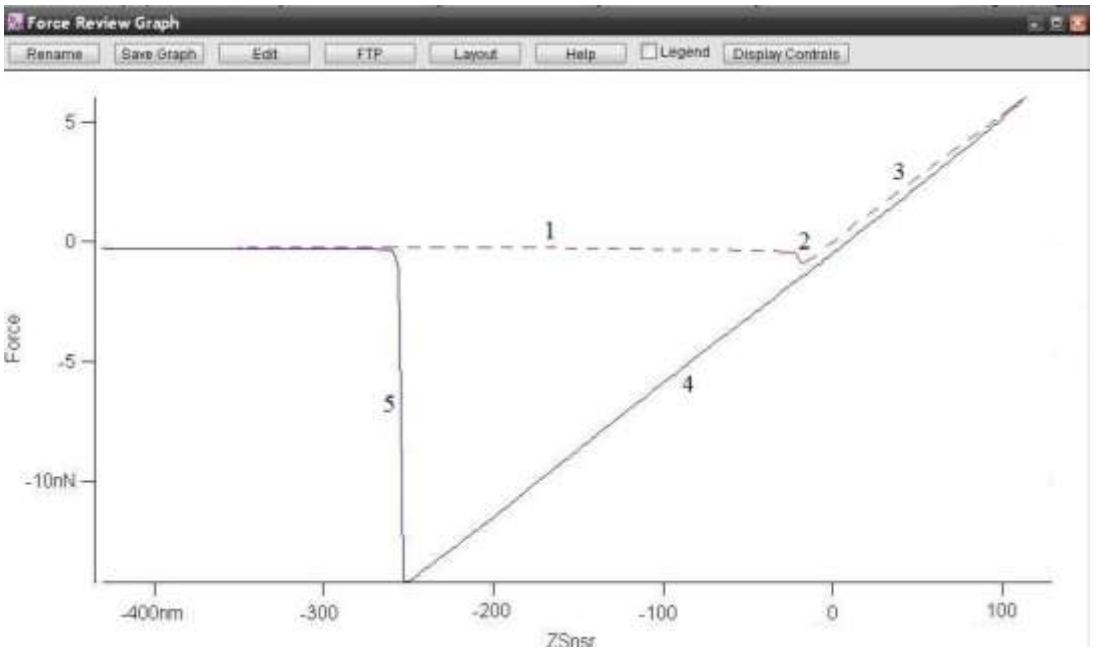

Figure 4.32 - A complete graph obtained from the AFM software

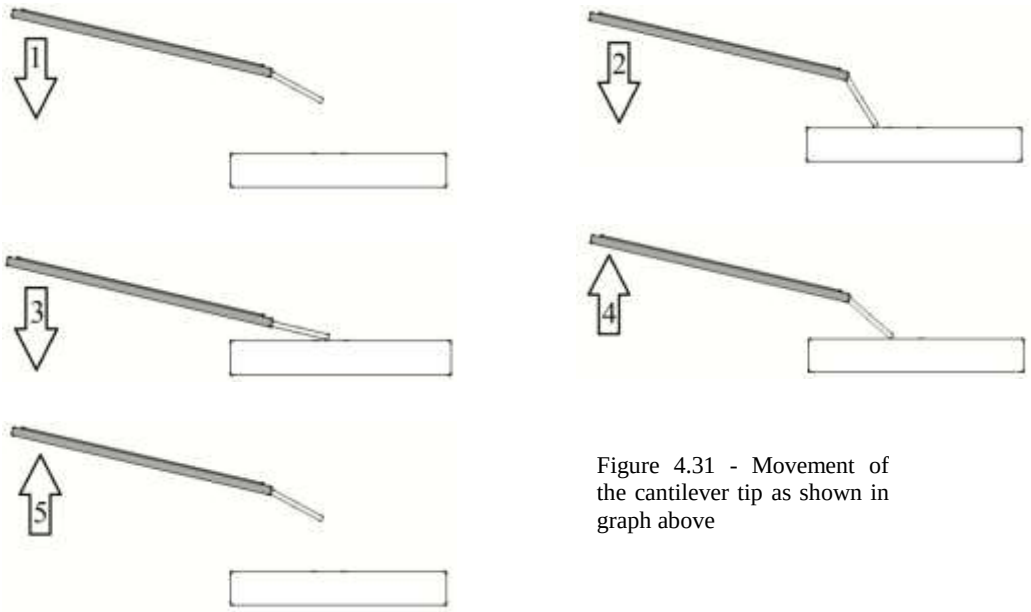

Figure 4.31 - Movement of the cantilever tip as shown in graph above

The previous representation works as desired when used on a hard, immobile substrate. Unfortunately, as the fibre is expected to deflect under the applied load, the cantilever tip and the fibre can be modelled as two springs in series both deflecting under the same load as seen in Figure 4.33

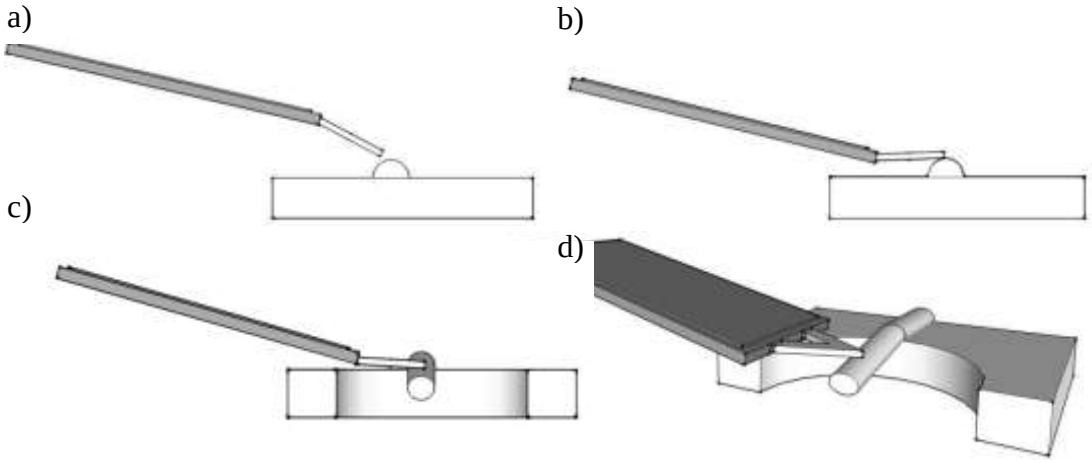

Figure 4.33 - Representation of force applied in two different scenarios

Figure 4.34 shows the movement of the Z-sensor when plotted against the force applied for both scenarios. The dashed line shows the deflection when a force is applied on the substrate, while the solid line shows the deflection when a force is applied on the fibre. The difference δ would signify the movement of the fibre alone and was the value of interest to us.

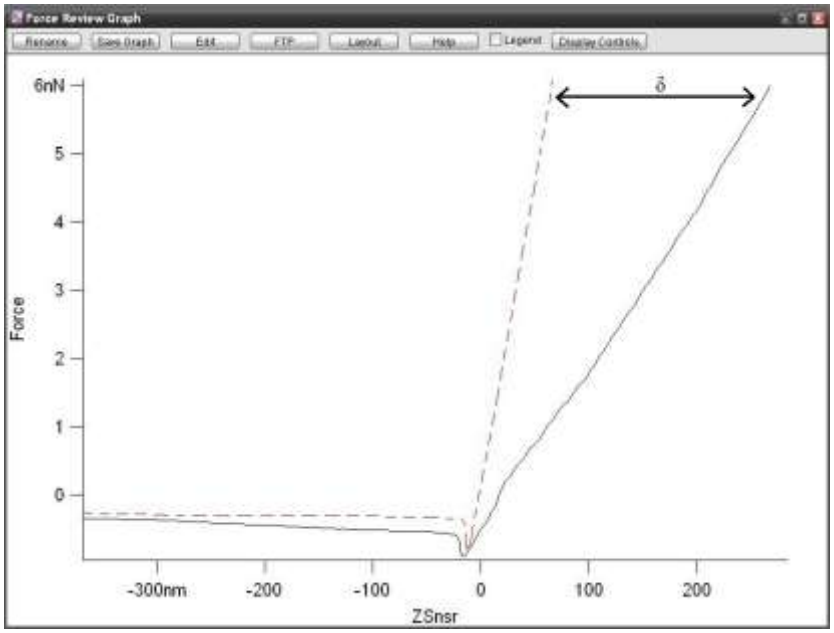

Figure 4.34 - Graph of Force against Z-Sensor. Dashed line showing a force applied to the substrate and the solid line showing a force applied on a suspended fibre.

The gradient of the plotted curves denotes their respective stiffness. From the gradient of the dashed line, the stiffness of cantilever k_c can be calculated while the gradient from the solid line, k_o represents the observed stiffness of the fibre and substrate. The stiffness of the nanofibre k_f is therefore given by:

$$\frac{1}{k_o} = \frac{1}{k_c} + \frac{1}{k_f} \qquad \text{Eqn 4.1}$$

To bypass this calculation every time the stiffness of the nanofibre had to be found, a graph was plotted with the gradient of the cantilever k_c as a straight line or a gradient of infinity as seen in Figure 4.35. The observed stiffness obtained from the new graph related directly to the stiffness of the fibre k_f. To do this, the force applied was plotted against Sep which is defined as the separation between the tip and surface and is sometimes used when indentation measurements are made.

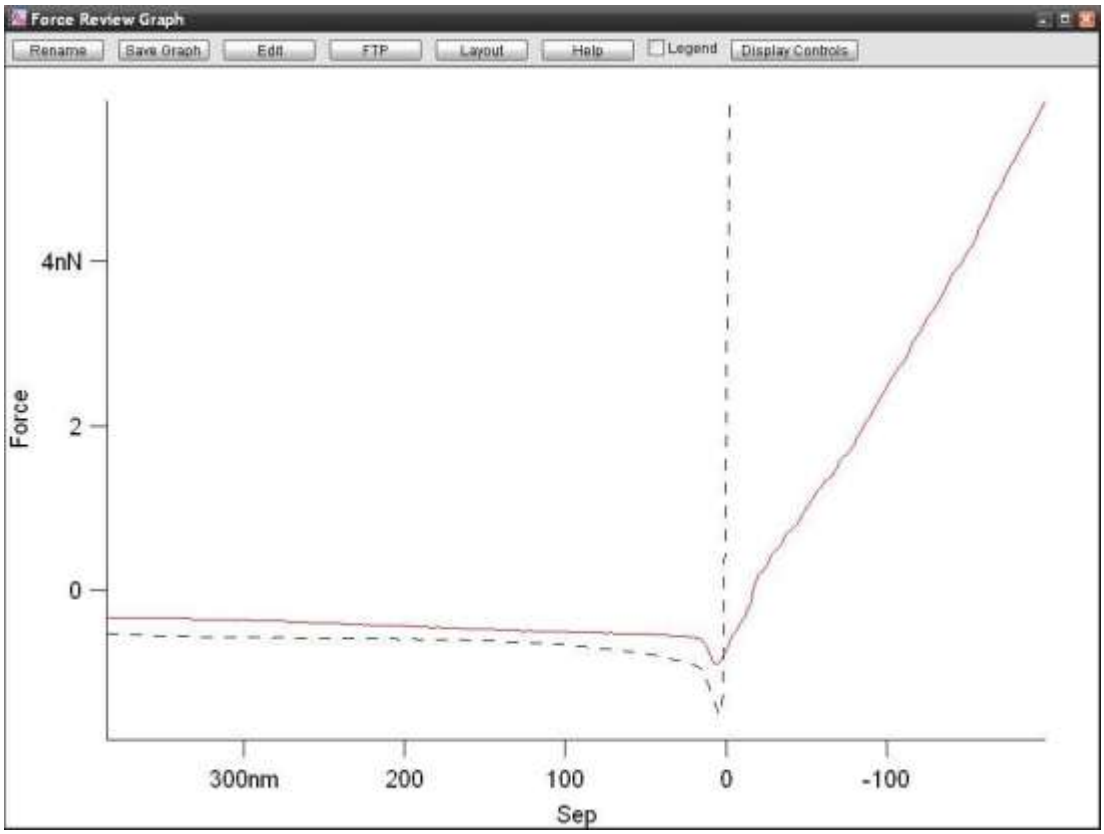

Figure 4.35 - Graph of Force against Sep. Dashed line showing a force applied to the substrate and the solid line showing a force applied on a suspended fibre.

An array of experiments was set up to confirm that the technique of three-point bending by AFM produced reliable results that could be reproduced elsewhere.

To confirm the reliability of the experiment, a set of fibres were tested both at the midpoint and at a quarter of the suspended length. The deflection observed at a quarter of the suspended length was expected to be half the deflection seen at the midpoint as the Young's modulus was constant throughout the fibre. Two values for Young's modulus could then be calculated and compared.

4.8 NANO-INDENTER

An *Asylum Research MFP NanoIndenter* was used for indentation of cast films. This system used the same vibration and acoustic isolation systems as the AFM. A separate optical camera could be used to allow for imaging of the sample. As it was designed for soft materials, it allowed for a maximum load of 4mN with a Z travel range of 15μm. A variety of nano-indenting tips were available, namely a Bercovich tip, a cube corner tip, a sapphire tip and a diamond flat punch. The accompanying software made the system versatile with multiple analysis tools such as inbuilt Hertz and Oliver-Pharr calculation options.

5 RESULTS

The results obtained from the *Bose ElectroForce* test machine for the tests performed on the macro scale are shown in Figure 5.1 and 5.2. The gradient of the graph was used to obtain the tensile modulus of specimen. The modulus observed for Z1A1 was 15MPa while the modulus obtained For Z3A1 was 81MPa.

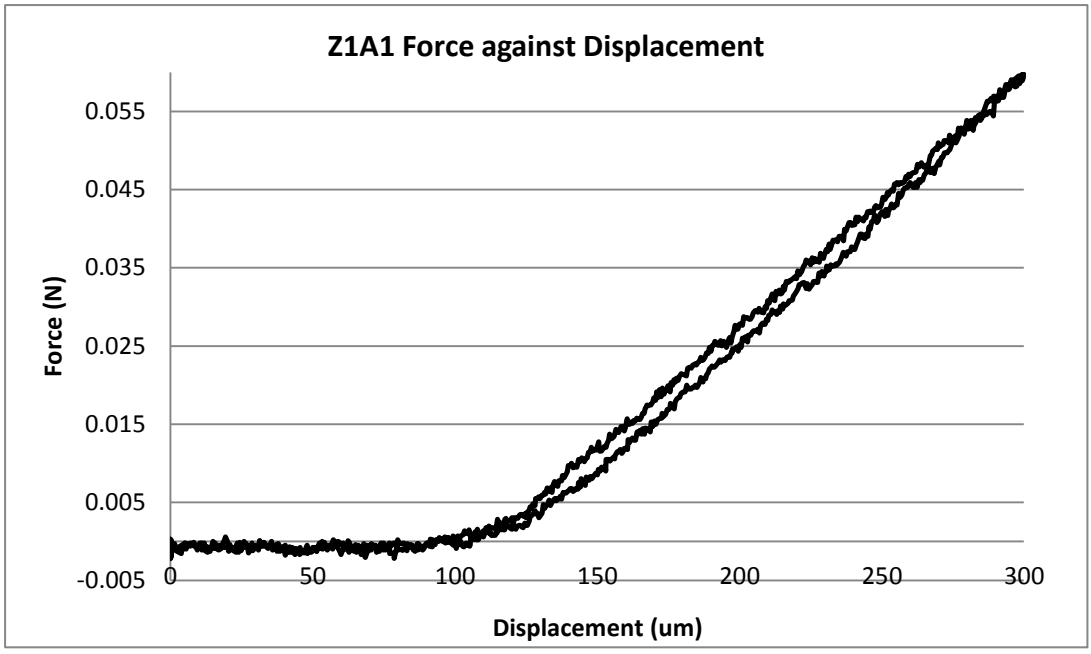

Figure 5.1 - Results from the tensile test on Z1A1

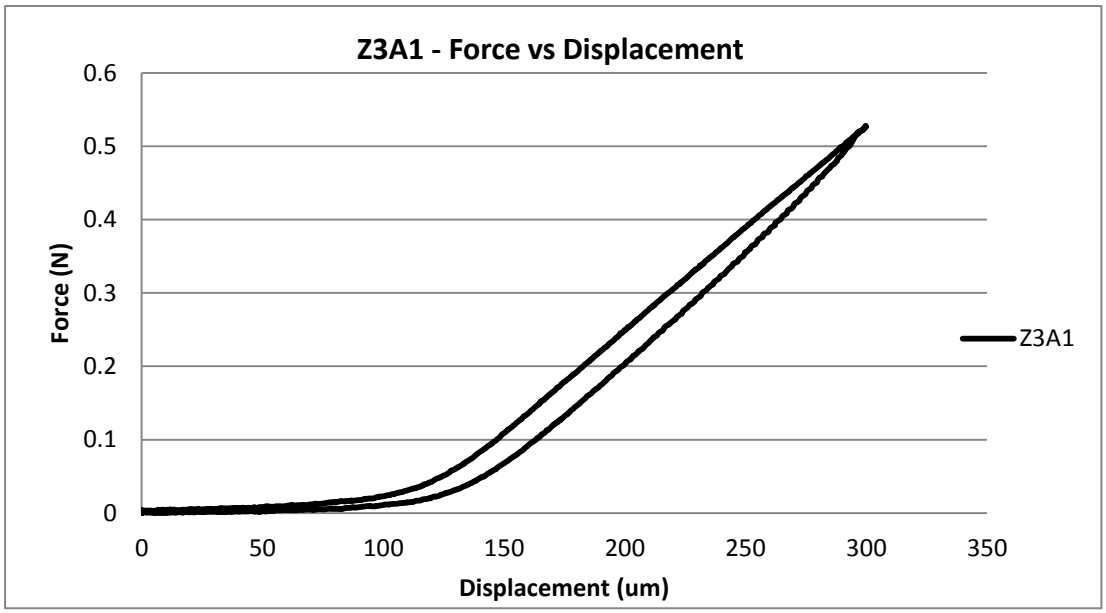

Figure 5.2 - Results from the tensile test on Z1A1

The results obtained from the AFM were more elaborate. A number of steps were involved in the data collection phase to ensure accurate and reliable data was collected as previously described.

The samples were stored at room temperature and atmospheric pressure in a secure place to avoid contamination. The tests were performed over a period of 3 weeks as data collection was significantly time consuming. The grades of polyurethane being used were non-degradable and therefore it was not expected that material properties would change over this period of time. All tests were performed in room temperature and atmospheric pressure.

30 fibres were tested for Z1A1 while 26 fibres were tested for Z3A1. The range of fibre diameter varied from 250nm to 650nm for Z1A1 and 120nm to 420nm in Z3A1. A Force was applied 4 times at the same position for each indent to obtain a repeated reading for every fibre. These repeats yielded a variation in moduli calculated and were included in the plotted graphs.

The equation used to calculate the elastic modulus was:

$$E = \frac{F L^3}{192\, d\, I} \qquad \text{Eqn 5.1}$$

Where: E – Young's modulus
F – Force applied at midpoint
L – Suspended length of the fibre
d – Deflection of the wire at midpoint
I – Sectional moment of area ($I = \frac{\pi r^4}{4}$ for a circle with radius *r*)

The diameter of the fibre was measured using the formula:

$$D = \sqrt{D_1 D_2} \qquad \text{Eqn 5.1}$$

Where: *D* - Reduced diameter
D_1 - Measured height
D_2 - Measured width

The data obtained from every fibre was then tabulated on *Microsoft Excel* including references to the date, specimen number, cantilever type and stiffness as shown below.

Suspended Length		Fibre Diameter	Extension	Force Applied	Moment of Area	Modulus	Modulus
μm		μm	m	N	m^4	Pa	MPa
#2	5	0.34641	6.7332E-08	3.2503E-09	7.0695E-28	44455143	**44.45**
	5	0.34641	6.6368E-08	3.115E-09	7.0695E-28	43223447	**43.22**
	5	0.34641	6.0287E-08	2.9817E-09	7.0695E-28	45547060	**45.54**
	5	0.34641	6.3407E-08	3.0028E-09	7.0695E-28	43612329	**43.61**
#3	5	0.41833	4.5093E-08	4.4187E-09	1.5035E-27	42431840	**42.43**
	5	0.41833	4.5276E-08	4.3545E-09	1.5035E-27	41646328	**41.64**
	5	0.41833	4.0301E-08	3.7808E-09	1.5035E-27	40623221	**40.62**
	5	0.41833	3.7107E-08	3.5573E-09	1.5035E-27	41511758	**41.51**

Figure 5.3 - Table of data collected for 2 fibres

All the data was then tabulated on a separate table for more convenient analysis as shown below.

Reference Number	Fibre Diameter	Average Modulus	Max Variation	Min Variation
	μm	MPa	MPa	MPa
2	0.35	44.2095	1.34	0.99
3	0.42	41.5532	0.88	0.93

Figure 5.4 - Format of a table with the summary of the data collected

The data obtained for both Z1A1 and Z3A1 was then plotted as seen in the following graphs to be analysed further.

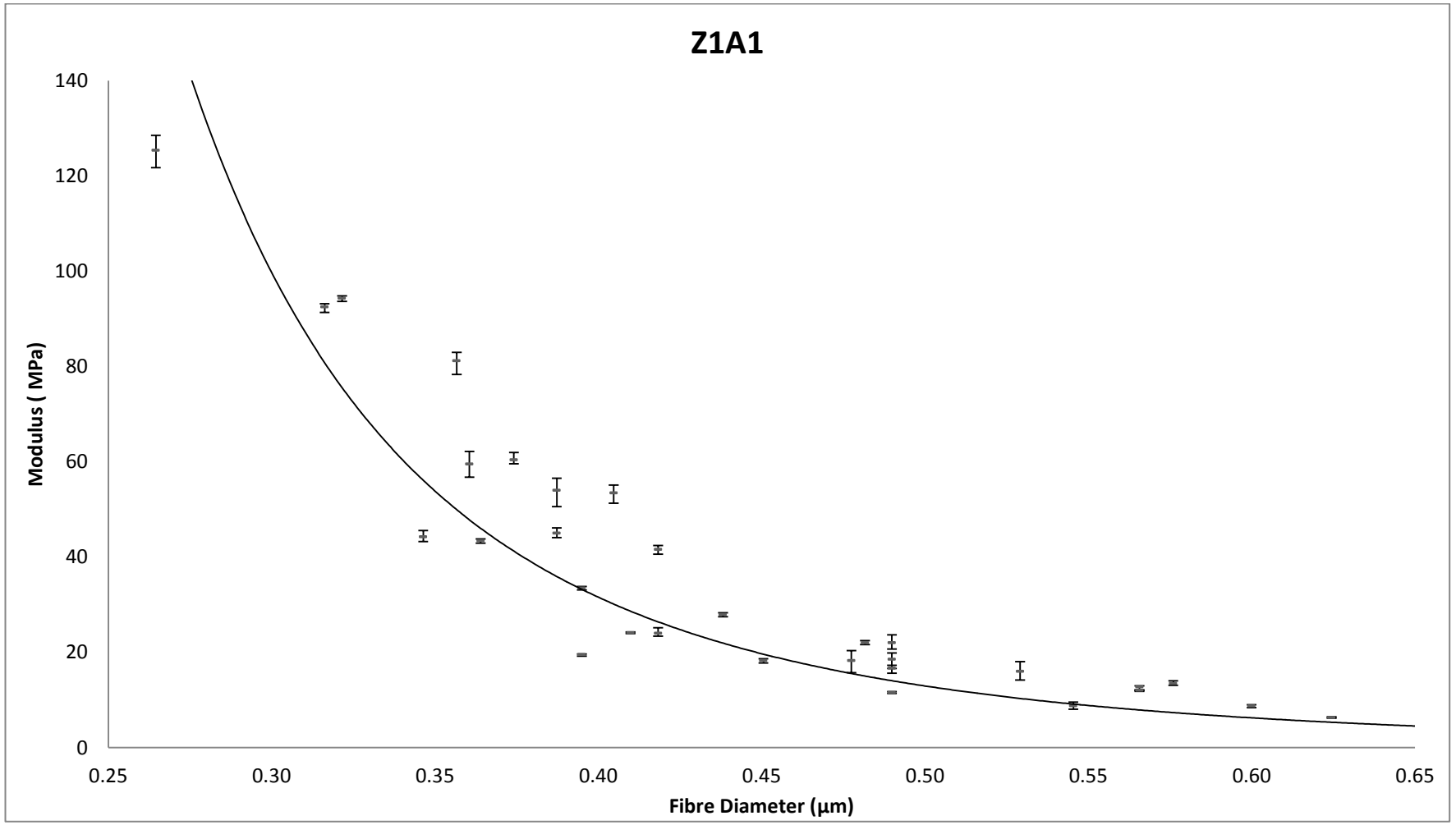

Figure 5.5 - Graph of modulus against fibre diameter for Z1A1

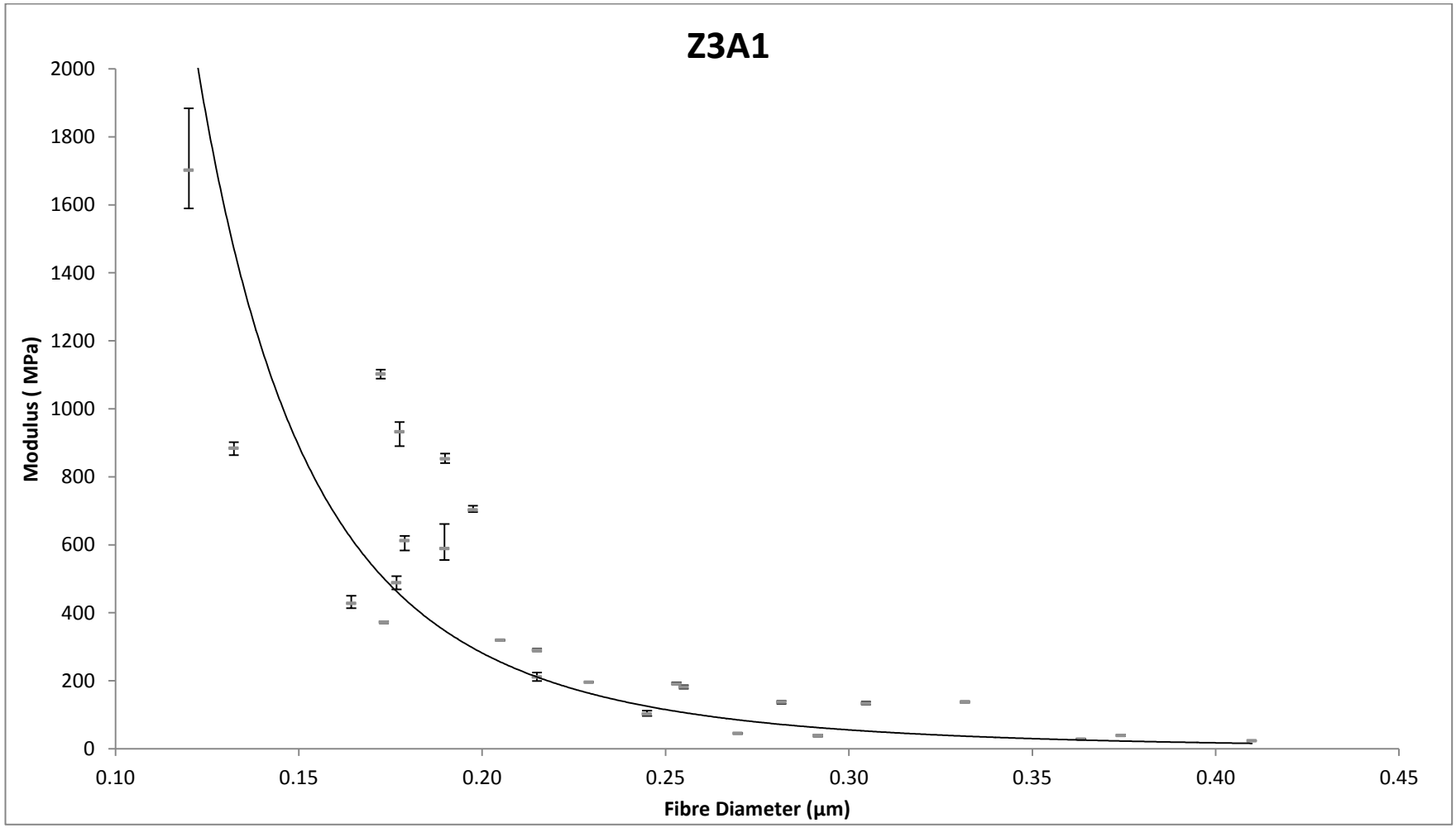

Figure 5.6 - Graph of modulus against fibre diameter for Z3A1

6 DISCUSSIONS

The main observation made for both Z1A1 and Z3A1 was that modulus increases considerably with a decrease in fibre diameter and a significant difference was seen from the moduli of the relative cast films. This observation could have a significant impact on the behaviour and mechanotransduction of cells on a scaffold with fibres of a varying diameter. The results obtained from the experiments conducted using the Atomic Force Microscope had a number of limitations that could compromise the reliability of the results. The experimental procedures used had to be scrutinised to reduce the number of assumptions taken when analysing the results obtained.

6.1 FIBRE ARTEFACTS

A number of considerations regarding the fibre profile and movement have been addressed during the data-collection phase of the experiments.

6.1.1 FIBRE TENSION

One of the concerns was that the suspended fibres sag over the suspended length of the pore. Fibres that are not firmly suspended over a pore can produce misleading results as the original length cannot be accurately measured. To prove that the fibres being tested were actually taut, an image obtained from the AFM while scanning parallel to the fibre was analysed as seen in Figures 6.1 and 6.2.

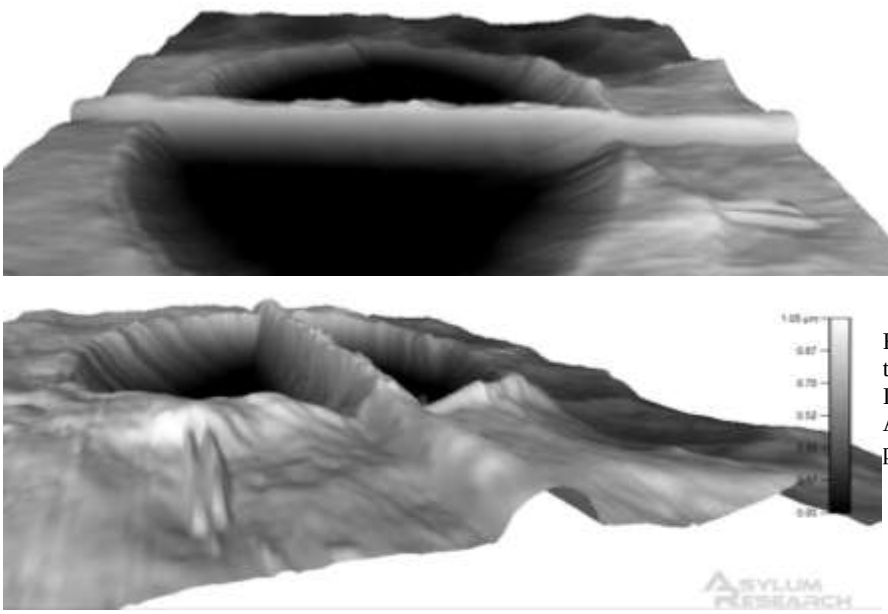

Figure 6.1 - Showing a taut fibre on a pore. Image obtained by AFM while scanning parallel to the fibre.

To prove this further, accurate measurements of the height could be obtained using the AFM software as shown below:

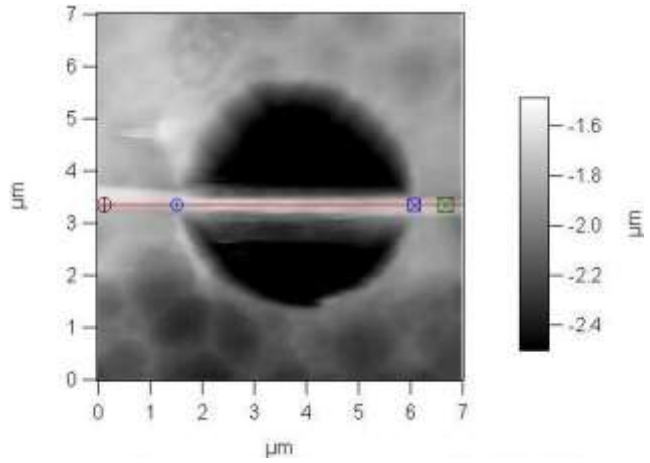

Figure 6.2 - Analysis of fibre height confirming a taut fibre including a measurement parallel to fibre (below).

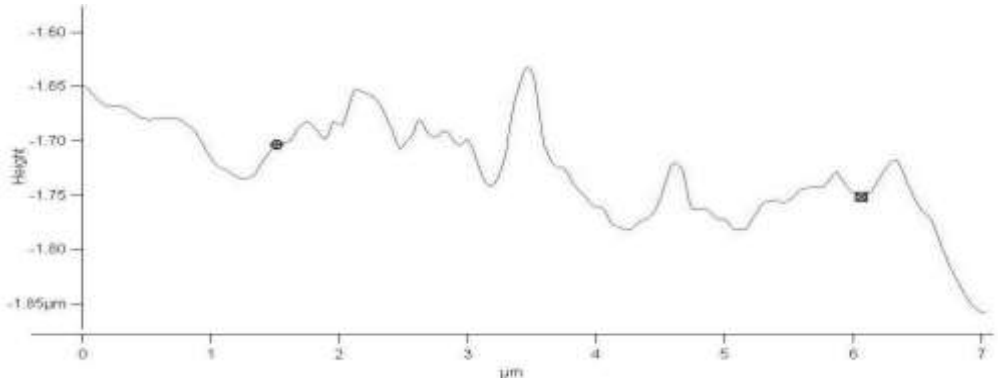

6.1.2 FIBRE MOVEMENT

The formula used to calculate the fibre modulus assumes that both ends of the fibre are fixed. If the fibres were free to move, the modulus calculated would decrease by a factor of 4. It was therefore essential to show that there was no movement of the fibre after each indent. To demonstrate this, Figure 6.3 shows four consecutive forces on the same position of a fibre were plotted on the same graph to show the position where the Z-sensor made contact on the fibre. While this variation in position seen was of about 5nm, the displacement of the fibre observed when a force is applied was about 60nm leading us to hypothesize that the movement of the fibre could be neglected. As the force was applied on the same position, we could also infer that no permanent indentation was seen on the fibre.

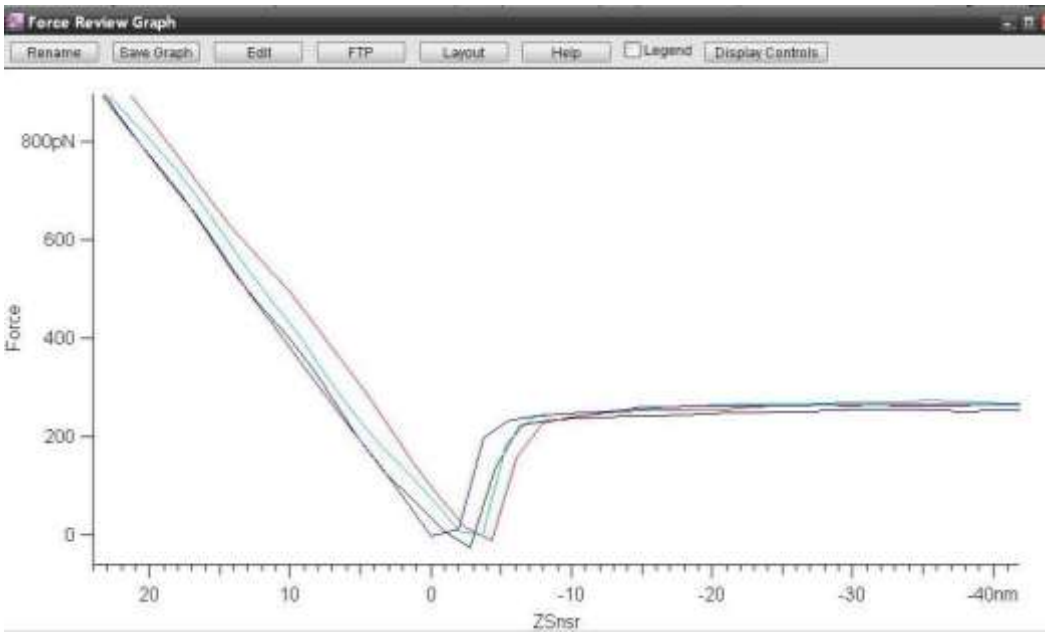

Figure 6.3 - Showing consecutive indents on the same position of a fibre

6.1.3 FIBRE NANO-INDENTATION

Elastic nano-indentation into the fibre while the force was being applied could also have affected our results. To demonstrate that this was not the case, a force was applied on a fibre lying on the substrate. Figure 6.4 shows three force curves plotted on an Sep – Force graph- the solid line was obtained from applying a force on the polycarbonate substrate, the dashed line was obtained from applying a force on a fibre lying on the substrate while the dotted line was obtained by applying a force on a suspended fibre. The difference in the gradient seen between the dashed and solid line shows the indentation made into the fibre. As this variation was very small, it could be considered to be negligible in this experiment and it was assumed that the range of forces applied were not enough to indent the nanofibres.

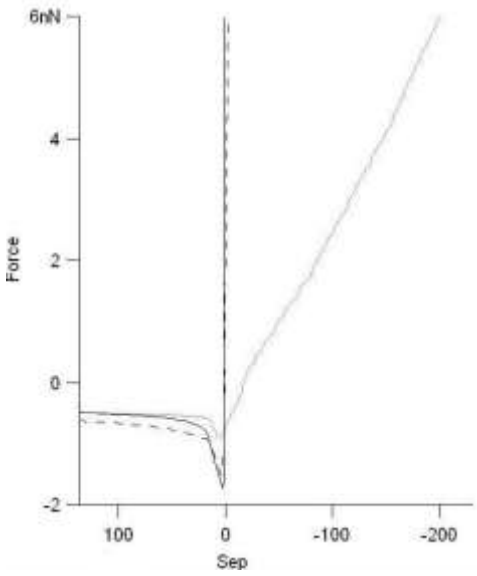

Figure 6.4 - Showing indentation on 3 different locations

The adhesion forces seen when applying a force on a fibre and on the polycarbonate were on the same scale, meaning that the adhesion observed was being caused by the surface energy on the polymers and not because of indentation.

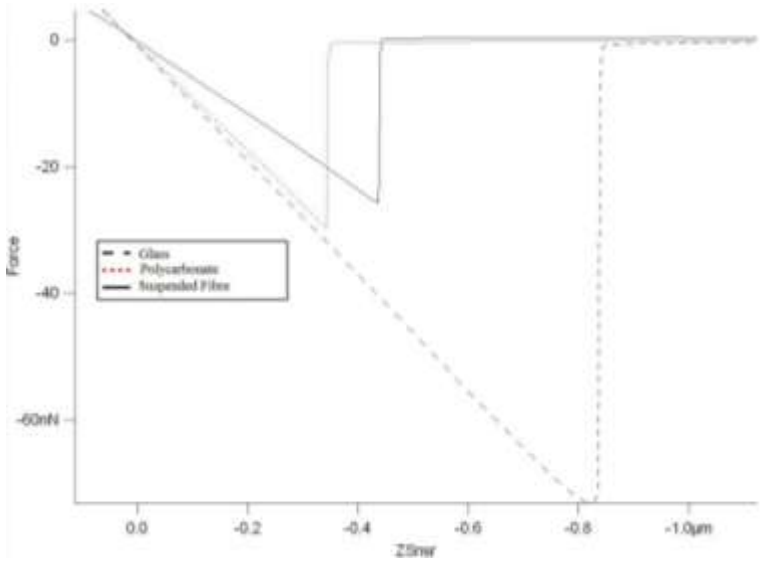

Figure 6.5 shows a significant increase in adhesion when a force is applied on glass. This confirms that the adsorbed layer, not indentation is the leading force behind this adhesion.

Figure 6.5 - Showing retracting graphs for forces applied on different surfaces.

The observations mentioned above were typical for the majority of the fibres found. On the other hand, thinner fibres proved to be more challenging to image and to provide reliable data from. In Figure 6.6, a thin fibre had adhered to the cantilever tip and was deposited to the side of the pore making it unusable. An observation that can be made from this image is that even though the suspended fibre had been moved, the fibre lying on the substrate at the top of the image seems to have remained in its original position and is well-adhered to the polycarbonate substrate.

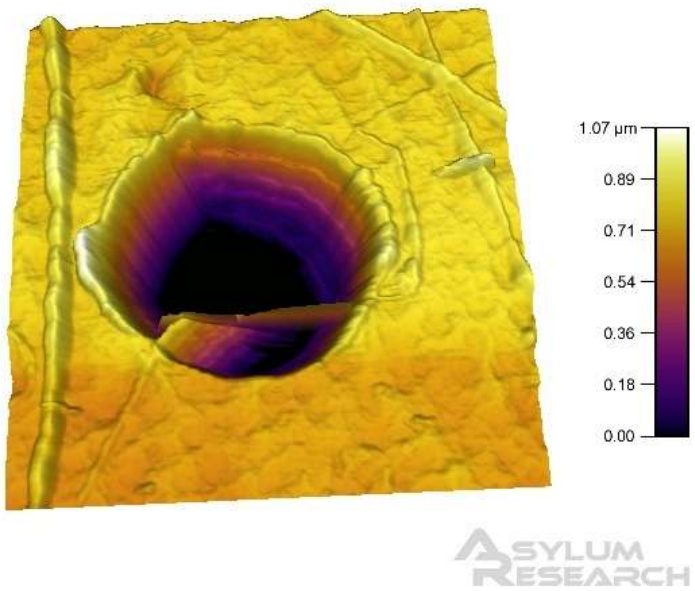

Figure 6.6 - A fibre damaged during AFM scanning by adhesion to the cantilever tip.

6.2 GEOMETRIC CONSIDERATIONS

As mentioned previously, the measured geometric properties have a significant impact on the calculated modulus. The equation being used to calculate the fibre modulus is: $E = \frac{F\,L^3}{48\,d\,\pi r^4}$ meaning that the modulus is proportional to the third power of the suspended length and the fourth power of radius.

6.2.1 L/D RATIO

Literature dictates that for the three-point bending formula to be valid, the ratio between the suspended length and the diameter of the suspended fibre should be higher than 10. If the ratio is smaller, shear forces would no longer be considered as negligible and the model would be invalid.

Data collected from Z3A1 was well above this threshold with the minimum ratio being 12.2 and the average ratio at 23. The fibres produced for Z1A1 had a larger diameter which led to smaller *L/d* ratios as the pore size (and hence suspended length) was the same for both polymers. The average *L/d* ratio for Z1A1 was 11.3 with 10 fibres having a ratio less than 10. These values were plotted on a graph to check whether any drastic change would be observed.

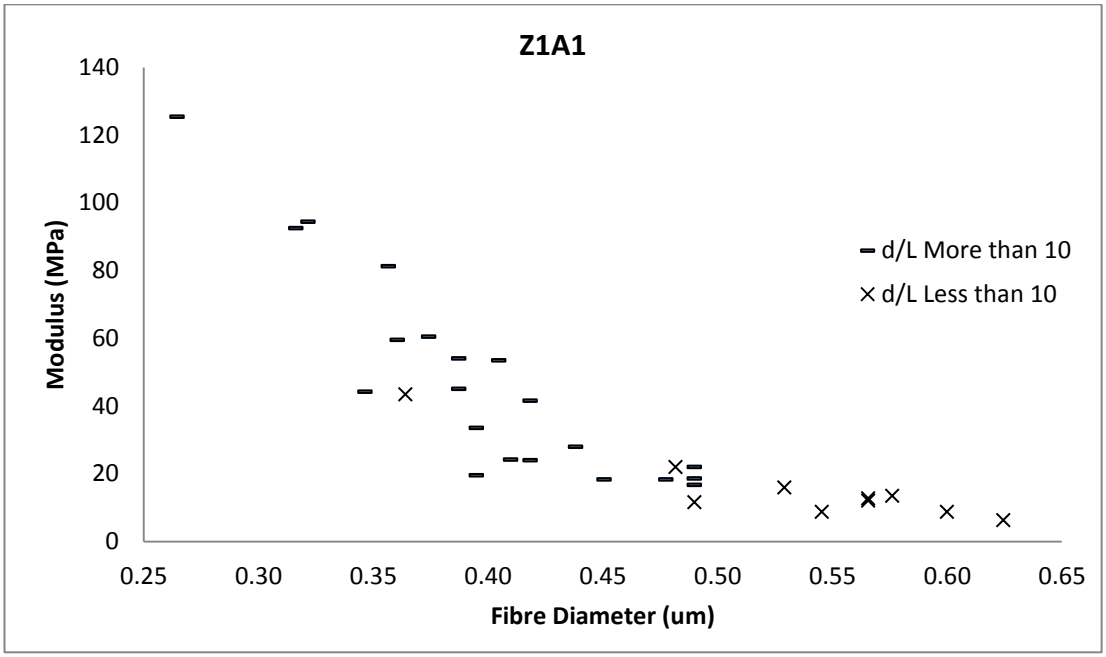

Figure 6.7 - Graph comparing fibres with different d/L ratios

As expected, most of the fibres with an *L/d* ratio less than 10 were below a fibre diameter of 0.5µm. The three fibres that had a diameter smaller than 0.5µm were suspended over a pore that was smaller than the 5µm nominal size specified by the supplier. The graph does not show any apparent difference in the trend of the modulus but this cannot be statistically confirmed as there were no fibres of large diameter suspended over pores larger than 5µm.

6.2.2 APPLYING FORCE AT QUARTER LENGTH

To increase the reliability of this experiment, a set of Z3A1 fibres were tested both at the mid-section and at the quarter-section of the fibre. The three-point bending formula was used to derive the modulus calculated from a force applied at this position. From the displacements observed, 2 values of modulus could therefore be plotted for the same suspended fibre as seen in Figure 6.8.

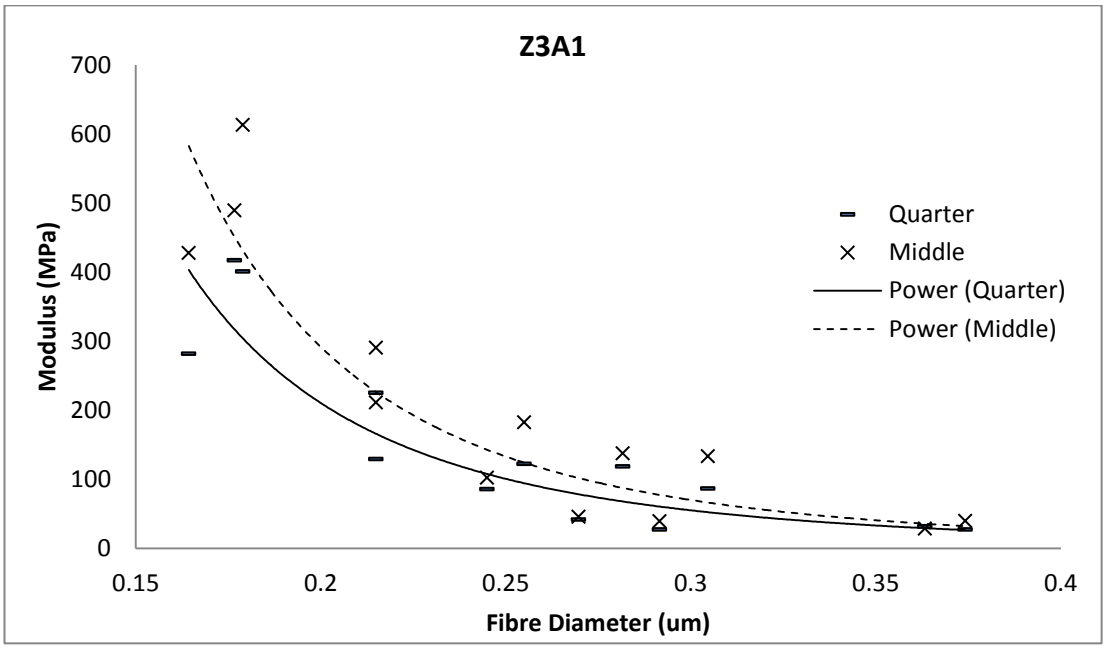

Figure 6.8 - Graph comparing values of moduli obtained from the middle and the quarter length of the fibre

When trend lines were added to the data, it was easy to see that there was a small difference in the calculated modulus. However, the initial observation claiming that the modulus increases with a decrease in fibre diameter was still very clear making the importance of the observed difference less relevant.

6.2.3 GEOMETRIC RELATIONSHIP

As the modulus varies with L^3/r^4, the observed increase in elastic modulus as the fibre diameter decreases could be induced by the measured dimensional changes. This would mean that the fibre modulus is not actually changing but the observed change is only due to an artefact created by the three-point bending formula.

To disprove this observation, the fibre modulus was plotted against the geometrical function relating both the suspended length and the radius as seen in Figure 6.9 for Z1A1 and Figure 6.10 for Z3A1.

As both figures still show an increase in the elastic modulus with a decrease in fibre diameter, it could be confirmed that this increase was actually brought around by a change in the intrinsic properties of the material. This relationship essentially proved that an increase in the stiffness of the nanofibres is responsible for the change in elastic modulus observed and not a geometric artefact.

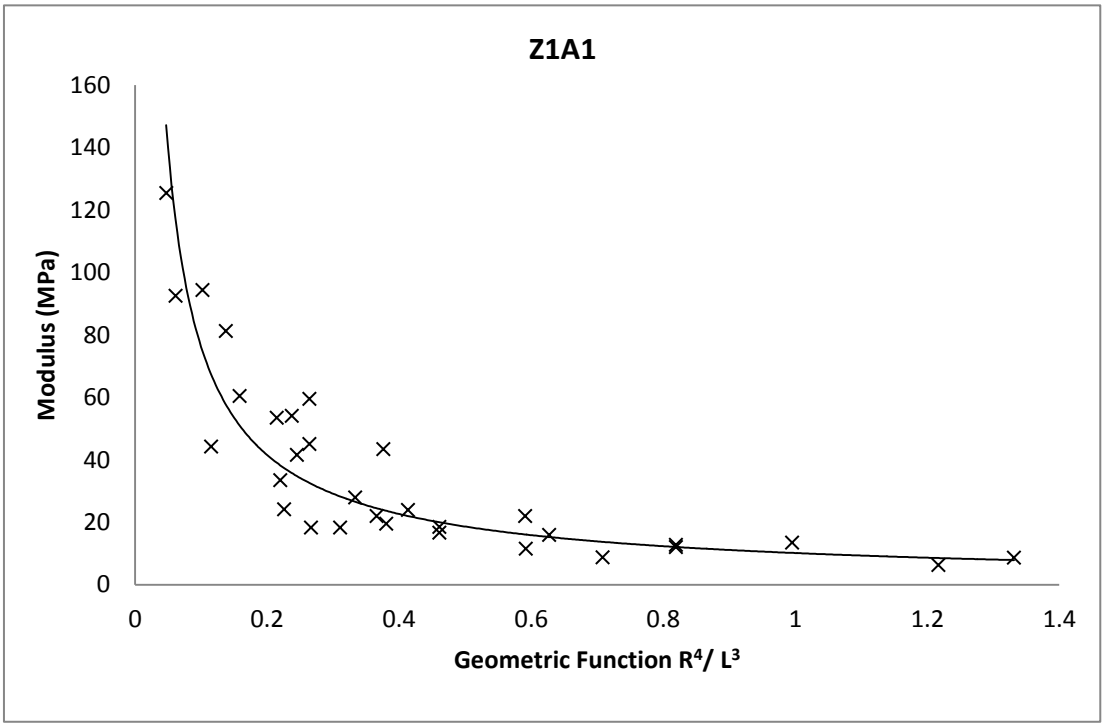

Figure 6.9 - Moduli of Z1A1 plotted against the geometric function

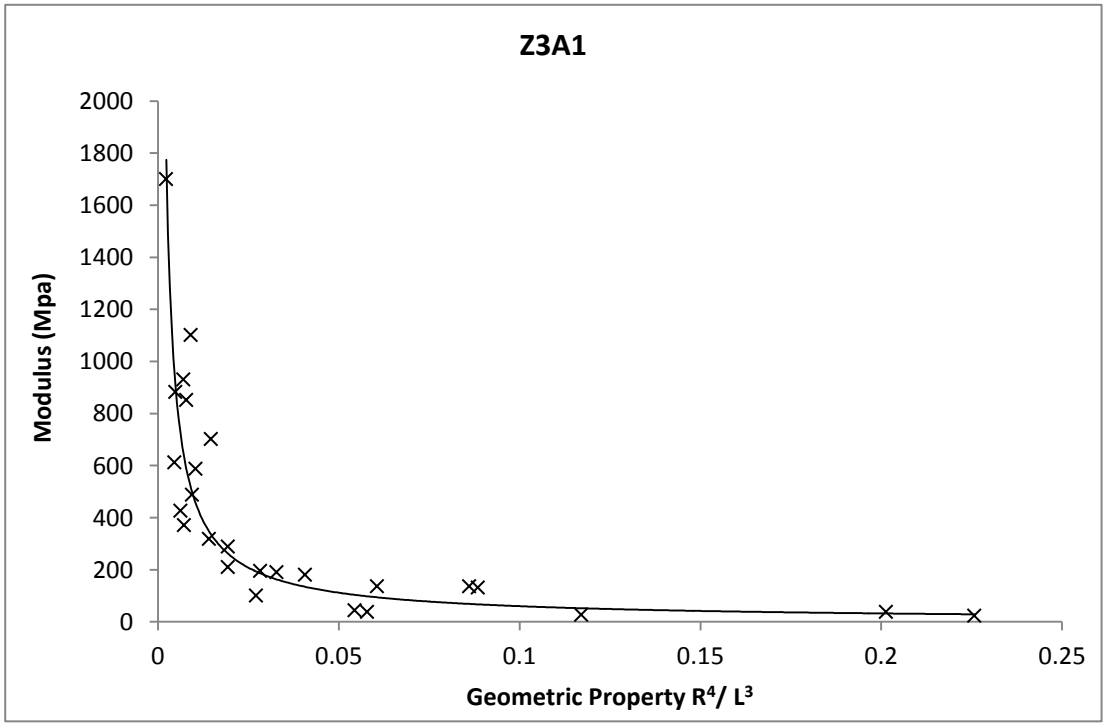

Figure 6.10 - Moduli of Z3A1 plotted against the geometric function

6.3 ALTERNATIVE APPROACH

All the experiments and data analysis carried out in this chapter follow the procedures performed in previous similar studies on different polymers, with the main assumption being that the polymer follows Euler's theorem for three-point bending. This theorem was derived for stiff materials and might not be entirely representative of what is happening in our experiments as the material under investigation is an elastomeric polymer. Euler's three-point bending assumes that the shape adopted by the fibre under three point bending is as shown in Figure 6.11 and the strains are distributed as shown in Figure 6.12. The strains are distributed over the whole area of the specimen under test and significant tensile and compressive forces can be seen on opposite sides of the specimen.

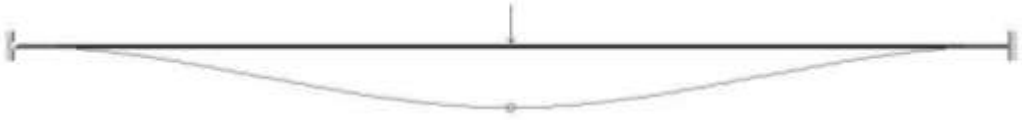

Figure 6.11 - Shape adopted by a beam with fixed ends under three-point bending

Figure 6.12 - Strain distribution for a fixed beam under 3 point bending

As polyurethane is an elastomeric material and it was assumed that both ends of the fibre were fixed to the substrate, the model being used could have been changed to two fixed springs in series with a force being applied in the middle, as shown in Figure 6.13. This model assumes that the tensile and compressive forces seen on opposite sides of the fibre at the clamping points and at the point where force is being applied was minimal and can be omitted. It therefore assumes that the forces seen along the fibre was in pure tension, and simple stress / strain calculations can be made to obtain the elastic modulus of the fibre.

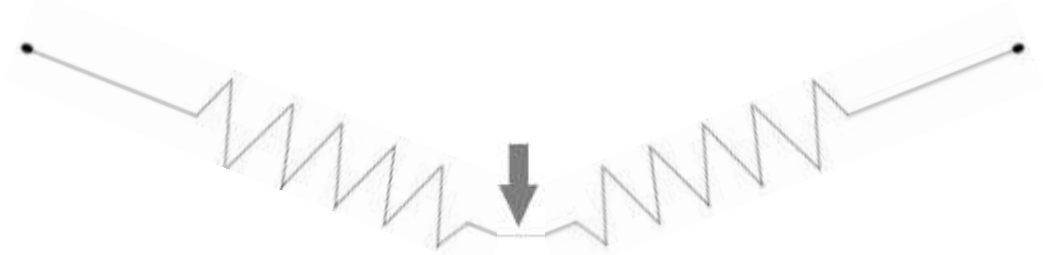

Figure 6.13 - Simple strain model

Simple trigonometry can be used to calculate the force and extension applied to each spring.

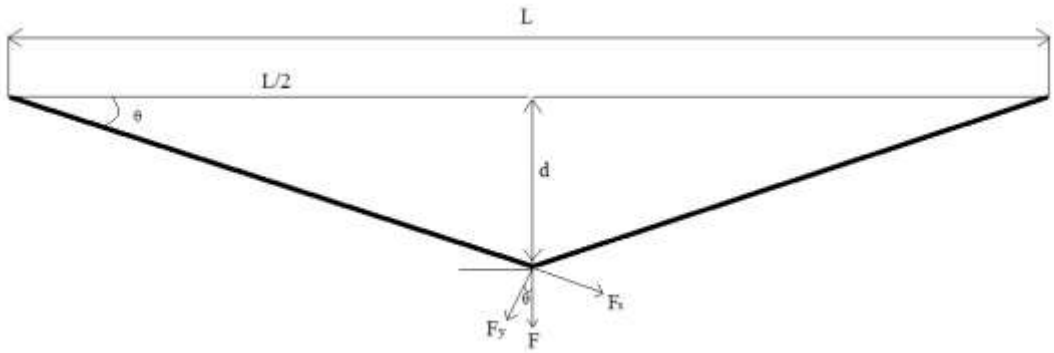

Figure 6.14 - Schematic diagram for the simple strain model

Taking half the fibre, for the displacement:

$$\Delta L = \left(\sqrt{\left(\frac{L}{2}\right)^2 + d^2}\right) - \frac{L}{2} \qquad \text{Eqn. 6.2}$$

For the force applied parallel to the extension:

$$\theta = \tan^{-1}\frac{d}{L/2} \qquad \text{Eqn. 6.3}$$

$$F_x = \frac{F}{2}\sin\theta \qquad \text{Eqn. 6.3}$$

To calculate the elastic modulus of a fibre of original length *L/2* and displacement *d*:

$$E = \frac{\sigma}{\varepsilon} = \frac{F_x}{A}\frac{L/2}{\Delta L} \qquad \text{Eqn. 6.4}$$

Where *A* is the cross-sectional area of the fibre.

As the deflection *d* is very small, the extension and force calculated are considerably smaller. The extension was calculated to be sub-nano meter while the force was only a few tens of pico-Newton. As this procedure acts as a gearing system where a large deflection is converted to a significantly smaller one, we could be confident that the values being used for the calculations were correct. The moduli obtained were plotted for both Z1A1 and Z3A1 against their diameter and a respective geometric function.

All the results obtained showed an increase in fibre modulus with a decrease in diameter as calculated in the previous model. The graphs plotting the moduli against the geometric function reconfirmed this observation, and thus reassured us that the increase in moduli observed was not created by geometric artefact.

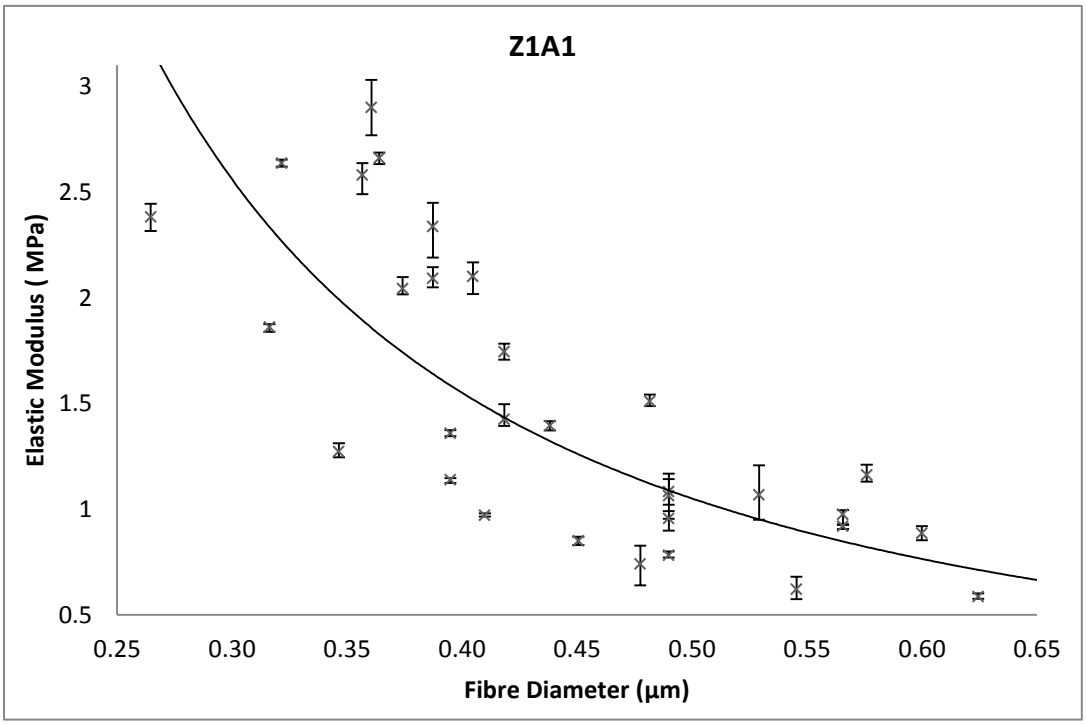

Figure 6.16 -Z1A1 - Moduli against fibre diameter for tensile analysis

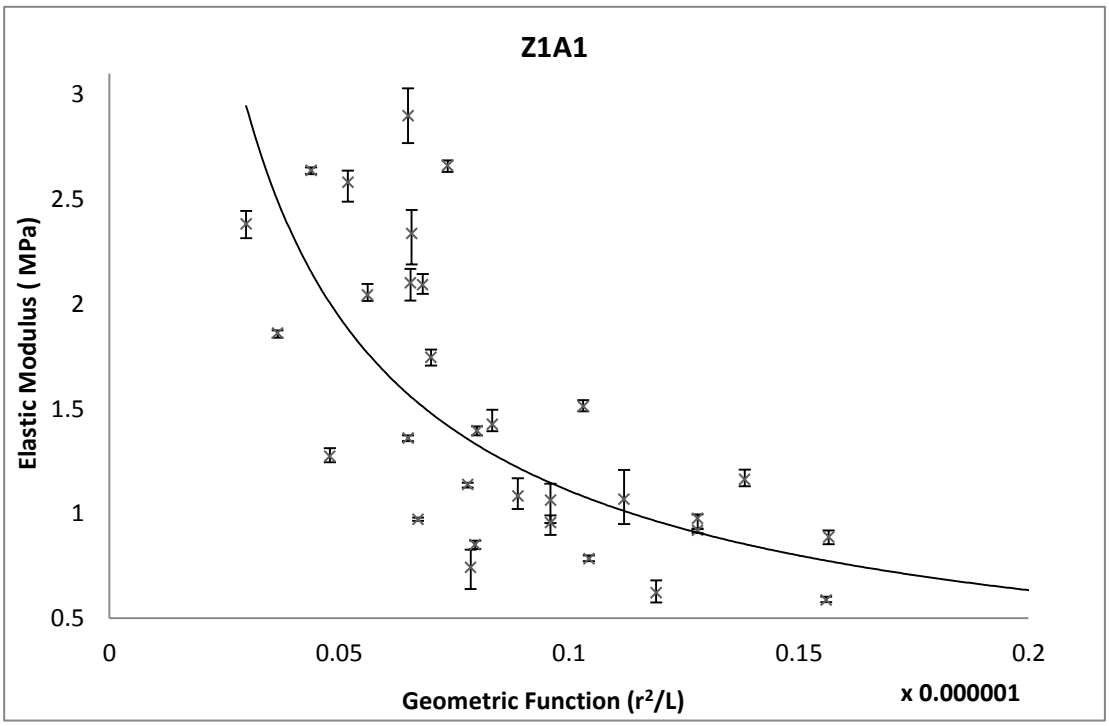

Figure 6.15 - Z1A1 – Moduli against geometric function for tensile analysis

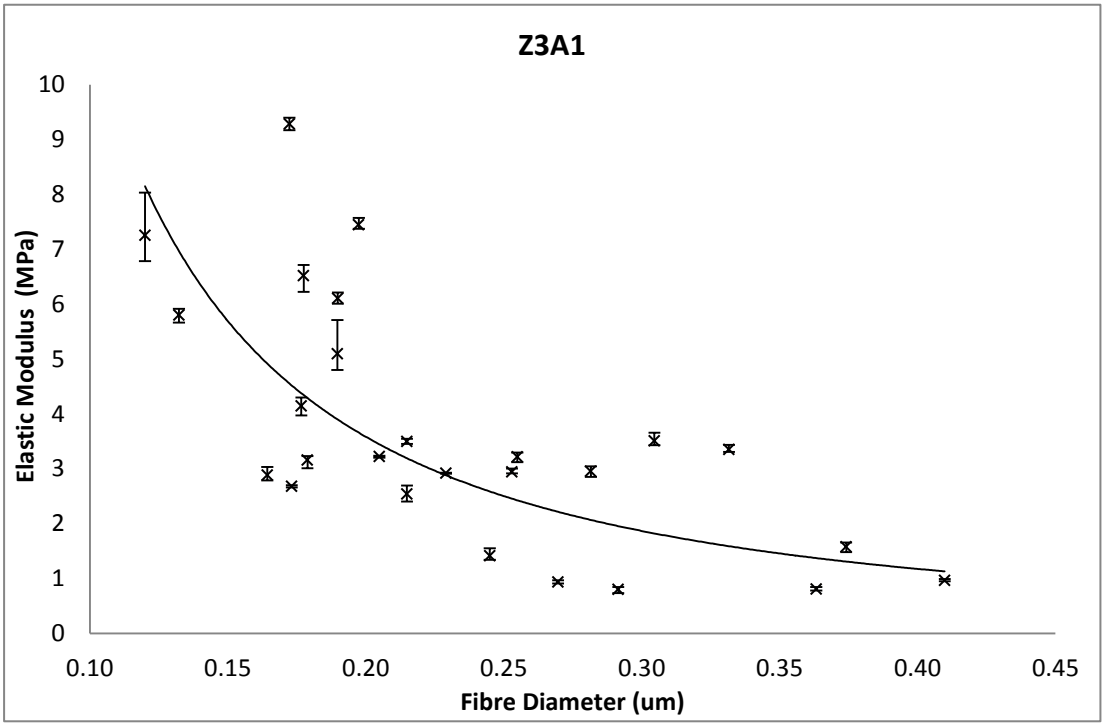

Figure 6.18 - Z3A1 - Moduli against fibre diameter for tensile analysis

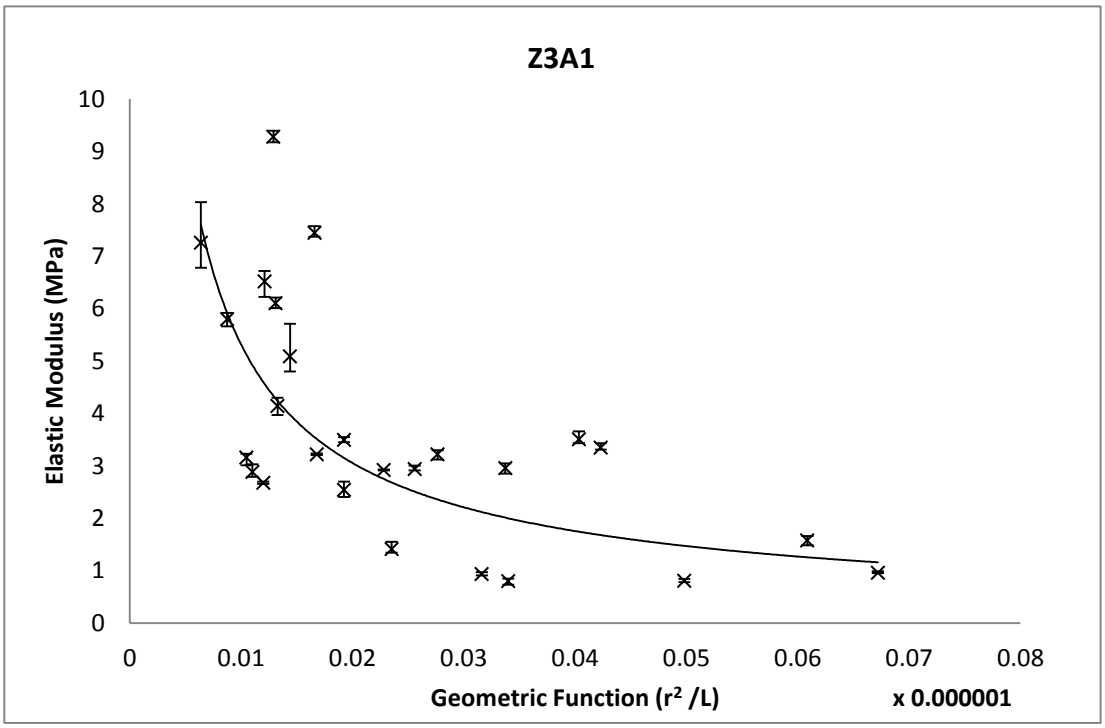

Figure 6.17 - Z3A1 - Moduli against geometric function for tensile analysis

The same analysis could be performed on the forces applied at a quarter distance of the fibre. These tests yielded two values of moduli for the same fibre which could be compared to test the reliability of the experiment.

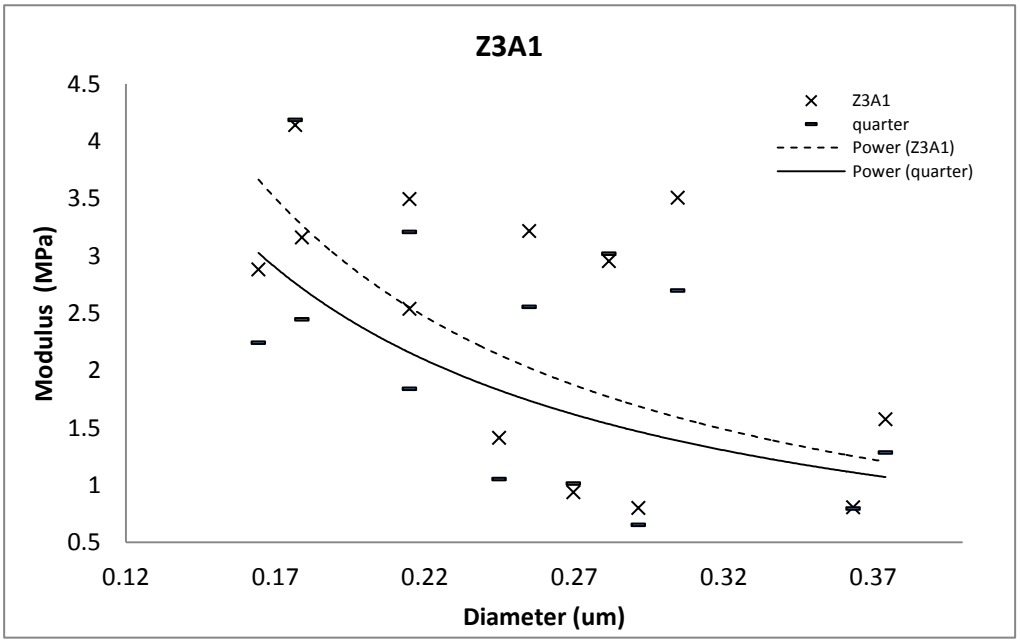

Figure 6.19 - Graph comparing values of moduli obtained from the middle and the quarter length of the fibre

The moduli calculated for both polymers were considerably lower to what was calculated when Euler's three-point bending theorem was used. This observation was expected as the simple tensile measurements completely disregards any compressive forces along the fibre and assumes homogeneous tension. Unfortunately, we could not confirm which of the two approaches best models the actual strain distribution along the fibre. Both approaches have their own advantages and we could only hypothesize that a realistic representation of the fibres under three-point bending act with a combination of the two models highlighted above.

Even though the simple strain method used a completely different approach and the values are on a different scale than what was calculated before, an increase in elastic modulus with the decrease in diameter could still be observed. This reconfirms the initial and most critical hypothesis being made in this thesis- with a decrease in fibre diameter, the fibre's intrinsic properties change leading to an increase in the fibre modulus.

The values calculated by the *Bose Electroforce* system in the tensile tests were significantly higher when compared to those obtained from the AFM experiment when the simple tensile method was used. It was difficult to compare these values as forces that are predominant on the nano-scale are not always predominant in the macro scale and a difference in moduli calculated was expected. An observation that could be made in this experiment was that the modulus for Z3A1 is 5 times higher than that of Z1A1. A higher modulus for Z3A1 has been observed in all our previous AFM experiments but the two polymers could not be compared against each other as the range of diameters for Z3A1 was smaller than that for Z1A1.

7 FURTHER EXPERIMENTS

After this critical observation was made, a series of experiments were set up in an attempt to explain why the fibre modulus was increasing with a decrease in diameter.

7.1 FLEXURE TEST

From literature, one of the major arguments for the mechanism that causes a change in the fibre modulus is a change in the molecular structure of the polymers caused by the electrospinning process. A paper published by *Tang et al.* investigated the surface properties of solvent cast films. In their study, they reported a significant difference between the surface that was in contact with air and the surface in contact with the glass petri dish while the polymer was setting. This difference was explained by a change in the assembly pattern of the molecules and depended on the hydrophobicity of the substrate [48].

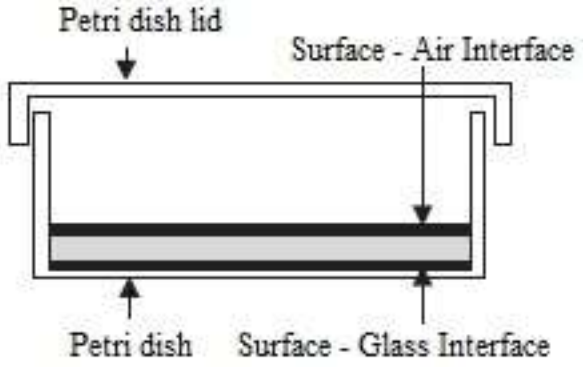

Figure 7.1 - Solvent cast film showing the two different interfaces **[48]**

Even though it was not investigated by *Tang et al*., this change in molecular structure could have contributed to a change between the moduli of the 2 different surfaces and that of the bulk. Furthermore, a change in the surface modulus could have influenced the overall modulus in our nanofibres and led to the increase in modulus observed with a reduction in diameter.

7.2 NANO-INDENTATION

The nano-indenter was then used to obtain a value for the elastic modulus using the Oliver-Pharr method. Data was obtained from shallow and relatively deep indents to investigate both the surface layer of the cast films and the bulk modulus. A Berkovich tip was used and nano-indentation was performed as instructed on the system's user manual. Multiple indents were made on the specimen to obtain readings from different areas. The results could then be tabulated on a picture graph by the software for easy comparison as shown below.

Z1A1 0.1µm indents

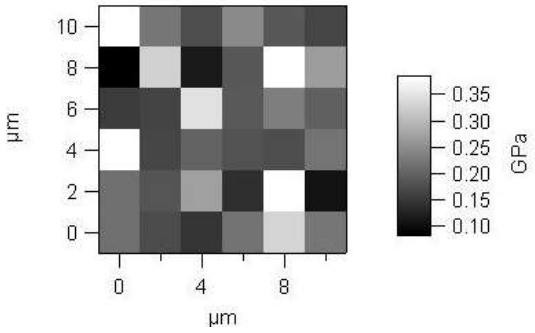

Z1A1 1.5µm indents

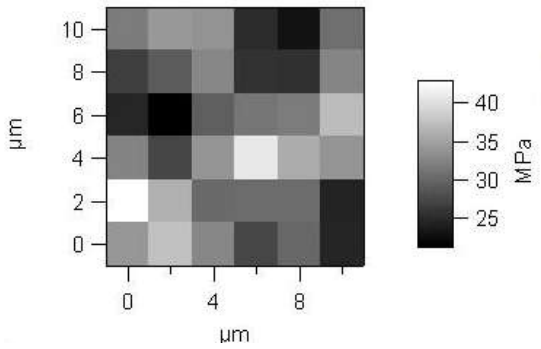

Z3A1 0.1µm indents

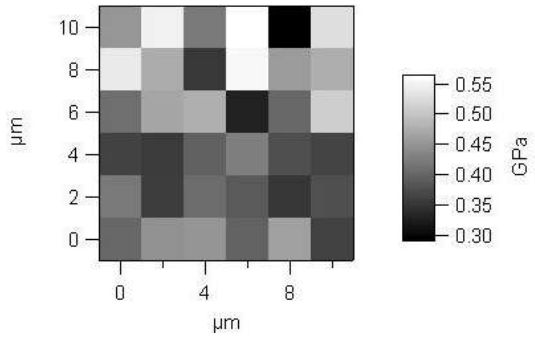

Z3A1 1.5µm indents

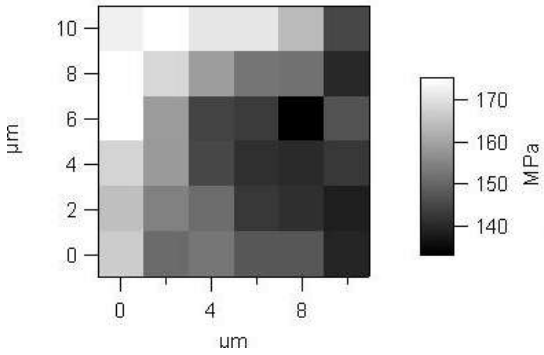

Even though the values for the moduli were different to those obtained from previous tests, there was still a 5 fold increase in the modulus between the two polymers. It was also easily visible that shallow indents yielded a much higher modulus than the indents made to greater depth. A statistical analysis of the data was performed to confirm this observation.

Z1A1 0.1µm

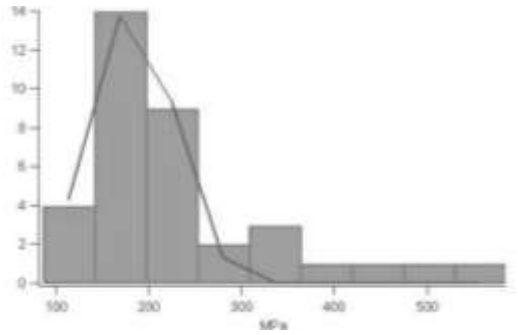

Z1A1 1.5µm

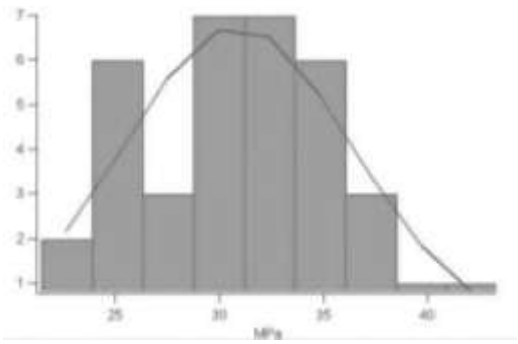

Z3A1 0.1µm

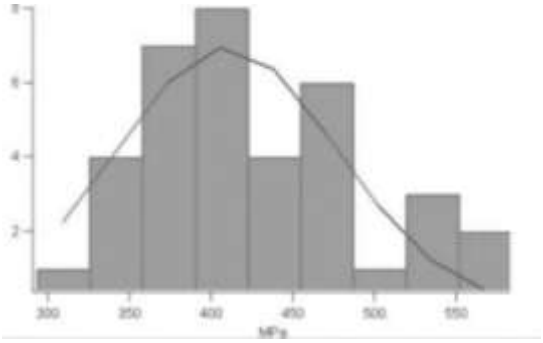

Z3A1 1.5µm

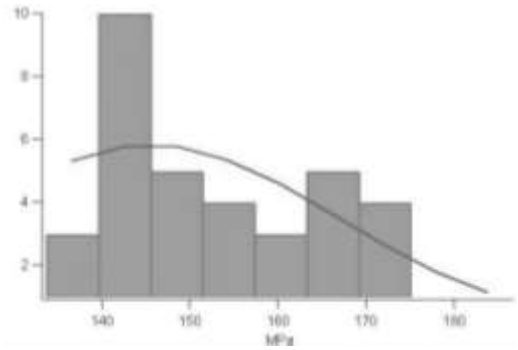

To confirm whether a change in the elastic moduli was observed on the different sides of the PU cast films, indentations were then performed on each side.

	0.1µm	1.5µm
Z1A1		
Air	182 ± 45 MPa	31 ± 5 MPa
Glass	186 ± 46 MPa	30 ± 1 MPa
Z3A1		
Air	409 ± 67 MPa	145 ± 21 MPa
Glass	223 ± 62 MPa	130 ± 4 MPa

A significant change in the distributions between indents made at 0.1µm and 1.5µm was observed and confirmed by t-tests, further confirming our hypothesis that a surface layer with a higher elastic modulus forms on top of the substrate as the solvent evaporates from the polymer dispersion.

The change in the properties observed for Z1A1 on different sides of the cast film seemed insignificant and was confirmed by a t-test which showed *t=0.052* for the 0.1μm indents and *t=0.744* for the 1.5μm indents. Z3A1 on the other hand showed a very significant difference between the two surfaces with the largest difference being observed in the shallow indents. The difference in the surface was also easily visible as one side of the film was shiny while the other was matt. Another observation was that cast films would flex under their own weight by a different amount depending direction in which they were held. These observations confirmed that the polymer molecules' alignment was influenced by the properties of the surface that was in contact while the film was being cast. As electrospun fibres are formed by evaporating the solvent from the polymer solution, the same phenomenon was expected to be observed on the nanofibres.

This shallow, hard surface layer might not have a significant impact on the elastic modulus of a comparatively large cast film. However, when nanofibres are produced, the effects of this layer would become predominant over the substrate layer leading to an overall increase in the modulus of the fibre. Even though the actual fibres` modulus most probably varies linearly form the centre of fibre, for ease of representation, Figure 7.2 shows two fibres of different diameter with a surface layer of the same thickness and higher modulus when compared to the bulk.

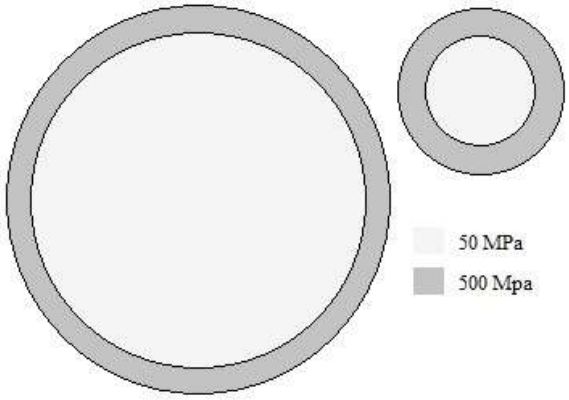

Figure 7.2 - Representation of hard surface layer on 2 fibres of different radius.

The overall modulus for the composite would therefore be expected to be higher in the smaller fibre as the hard surface layer has a higher influence on the modulus in the small fibre than in the large fibre.

In an attempt to prove this hypothesis, nano-indentation was performed on a specimen that was used for mechanical characterisation on the AFM. As the polycarbonate membrane was only 7μm in thickness, the nano-indenter could not be used as the hardness of the glass slide had a large impact on the values obtained. Nano-indentation has to be performed on materials that are at least 10 times thicker than the depth of the indentation to avoid effects from the substrate.

7.3 NANO-INDENTATION USING AFM

The Atomic Force Microscope was then used with a cantilever of nominal stiffness at 10N/m aiming to perform nano-indentation on the fibres. The main advantages of using the AFM for this procedure were the increased sensitivity over the nano-indenter and the ability to obtain an image of the area to locate the position of a fibre before performing nanoindentation. The indentations effected using the AFM were shallower than those made on the nano-indenter as the fibre thickness was only a few hundreds of nanometres.

	8nm	40nm
Z1A1	661 ± 171 MPa	95 ± 11 MPa
Z3A1	1558 ± 226MPa	685 ± 87 MPa

Even though this procedure had a considerable number of limitations associated with it, a significant increase could still be seen in the modulus calculated by the Oliver- Pharr model when indentation was only made to a shallower depth. This further supports our initial hypothesis that a thin surface layer with a higher modulus forms on top of the fibres leading to an increase in elastic modulus as the fibre diameter decreases.

One of the main problems with the Oliver-Pharr method is that it did not account for pile-up of material around the contact impression as is observed in most elastic materials. This pile-up of material increases the contact area, making it greater than what would be predicted by the model. This increase in contact area would overestimate the values calculated modulus as shown in Eqn. 2.1. As the indentation depth increases, this pile-up of material around the tip would be expected to increase. This would lead to inaccurate, higher values for the calculated moduli when indentation is performed to an increased depth. The values obtained when indentations were made to a higher depth might have therefore been artificially raised by this artefact. A more important observation is that in our case, a higher modulus was observed when indentations were made to a shallow depth. As this artefact has a less significant role at shallower indents, it could be assumed that the increase in moduli observed was real and not created by this artefact brought around by the Oliver-Pharr model.

Even though indentation using AFM is suitable for testing the mechanical properties of soft materials, a number of limiting factors have to be considered. Indenting in thin nanofibres could lead to an overestimation of the moduli as the effects of the substrate could be predominant. The cantilever tips used to perform nano-indentation are not as accurate as those used in purpose-built nano-indenters. This might lead to inaccurate estimates of nominal tip radius and shape. Another concern is the curvature of the fibre as this would alter the contact area of indentation if the fibre diameter is close to the tip radius. When these limiting factors are considered, nano-indentation using an AFM would not be considered as an ideal method, but as there is no other feasible alternative, this method would have to be accepted while keeping in mind its limitations.

The results obtained from this method nevertheless supported our initial hypothesis as a surface layer with a high elastic modulus was still described.

8 CONCLUSIONS

The main observation being made in this thesis is that the mechanical properties, namely the elastic modulus, are not constant over a range of fibre diameters. An attempt was made to disprove the major concerns that were associated with our experiments to further confirm that our observations were scientifically correct. As multiple experiments have pointed to the same conclusion, we can be confident in confirming this observation. Even though the same general trend was observed, the experiments conducted yielded varying figures for the moduli, rendering us unable to give exact figures of the fibre moduli with a varying diameter. Further work would have to be done using different approaches to find a more suitable model that accurately represents the real fibre response.

The behaviour of cells strongly depends on the substrate's properties such as the elastic modulus, and normal electrospun scaffolds have a wide range of fibre diameters. This variation could be disregarded if the overall modulus of the fibre mesh is calculated, but it would lead to an important variation in the local elastic moduli of each fibre. As individual cells only interact with single nanofibres, and not the mesh as a whole, an alteration in the local elastic modulus would have a significant impact on the mechanotransduction of cells. This variation in cellular response could lead to an inhomogeneity in the distribution of cells, rendering the scaffold less suitable for the engineered tissue's needs. This thesis therefore highlights the need for an optimisation in the control of fibre diameter when building cell scaffolds. An ideal scaffold built from these polymers would therefore have a very limited variation in fibre diameter to reduce the variation in local moduli.

In a recent study published by *Curtis et al.*, cells are shown to exert forces in the range of 10pN to 1nN [49]. In our experiments, the forces were applied on individual nanofibres and were in the range of 4nN. This therefore closely mimics the forces and environment experienced by the cells *in situ*. Applying larger forces could have led to an elastic hardening and the calculations obtained would therefore not have been representative of what is experienced by an individual cell. Artificial scaffolds can act like chainmail, where even though the scaffold is pliable and easy

to manipulate, the modulus of individual strands is in fact considerably high. Rather than testing the bulk modulus of the scaffold, tests were performed on single nanofibres as cells only interact with the latter, thus further mimicking cellular environment.

Experiments were also made in an attempt to explain the stiffening mechanism observed in the fibres. Results point to an increase in the surface modulus formed as solvent evaporates from the nanofibres during synthesis. This hypothesis has been backed up by two experiments, both of which used the Oliver-Pharr model to derive the calculations made. As the Oliver-Pharr model has a number of limitations associated with it, the reliability of these results can be challenged. Nonetheless, the impact that a change in fibre modulus has on mechanotransduction would be evident regardless of the stiffening mechanism at play.

8.1 SUGGESTIONS FOR FURTHER WORK

Most of the limitations that could compromise the results of our experiments have been dealt with and disproved. To further confirm these results, a technique to investigate the shape adopted by the fibre during three-point bending could be used. This could confirm which model best fits the obtained data and would therefore result in a more accurate calculation of the elastic moduli. A different technique other than three-point bending could be used to calculate the elastic modulus of the fibres. Tensile tests using AFM could be performed along with single fibre analysis using the *Bose ElectronForce* test machine.

Even though an increase in the surface modulus was observed, the mechanism by which this was created was not fully described. If this mechanism is successfully explained, further experiments could be made in an attempt to control or remove this surface phenomenon. Another feasible approach to this problem would be the application of post-processing techniques to the scaffold such as annealing, in an attempt to homogenise the fibre moduli. The outcome of this procedure would be a scaffold with a range of fibre diameters but a constant fibre modulus. This would

create a more homogenous substrate for cells and could therefore increase cell proliferation and survival rate.

Further tests that could be performed include an investigation into whether the fibre properties change after being submerged into physiological solutions. Even though the material is listed as being bio-stable, changes can occur on the nanoscale and these can be amplified by the large surface area to volume ratio that is naturally present in scaffolds. Changes in the surface topography of individual nanofibres could be monitored as these might further influence cellular behaviour on a scaffold. Another challenging area that could be investigated is the change in mechanical properties seen in degradable nanofibres. These resorbable fibres have a strong role in tissue engineering as they are sometimes used as a temporary scaffold and in drug-releasing applications. Monitoring the change in their mechanical properties could provide an insight on the environment being encountered by cells.

As scaffolds are three-dimensional structures, it would be relevant to attempt to characterise the scaffold properties in three dimensions. A complex computer model could be used to re-create the structure of electrospun scaffolds along with the knowledge obtained from this thesis in an attempt to accurately predict local stresses and strains and analyse the environment encountered by cells.

Using the knowledge acquired from this thesis, experimentation should be taken to the next stage and *in-vitro* analysis could be performed using various cell types. The proliferation of cells on scaffolds with different ranges of fibre diameter can be compared. Different mean fibre diameter, as well as different distribution can be compared in an effort to find which range is most suited for specific cell types to grow on. The effect that fibre modulus homogenisation has on the proliferation of cells can also be investigated and compared to the results obtained from previous experiments. Fibre alignment could also be investigated as this can have a significant impact on cell propagation as well as the overall mechanical properties of the scaffold.

The set of experiments described above could be used to optimise a scaffold for use in *in-vivo* experiments to help progress the application of tissue engineering.

9 BIBLIOGRAPHY

[1] W. M. Saltzman, Tissue Engineering - Principles for the design of replacement organs and tissues, Oxford: Oxford University Press, 2004.

[2] B. Palsson, J. A. Hubbell, R. Plonsey and J. D. Bronzino, Tissue Engineering, Florida: CRC Press, 2000.

[3] S. Ramakrishna, An Introduction to Electrospinning And Nanofibers, Singapore: World Scientific Publishing Co.Pte. Ltd, 2005.

[4] S. Agarwal, "Use of electrospinning technique for biomedical applications," *Polymer*, pp. 5603-5621, 2008.

[5] Y. Gogotsi, Nanomaterial Handbook, Florida: CRC Press, 2006.

[6] V. Leung, "Biomedical applications of nanofibers," *Polymers advanced technologies,* no. 22, pp. 350-365, 2010.

[7] J. Venugopal, "Applications of Polymer Nanofibers in Biomedicine and Biotechnology," *Biochemistry,* vol. 125, no. 5, pp. 147 - 157, 2005.

[8] B. B. Association, "Standards," [Online]. Available: http://www.britishburnassociation.org/standards. [Accessed 15 4 2012].

[9] E. T. Vargas, "Hyperbranched polyglycerol electrospun nanofibers for wound," *Acta Biomaterialia,* no. 6, pp. 1069 - 1078, 2010.

[10] D. A.Soscia, "Antibiotic-Loaded PLGA Nanofibers for Wound Healing," *Advanced Biomaterials,* no. 12, pp. B83 - B88, 2010.

[11] M. Goldberg, . R. Lange and J. Xinqiao, "Nanostructured materials for applications in drug delivery and tissue engineering," *Journal of Biomaterial Science,* vol. 18, no. 3, pp. 241 - 268, 2007.

[12] M. Prabaharan, R. Jayakumar and N. SV, "Electrospun Nanofibrous Scaffolds-Current Status and Prospects in Drug Delivery," *Advances in polymer sceince,* vol. 246, pp. 241-262, 2012.

[13] Y. Dong, "Aligned Nanofiber covered stent". Patent PCT application, 2009.

[14] K. Keita, "Development of Nanofiber-Covered Stents Using Electrospinning: In Vitro and Acute Phase In Vivo Experiments," *Journal of Biomaterial science,* vol. 88B, no. 1, pp. 230-239, 2009.

[15] A. Campillo-Fernandez, R. Unger, K. Peters, S. Halstenberg, M. Santos, M. Sanchez and Duenas, "Analysis of the Biological Response of Endothelial and Fibroblast Cells Cultured on Synthetic Scaffolds with Various Hydrophilic/Hydrophobic Ratios: Influence of Fibronectin Adsorption and Conformation," *Tissue Engineering,* vol. 15, no. 6, pp. 1331 - 1341, 2009.

[16] Abrams, G. A. and S. L. Goodman, "Nanoscale topography of the basement membrane underlying the corneal," *Cell Tissue Research,* vol. 299, no. 1, pp. 39-46, 2000.

[17] T. A. Ulrich, E. M. d. J. Pardo and S. Kumar, "The Mechanical Rigidity of the Extracellular Matrix Regulates the Structure, Motility, and Proliferation of Glioma Cells," *Cancer Research,* vol. 69, no. 1, pp. 4167 -4174, 2009.

[18] M. J. Paszek, N. Zahir, K. R. Johnson and J. N. Lakins, "Tensional homeostasis and the malignant phenotype," *Cancer Cell,* vol. 8, no. 1, pp. 241 - 254, 2005.

[19] A. S. Kulshrestha and A. Mahapatro, "Polymers for Biomedical Applications," *American Chemical Society,* 2008.

[20] W. -. J. Li and R. S. Tuan, "Polymeric Scaffolds for Cartilage Tissue Engineering," *International Union of Pure and Applied Chemistry,* vol. 227, pp. 65 - 75, 2005.

[21] L. S. Naira and C. T. Laurencin, "Biodegradable polymers as biomaterials," *Progress in Polymer Science,* vol. 32, pp. 762 - 798, 2007.

[22] B. Carlberg, M. Z. Axell, U. Nannmark, J. Liu and H. G. Kuhn, "Electrospun polyurethane scaffolds for proliferation and neuronal differentiation of human embryonic stem cells," *Biomedical Materials,* vol. 4, no. 4, 2009.

[23] S. Grenier, M. Sandig, D. W. Holdsworth and K. Mequanin, "Interactions of coronary artery smooth muscle cells with 3D porous polyurethane scaffolds.," *Journal of Biomaterial Research ,* vol. 89, pp. 293 - 303, 2009.

[24] S. Grenier, M. Sandig and K. Mequanint, "Polyurethane biomaterials for fabricating 3D porous scaffolds and supporting vascular cells," *Journal of biomedical materials research,* vol. 82A, no. 4, pp. 802 - 809, 2007.

[25] A. L. Andrady, Science and Technology of Polymer Nanofibers, New Jersey: John Wiley & Sons, 2008.

[26] N. Bhardwaj, "Electrospinning: A fascinating fiber fabrication technique," *Biotechnology Advances,* no. 28, pp. 325 - 347, 2010.

[27] J. H. Wendorff, S. Agarwal and A. Greiner, Electrospinning: Materials, Processing and Applications, Weinheim: Wiley, 2012.

[28] Z.-M. Huang, “Electrospinning and mechanical characterization of gelatin nanofibers,” *Polymer,* no. 45, pp. 5361 - 5368, 2004.

[29] Lim and C. Tan, “Mechanical characterization of a single nanofiber,” *Nanomechanics of Materials and Structures,* pp. 121 - 136, 2006.

[30] Y. Zhang, “Nanomechanical Characterization of One-Dimensional Nanostructures,” in *Micro and Nano Mechanical Testing of Materials and Devices,* Kentucky, Springer, 2008, pp. 105 - 120.

[31] W. Oliver and G. Pharr, “Measurement of hardness and elastic modulus by instrumented indentation: Advances in understanding and refinements to methodology,” *Journal of Materials Research,* vol. 19, no. 1, pp. 3 - 20, 2003.

[32] W. Oliver and G. Pharr, “An improved technique for determining hardness and elastic modulus using load and displacement sensing indentation experiments,” *Journal of Materials,* vol. 7, no. 6, pp. 1564 - 1583, 1992.

[33] P. Zhou, “Three-point bending Young’s modulus of nanowires,” *Measurement science and technology,* no. 19, 2008.

[34] G. Binnig and C. Quate, “Atomic Force Microscope,” *Physical Review Letters,* vol. 56, no. 9, pp. 930 - 933, 1986.

[35] P. C. Braga, Atomic Force Microscopy - Biomedical Methods and Applications, New Jersey: Humana Press Inc., 2004.

[36] W. Bowen, Atomic Force Microscopes in Process Engineering, Oxford: Elsevier Ltd., 2009.

[37] “Atomic Force Microscopy,” nanoScience instruments, [Online]. Available: http://www.nanoscience.com/. [Accessed 29 3 2012].

[38] Bhushan, Handbook of Nano-technology, Berlin: Springer, 2004.

[39] P. West, “A Guide to AFM Image Artifacts,” Pacific Nanotechnology.

[40] P. Eaton, “Other Artifacts - Flying tip,” 11 August 2009. [Online]. Available: http://afmhelp.com. [Accessed 29 3 2012].

[41] B. Wu, A. Heidelberg, J. Boland, J. Sader, X. Sun and Y. Li, “Microstructure-hardened silver nanowires,” *Nano Letters,* vol. 6, no. 3, pp. 468 - 472, 2006.

[42] H. Ni, X. Li and H. Gao, “Elastic modulus of amorphous SiO2 nanowires,” *Nanoscale Science and Design,* vol. 88, no. 4, 2005.

[43] S. Lee, C. Tekmen and W. Sigmund, “Three-point bending of electrospun TiO2 nanofibers,” *Material science and engineering,* vol. 398, no. 1-2, pp. 77 - 81,

2005.

[44] S. Cuenot, S. Demoustier-Champagne and B. Nysten, “Elastic Modulus of Polypyrrole Nanotubes,” *Physical Review Letters,* vol. 85, no. 8, pp. 1690 - 1693, 2000.

[45] E. P. S. Tan and C. T. Lim, “Effects of annealing on the structural and mechanical properties of electrospun polymeric nanofibres,” *Nanotechnology,* vol. 17, pp. 2649 - 2654, 2006.

[46] M. K. Shin, S. I. Kim and S. J. Kim, “Size-dependent elastic modulus of single electroactive polymer nanofibers,” *Applied Physics Letters,* vol. 89, 2006.

[47] Q. Fu, Y. Jin, X. Song, J. Gao and X. Han, “Size-dependent mechanical properties of PVA nanofibers reduced via air plasma treatment,” *Nanotechnology,* vol. 21, pp. 1 - 5, 2010.

[48] L. Sun, R. P. S. Han, J. Wang and C. T. Lim, “Modeling the size-dependent elastic properties of polymeric nanofibers,” *Nanotechnology,* vol. 19, no. 45, 2008.

[49] A. Arinstein, M. Burman, O. Gendelman and E. Zussman, “Effect of supramolecular structure on polymer nanofibre elasticity,” *Nature Publishing Group,* vol. 2, pp. 59 - 62, 2007.

[50] Z. Tang, R. Black, J. Curran, J. Hunt, N. Rhodes and D. Williams, “Surface properties and biocompatibility of solvent-cast poly[e-caprolactone] films,” *Biomaterials,* vol. 25, pp. 4741 - 4748, 2004.

[51] A. Curtis, L. Sokolikova-Csaderova and G. Aitchison, “Measuring Cell Forces by a Photoelastic Method,” *Biophysical Journal,* vol. 92, pp. 2255 - 2261, 2007.

[52] Y. Xin, “Fabrication of well-aligned PPV/PVP nanofibers by electrospinning,” *Materials Letters,* no. 62, pp. 991 -993, 2008.

[53] K. Zhang, “Degradation of electrospun SF/P(LLA-CL) blended nanofibrous scaffolds in vitro,” *Polymer Degradation and Stability,* no. 96, pp. 2266 - 2275, 2011.

[54] J. Ba, Q. Yang, S. Wang and Y. Li, “Preparation and characterization of electrospun Ag/polyacrylonitrile composite nanofibers,” *Korean Journal of chemical engineering,* vol. 28, no. 8, pp. 1761 - 1763, 2011.

[55] W. Yan, C. L. Pun and G. P. Simon, “Conditions of applying Oliver–Pharr method to the nanoindentation of particles in composites,” *Composites Science and Technology,* vol. 72, pp. 1147 - 1152, 2011.

10 APPENDIX

BIOMER TECHNOLOGY LTD
MATERIAL SAFETY DATA SHEET
Z1A1

1. IDENTIFICATION	
Chemical Name Product Code Supplier	Polyetherurethane. Z1A1 Part Number 3100001. Biomer Technology Ltd.
2. COMPOSITION	
Composition	100% polyurethane pellets.
3. REGULATORY INFORMATION	Risk free.
Safety Phrase	Chemically unreactive/ biologically compatible. Ingestion to be avoided as choking hazard. S16 Keep away from sources of ignition.
4. HAZARD IDENTIFICATION	Z1A1 will melt at 190 - 235 deg. C.
	Decomposition above 280 deg. C. may release carbon monoxide and hydrogen cyanide.
5. FIRE FIGHTING MEASURES	Evacuate building. Call fire brigade. Full self -contained breathing apparatus must be worn. All commonly available extinguishers useable.
6. FIRST AID MEASURES	Safe normally. In event of fire / medical aid on hand.
7. ACCIDENTAL SPILLAGE/ RELEASE	Sweep up as pellets are a slipping hazard.
8. HANDLING AND STORAGE	Keep away from sources of ignition.
9. STABILITY AND REACTIVITY	Chemically inert. Stable under normal conditions.
10. EXPOSURE CONTROLS	Follow good industrial hygiene procedures, with masks, gloves eye protection available.
11. PHYSICAL AND CHEMICAL PROPERTIES	Solid pellet, odourless, melting range 190-235 deg. C.
12. TOXICOLOGICAL INFORMATION	Safe, medical grade polymer.
13. ECOLOGICAL INFORMATION	Ecotoxicity –Z1A1 will not contaminate ground water. Non biodegradable.
14. DISPOSAL CONSIDERATIONS	Z1A1 can be recycled or disposed of in a landfill without detriment to the environment.
15. TRANSPORT INFORMATION	Bagged in high density polyethylene bag inner and tri-ply paper outer.
16. OTHER INFORMATION	Contact Biomer Technology Limited. Tel: 44 (0) 1928 531888 Fax: 44 (0) 1928 531817

Biomer Technology Ltd
10 Seymour Court, Tudor Road
Manor Park, Runcorn
Cheshire WA7 1SY
United Kingdom.

BIOMER TECHNOLOGY LTD
MATERIAL SAFETY DATA SHEET
Z3A1

1. IDENTIFICATION	
Chemical Name Product Code Supplier	Polyetherurethane. Z3A1 Part Number 3100004. Biomer Technology Ltd.
2. COMPOSITION	
Composition	100% polyurethane pellets.
3. REGULATORY INFORMATION	Risk free. Chemically unreactive/ biologically compatible.
Safety Phrase	Ingestion to be avoided as choking hazard. S16 Keep away from sources of ignition.
4. HAZARD IDENTIFICATION	Z3A1 will melt at 200 - 235 deg. C.
	Decomposition above 280 deg. C. may release carbon monoxide and hydrogen cyanide.
5. FIRE FIGHTING MEASURES	Evacuate building. Call fire brigade. Full self -contained breathing apparatus must be worn. All commonly available extinguishers useable.
6. FIRST AID MEASURES	Safe normally. In event of fire / medical aid on hand.
7. ACCIDENTAL SPILLAGE/ RELEASE	Sweep up as pellets are a slipping hazard.
8. HANDLING AND STORAGE	Keep away from sources of ignition.
9. STABILITY AND REACTIVITY	Chemically inert. Stable under normal conditions.
10. EXPOSURE CONTROLS	Follow good industrial hygiene procedures, with masks, gloves eye protection available.
11. PHYSICAL AND CHEMICAL PROPERTIES	Solid pellet, odourless, melting range 200-235 deg. C.
12. TOXICOLOGICAL INFORMATION	Safe, medical grade polymer.
13. ECOLOGICAL INFORMATION	Ecotoxicity –Z3A1 will not contaminate ground water. Non biodegradable.
14. DISPOSAL CONSIDERATIONS	Z3A1 can be recycled or disposed of in a landfill without detriment to the environment.
15. TRANSPORT INFORMATION	Bagged in high density polyethylene bag inner and tri-ply paper outer.
16. OTHER INFORMATION	Contact Biomer Technology Limited. Tel: 44 (0) 1928 531888 Fax: 44 (0) 1928 531817

Biomer Technology Ltd
10 Seymour Court, Tudor Road
Manor Park, Runcorn
Cheshire WA7 1SY
United Kingdom.

Registered in England 4948804
Registered Office: 10 Seymour Court, Manor Park Runcorn, Cheshire

LIST OF ELECTROSPINNING TRIALS FOR Z3A1

Mandrell V	Electric Field V	Distance to Collector	Volume	Rate of Flow
kV	kV	cm	ml	ml/hr
Humidity 34%			Temperature 23.6 °C	
23	18	16	0.014	0.2
23	18	16	0.014	0.25
18	18	16	0.01	0.2
18	18	16	0.02	0.2
18	18	16	0.01	0.15
23	18	16	0.02	0.15
18	18	16	0.02	0.15
18	18	16	0.02	0.1
18	18	16	0.03	0.15
18	18	16	0.025	0.15
18	18	16	0.01	0.13
18	18	16	0.015	0.13
18	18	16	0.01	0.13
18	18	16	0.01	0.13
18	17.5	16	0.01	0.13
18	17.5	16	0.01	0.15
Humidity 32%			Temperature 22.6 °C	
23	18	16	0.01	0.2
18	18	16	0.01	0.13
23	18	16	0.01	0.12
18	18	16	0.01	0.2
18	18	16	0.01	0.13
23	18	16	0.01	0.13
23	18	16	0.005	0.1
23	18	16	0.001	0.1
23	18	16	0.006	0.1
23	18	16	0.0085	0.05
23	18	16	0.1	0.05
23	18	16	0.2	0.05

Humidity 30% Temperature 22.2 °C

18	18	16	0.016	0.2
18	18	16	0.016	0.18
18	18	16	0.016	0.17
18	18	16	0.017	0.18
15	18	16	0.017	0.18
18	18	16	0.017	0.18
18	18	16	0.016	0.19
18	18	16	0.018	0.19
18	18	16	0.02	0.19
18	18	16	0.018	0.19
18	18	16	0.016	0.19

Humidity 34% Temperature 22.6 °C

18	18	16	0.004	0.19
18	18	16	0.005	0.185
18	18	16	0.005	0.195
18	18	16	0.005	0.19
18	18	16	0.005	0.19
18	23	16	0.005	0.19
18	18	16	0.005	0.19
15	18	15	0.005	0.19
15	23	15	0.005	0.19
15	18	15	0.003	0.19

Humidity 29% Temperature 23.7 °C

15	18	15	0.003	0.19
15	18	15	0.003	0.2
15	18	15	0.003	0.1
15	18	15	0.003	0.05
15	18	15	0.004	0.15
15	18	15	0.004	0.1
15	18	15	0.004	0.06

LIST OF ELECTROSPINNING TRIALS FOR Z1A1

Mandrell V	Electric Field V	Distance to Collector	Volume	Rate of Flow
kV	kV	cm	ml	ml/hr
Humidity 35%			Temperature 23°C	
23	18	15	0.008	0.1
23	18	15	0.005	0.1
23	18	15	0.003	0.1
23	18	15	0.002	0.1
23	18	15	0.0023	0.1
23	18	15	0.003	0.1
23	18	15	0.003	0.1
Humidity 31%			Temperature 21.1 °C	
23	18	16	0.003	0.1
23	18	15	0.003	0.1
23	18	15	0.003	0.05
23	18	15	0.003	0.02
Humidity 32%			Temperature 22.6 °C	
23	18	15	0.003	0.1
23	18	15	0.005	0.1
23	18	15	0.003	0.12
23	18	15	0.003	0.15
23	18	15	0.007	0.2
23	18	16	0.008	0.2
23	18	16	0.008	0.19
23	18	16	0.008	0.15
23	18	16	0.007	0.15
23	18	15	0.007	0.15
23	18	15	0.005	0.15
23	18	15	0.003	0.15
23	18	15	0.003	0.18
23	18	15	0.003	0.2